UNIVERSITY OF NOVA GORICA
GRADUATE SCHOOL

NON-SINGULAR METHOD OF FUNDAMENTAL SOLUTIONS FOR PROBLEMS IN MICROMECHANICS

DISSERTATION

Qingguo Liu

Mentor: Prof. Dr. Božidar Šarler

Nova Gorica, 2014

UNIVERZA V NOVI GORICI
FAKULTETA ZA PODIPLOMSKI ŠTUDIJ

NESINGULARNA METODA FUNDAMENTALNIH REŠITEV ZA MIKROMEHANSKE PROBLEME

DISERTACIJA

Qingguo Liu

Mentor: Prof. Dr. Božidar Šarler

Nova Gorica, 2014

Acknowledgements

My deepest gratitude goes first and foremost to my advisor prof. Božidar Šarler, for his constant support, encouragement, guidance and specially for giving me opportunity to independently explore the topic I am presenting in this dissertation, during last few years.

I would like to express my heartfelt gratitude to co-workers of the laboratory dr. Eva Sincich, dr. Agnieszka Zuzanna Lorbiecka, dr. Robert Vertnik and dr. Gregor Kosec for uncountable useful discussions, ideas and encouragements they gave me. Especially thanks to Umut Hanoglu for making calculations with Deform code in Figures 4.12 and 4.15.

I am also greatly indebted to all my co-workers from COBIK, specially to dr. Igor Grešovnik, Todej Kodelja and Katarina Mramor for having great time with them.

Last, but not least, my thanks would go to my beloved family for their loving considerations and great confidence in me all through these years. I also owe my sincere gratitude to my friends who gave me their help and time in listening to me

Finally, I would like to express gratitude to Slovenian Research Agency for support in the framework of the project Young Researcher Programme 1000-12-1540.

Non-Singular Method of Fundamental Solutions for Problems in Micromechanics

Abstract

The research described in this dissertation is focused on development of a novel Method of Fundamental Solutions (MFS) for solving two-dimensional linear elasticity problems. The purpose of the developments is the use of the developed method for numerical modelling and simulation of deformation of microstructure of multi-grain materials such as metals. This approach enables to calculate the deformation of multi-grain materials as a function of the shape and mechanical properties of each of the grains that can be anisotropic and differently oriented. Respectively, the macroscopic mechanical response can be obtained from the defined properties of its microscopic constituent parts. The novelty of the developed approach is in the removal of the fictitious boundary where in MFS the poles of the fundamental solution are placed. The fictitious boundary represents the main drawback of MFS. This drawback makes the application of MFS to multi-grain materials very complicated. With the goal to make the artificial boundary coincide with the physical boundary of the grain are the singular point sources of the fundamental solution replaced by distributed sources over circular discs around the singularity. The magnitude and the shape of the fundamental solution inside the disk is adjusted by the average value of the domain integral of the fundamental solution over the disk and by coinciding of the shape of the related function with the fundamental solution and its first derivatives on the border of the disc.

In case of displacement (Dirichlet) boundary conditions, the values of distributed sources are calculated directly and analytically for isotropic problems and numerically for anisotropic problems. In case of traction (Neumann) boundary conditions, the respective desingularized values of the derivatives of the fundamental solution in the coordinate directions, as required in the calculations, are calculated indirectly from the construction of two reference solutions of the linearly varying simple displacement fields in the first variant of the novel method, termed Non-singular Method of Fundamental Solutions (NMFS). However on the expense of solving three times the systems of algebraic equations in comparison with only one solution in MFS. In addition, the related reference fields have to be carefully chosen in order to get the proper solution. In the second variant of the novel method, termed Improved Non-singular Method of Fundamentals Solutions (INMFS), the respective desingularized values of the derivatives of the fundamental solution in the poles are calculated from the assumption that the sum of the forces on the body should vanish in mechanical equilibrium. The system of algebraic equations is solved only once as in the MFS and there is no need to employ the two reference solutions as in NMFS. A free parameter – radius of the desingularization disk appears in both non-singular methods. It turns out that a suitable choice for this parameter is around 20% of the distance between the neighbouring nodes on the boundary.

In order to demonstrate the feasibility, accuracy and convergence of the newly developed methods, the NMFS and the INMFS solutions are compared to the MFS

solution and analytical solutions for a spectra of plane strain problems. Analysis of the method includes isotropic and anisotropic materials, single and multi-grain problems. Special attention is devoted to problems with elastic or rigid inclusions as well as voids.

Both, the NMFS and the INMFS methods, turn out to give similar results than the classical MFS method in all spectra of the performed tests. Because INMFS is simpler and more efficient than the NMFS, INMFS is a preferred method for use. The dissertation is concluded with simulation of deformation of a piece of a realistic microstructure of a spring steel 51CrMoV4 on a square 50μm with 24 grains.

The represented work display a first use of MFS for solid mechanics problems without the fictitious boundary. The developed approach is clearly better than the classical finite element method for this type of problems, since discretisation is performed only on the boundary. The newly generated knowledge will be incorporated in microstructure deformation model, coupled with the macroscopic simulation system for continuous casting, hot rolling and heat treatment of metals.

Key words:

Micromechanics, microstructure, isotropic elasticity, anisotropic elasticity, plane strain problems, Method of Fundamental Solutions, displacement boundary conditions, traction boundary conditions, fundamental solution, Non-Singular

Nesingularna metoda fundamentalnih rešitev za mikromehanske probleme

Povzetek

Raziskave, opisane v disertaciji, so osredotočena na razvoj nove Metode Fundamentalnih Rešitev (MFS) za reševanje dvo-dimenzionalnih linearnih elastičnih problemov. Namen razvoja nove metode je njena uporaba za numerično modeliranje in simulacijo deformacije mikrostukture snovi z več zrni, kot so na primer kovine. Ta omogoča izračun deformacije zrnatega materiala kot funkcijo oblike in mehanskih lastnosti posameznega zrna, ki so lahko anizotropna in različno orientirana. Zato lahko makroskopske mehanske lastnosti materiala izračunamo iz definiranih lastnosti njihovih mikroskopskih delov. Novost razvitega računskega postopka je odstranitev fiktivnega roba, kjer so pri MFS postavljeni poli fundamentalne restive. Fiktivni rob predstavlja glavno slabost MFS. Zaradi te slabosti je uporaba MFS za zrnate materiale zelo zapletena. S ciljem narediti sovpadanje fiktivnega roba s fizikalnim robom so singularni točkovni izvori fundamentalne reštive zamenjani s porazdeljenimi izvori po krožnih diskih okoli singularnosti. Velikost in oblika fundamentalne rešitve znotraj diska je prilagojena povprečni velikosti območnega integrala fundamentalne reštive po disku in z sovpadanjem oblike funkcije znotraj diska s fundamentalno rešitvijo in njenimi prvimi odvodi na meji diska.

V primeru robnih pogojev premika (Dirichletovi robni pogoji) so vrednosti distribuiranih izvorov izračunane direktno in analitično za izotropne probleme in numerično za anizotropne probleme. V primeru obremenitvenih robnih pogojev (Neumanovi robni pogoji) so desingularizirane vrednosti odvodov fundamentalne reštive v smeri koordinatnih osi, kot jih potrebujemo v izračunih, v prvi varianti nove metode, ki jo imenujemo Nesingularna metoda fundamentalnih rešitev (NSMFS), izračunane nedirektno iz konstrukcije dveh referenčnih rešitev linearno spremenljivega preprostega polj premikov. Vendar na račun trikratnega računanja sistema nastopajočih algebrajskih enačb, namesto samo enega izračuna kot v primeru MFS. Dodatno pa morajo biti referenčna polja skrbno izbrana za pravilno rešitev. V drugi varianti nove metode, ki jo imenujemo Izboljšana nesingularna metoda fundamentalnih rešitev (INMFS) pa so desingularizirane vrednosti odvodov fundamentalne rešitve v polih izračunane na podlagi predpostavke, da mora biti vsota vseh sil na telo v ravnovesju enaka nič. Sistem algebrajskih enačb v tem primeru rešimo samo enkrat, tako kot pri MFS, ne potrebujemo pa dveh referenčnih rešitev kot pri NMFS. V obeh nesingularnih metodah nastopa prosti parameter - polmer desingularizacijskega diska. Izkaže se, da dobimo natančne rezultate, če za polmer izberemo okoli 20% razdalje med sosednjimi točkami na robu.

S ciljem demonstracije izvedljivosti, natančnosti in konvergence novo razvite metode, sta NMFS in INMFS rešitvi primerjani z MFS in analitičnimi rešitvami za spekter problemov ravninske deformacije. Analiza metode vsebuje izotropne in anizotropne materiale, probleme na enem in več območjih. Posebna pozornost je namenjena poblemom z elastičnimi in togimi vključki in prazninami.

NMFS in INMFS dajeta podobne razultate kot klasična MFS na celotnem spektru izdelanih testov. Zaradi tega, ker je INMFS bolj preprota in bolj efektna kot NMFS, je INMFS primerna izmed obeh. Disertacijo sklenemo z deformacijo dela realistične mikrostukture vzmetnega jekla 51CrMoV4 na kvadratu dimenzije 50μm s 24 zrni.

Predstavljeno delo prikazuje prvo uporabo MFS brez fiktivnega roba za probleme mehanike trdnin. Metoda bo v prihodnosti dopolnjena tudi za plastično obnašanje materiala in uporabljena v modelu deformacije mikrostrukture, ki bo sklopljen z makroskopskimi simulacijami kontinuirnega ulivanja, vročega valjanja in toplotne obdelave kovin.

Ključne besede:

Mikromehanika, mikrostruktura, izotropna elastičnost, anizotropna elastičnost, ravninski deformacijski problemi, metoda fundamentalnih rešitev, robni pogoji premika, robni pogoji obremenitve, fundamentalna rešitev, nesingularna metoda fundamentalnih rešitev, izboljšana nesingularna metoda fundamentalnih rešitev.

Contents

List of Figures

List of Tables

List of Symbols

General notation

$\lvert\bullet\rvert$	determinant of a matrix
$\mathbf{x}$	vector or matrix
$\overline{f}$	known function
x_i	i -th component of vector
x_{ij}	i, j -th component of matrix

symbols

α, β	arbitrary constants
χ_{ς}^{D}	ς -direction Dirichlet type of boundary condition indicator
χ_{ς}^{T}	ς -direction Neumann type of boundary condition indicator
$\boldsymbol{\varepsilon}$	strain vector
$\varepsilon_{\varsigma\varsigma}$	normal strain
$\varepsilon_{\varsigma\xi}$	shear strain
μ	shear modulus of elasticity
ρ	complex constant
$\overline{\rho}$	conjugate complex of ρ
$\boldsymbol{\sigma}$	stress vector
$\sigma_{\varsigma\varsigma}$	normal stress
$\sigma_{\varsigma\xi}$	shear stress
A	disk covering the source point
$\mathbf{b}$	body force
b_{ς}	component of the body force in direction ς
$\mathbf{C}$	stiffness matrix
$C_{\varsigma\xi\upsilon\tau}$	fourth rank stiffness matrix component
c_{ij}	i, j -th component of the reduced stiffness matrix
d	the smallest distance between two nodes
E	Young's modulus
F	pressure

G	shear modulus
m_ς	the directional cosines of the angle between a normal and ς axes
N^Γ	number of boundary nodes
N^Ω	number of domain nodes
$N^{\Gamma^{m\cap k}}$	number of interface nodes between $m-$th and $k-$th domain
$\mathbf{n}$	normal vector
n_ς	component of the normal in direction ς
P	point
$\mathbf{p}$	collocation point
R	radius of A
R_M	distance between the fictitious and the true boundary in MFS
$\mathbf{S}$	compliance matrix
$S_{\varsigma\xi\upsilon\tau}$	fourth rank compliance matrix component
$\mathbf{s}$	source point
s_{ij}	i, j -th component of the reduced compliance matrix
$T_{\varsigma\xi}$	fundamental traction
$\tilde{T}_{\varsigma\xi}$	desingularized fundamental traction
$\mathbf{t}$	traction vector
t_ς	traction component in direction ς
$U_{\varsigma\xi}$	fundamental solution
$\tilde{U}_{\varsigma\xi}$	desingularized fundamental solution
$\mathbf{u}$	displacement vector
u_ς	component of the displacement in direction ς
$\underline{u}_\varsigma$	component of the analytical solution in direction ς
ν	Poisson's ratio
Γ	boundary
Γ^D	Dirichlet part of the boundary
Γ^N	Neumann part of the boundary
Ω	domain
Ω^m	$m-$ th sub-domain

Acronyms and abbreviations

BC	Boundary Condition
Eq.	equation
FDM	Finite Difference Method

FEM	Finite Element Method
FVM	Finite Volume Method
INMFS	Improved Non-Singular Method of Fundamental Solutions
MFS	Method of Fundamental Solutions
NMFS	Non-Singular Method of Fundamental Solutions
PDE	Partial Differential Equations
Re	real part of complex number
Ref.	Reference

1. Introduction

1.1 Overview of Dissertation

Micromechanics [Qu and Cherkaoui (2006)] represents analysis of composite or heterogeneous materials on the level of the individual constituent grains that form these materials. One of the main tasks of micromechanics of materials is localization, which aims at evaluating the local (stress and strain) fields in the phases for given macroscopic load states, phase properties, and phase geometries. Such knowledge is especially important in understanding and describing material elastic and plastic deformation damage and failure. The micromechanics of materials is mostly based on continuum mechanics principles. The computational solution of continuum micromechanics usually involves Finite Difference Method (FDM) [Mitchell and Griffiths (1980)], Finite Volume Method (FVM) [Patankar (1980)], Finite Element Method (FEM) [Zienkiewicz and Taylor (2000)], and Boundary Element Method (BEM) [Wrobel (2002); Aliabadi (2002)].

The BEM is a numerical computational method for solving linear Partial Differential Equations (PDE) which have been formulated as integral equations (i.e. in boundary integral form). The integral equation may be regarded as an exact solution of the governing partial differential equation. The BEM attempts to use the given boundary conditions to fit the boundary values into the integral equation, rather than values throughout the space defined by a partial differential equation. Once this is done, in the post-processing stage, the integral equation can then be used again to calculate numerically the solution directly at any desired point in the interior of the solution domain. Comparing to the more popular numerical methods, such as FEM and FDM, which can be classified as the domain methods, the BEM distinguish itself as a boundary method, meaning that the numerical discretization is conducted at reduced spatial dimensions. This reduced dimension leads to smaller linear systems, less computer memory requirements, and sometimes more efficient computation. This effect is most pronounced when the domain is unbounded. Unbounded domain needs to be truncated and approximated in domain methods. The BEM, on the other hand, automatically models the behaviour at infinity without the need of deploying a mesh to approximate it.

In scientific computation and simulation, the Method of Fundamental Solutions (MFS) [Chen, Karageorghis and Smyrlis (2008)] is getting a growing attention. The method also belongs to boundary methods. It is referred to by many other names such as the F-Trefftz method [Golberg and Chen (1997)], charge simulation method

[Golberg and Chen (1998)] or singularity method [Chen, Karageorghis and Smyrlis (2008)]. The main idea of MFS consists of approximating the solution of the partial differential equation by a linear combination of fundamental solutions, defined in source points. The expansion coefficients of the solution in MFS are determined so that the solution satisfies the boundary condition with the help of direct collocation [Fairweather and Karageorghis (1998); Balakrishnan and Ramachandran (2001)], least squares approximation [Chen (1995)], or by an integral fit of the boundary data [Balakrishnan and Ramachandran (2001); Karageorghis (1987)]. The fundamental solution is for certain PDE's singular in the source points and this is the reason why the source points have to be located outside the domain in the classical MFS for such situations. Then, the original problem is reduced to determining the unknown coefficients of the fundamental solutions and the coordinates of the source points by requiring the approximation to satisfy the boundary conditions and hence solving a non-linear problem. If the source points are a priori fixed (on a fictitious boundary) then the coefficients of the approximation are determined by solving a linear problem. In contrast to the BEM, the MFS avoids numerical integration of singular fundamental solution and is an inherent meshless method.

In the traditional MFS, the fictitious boundary, positioned outside the problem domain, is required to place the source points. This avoids the singularity of the solution at the boundary which would prevent the proper compliance with the boundary conditions. The determination of the distance between the real boundary and the fictitious boundary is based on experience and therefore troublesome. In recent years, various efforts have been made, aiming to remove this drawback of the MFS, so that the source points can be placed on the real boundary directly. The present dissertation essentially develops such a method for solution of a class of micromechanics problems.

1.2 The Meshless Methods

In the field of numerical simulation methods, meshless methods, sometimes named also meshfree or mesh reduction methods**,** are those that do not require that a mesh connects the data points of the simulation domain. Meshless methods enable the simulation of some otherwise difficult types of problems, at the cost of extra computing time and programming effort. There exist several meshless methods such as Element-free Galerkin Methods (EFGM) [Belytschko, Lu and Gu (1994)], the Meshless Local Petrov-Galerkin (MLPG) method [Atluri and Shen (2002)], Finite Mass Method (FMM) [Gauger, Leinen and Yserentant (2000)], Smoothed Point Interpolation Method (S-PIM) [Liu (2009)], Meshfree local Radial Point Interpolation Method (RPIM) [Liu (2009)], Local Radial Basis Function Collocation Method (LRBFCM) [Šarler and Vertnik (2006)], Repeated Replacement Method (RRM) [Walker (2012)], Radial Basis Integral Equation Method [Ooi and Popov (2012)]. A practical overview of meshless methods (for solid mechanics) based on global weak forms is given by [Nguyen, Rabczuk, Bordas and Duflot (2008)] and in the book [Chen, Lee and Eskandarian (2006)]. This dissertation is focused on development of modified Method of Fundamental Solutions, based on the classical MFS.

1.2.1 Method of Fundamental Solutions

The ideas behind the MFS have been around for a few decades and were developed primarily by [Kupradze and Alexidze (1964)] in the late 1950s and early 1960s. However, the method was proposed as a computational technique much later by [Mathon and Johnston (1977)] in the late 1970s, followed by a number of papers by Mathon, Johnston and Fairweather with applications. Slowly, but surely, the MFS become a useful tool for solution of a large variety of physical and engineering problems see [Fu, Chen and Yang (2009); Chen, Lin and Wang (2011); Chen and Wang (2010); Jiang and Chen (2011)].

A major obstacle was overcome when, in the 1990s, [Golberg and Chen (1994); Golberg, Chen, Bowman and Power (1998)] extended the MFS to deal with inhomogeneous equations and time-dependent problems. Recent developments indicate that the MFS can be used to solve partial differential equations with variable coefficients [Fan, Chen and Monroe (2009)]. For instance, Laplace equation [Bogomolny (1985); Katsurada and Okamoto (1996); Mathon and Johnston (1977)], biharmonic [Karageorghis and Fairweather (1987)], elastostatic problems [Poullikkas, Karageorghis and Georgiou (2002)], wave scattering problems [Kondapalli, Shippy and Fairweather (1992a); Kondapalli, Shippy and Fairweather (1992b)], inverse obstacle scattering problems [Karageorghis and Lesnic (2011)]，inverse problems of Laplace equation [Young, Tsai, Chen, Fan (2008)], multidimensional inverse heat conduction problems [Hon and Wei (2005)]. More recently, the MFS has successfully been applied to approximate the solutions of non-homogeneous linear and nonlinear Poisson equations [Balakrishnan and Ramachandran (2001); Golberg (1995)]. Details can be found in the review papers of [Fairweather and Karageorghis (1998); Golberg and Chen (1998); Kołodziej (1987; 2001)], and also in the excellent book written by [Golberg and Chen (1997)]. The expansion coefficients in the solution are determined so that the solution satisfies the boundary condition with the help of direct collocation [Chen (1995); Balakrishnan and Ramachandran (2001)], least squares fit [Karageorghis and Fairweather (1987)] or by an integral fit of the boundary data [Herrera (1984); Zielinski and Herrera (1987)].
The method has been widely used for the solution of problems in linear elasticity. The first application of the MFS for elasticity problems can be found in the paper [Kupradze and Aleksidze (1964)], whereas a theoretical analysis and density results for problems of linear elasticity may be found in the papers [Kupradze (1964); Smyrlis (2009)]. The solution of anisotropic elasticity problems was considered in [Berger and Karageorghis (2001); Maharejin (1985)]. In the paper of [Marin and Lesnic (2004)], inverse problems in planar elasticity were considered, whereas axisymmetric elastic problems were studied in [Redekop and Thompson (1983); Karageorghis and Fairweather (2000)]. The MFS has been applied to the computation of stress intensity factors in linear elastic fracture mechanics [Berger, Karageorghis and Martin (2005); Karageorghis, Poullikkas and Berger (2006)] as well. The MFS was applied to thermo-elasticity problems in [Aleksidze (1991); Kupradze, Gegelia, Basheleshvili and Burchuladze (1976)]. Further applications of the MFS to elasticity problems can be found in [Patterson and Sheikh (1982); Redekop (1982); Burgess and Maharejin (1984); Redekop and Cheung (1987); Raamachandran and Rajamohan (1996); Fenner (2001); Poullikkas, Karageorghis

and Georgiou (2002); Tsai (2007); Marin (2011)]. Multi-domain (multi-zone) formulations play an important part in numerical analysis when dealing with problems involving interfaces or dissimilar materials, such as composite materials, etc. [Berger and Karageorghis (2001)] present a MFS solution of a multi-domain anisotropic elasticity problem.

1.2.2 Modified Method of Mundamental Solutions

In recent years, various efforts have been made, aiming to remove the fictitious boundary of the MFS, so that the source points can be placed on the real boundary directly. [Young, Chen and Lee (2005); Young, Chen, Chen and Kao (2007); Chen, Kao, Chen, Young and Lu (2006)] proposed to place the source points on the boundary in the MFS. They introduce novel ways to determine the diagonal collocation matrix coefficients. The diagonal coefficients were determined directly for simple geometries or by using the results from the BEM, based on the fact that the MFS and the indirect boundary integral formulation are similar in nature. In their approach, information of the neighbouring points before and after each source point is needed, in order to form line segments for integrating the kernels to obtain the diagonal coefficients. This is essentially the same information of the element connectivity as in a BEM mesh. [Šarler (2009)] proposed a similar modified MFS, where the diagonal terms are determined by the integration of the fundamental solution on the line segments formed by using neighbouring points, and the use of a constant solution to determine the diagonal coefficients of the derivatives of the fundamental solution in different coordinate directions. This approach is very stable, but it amounts to solve the problem twice. [Chen and Wang (2010)] proposed a similar method for determining the diagonal coefficients in the modified MFS by applying a known solution inside the domain, so that the diagonal coefficients from both the fundamental solution and its derivatives can be determined indirectly, without using any element or integration concept. Again, this approach is appealing, stable and accurate, but it is costly for solving large-scale problems due to the need to solve the problem twice. The solution also depends on the choice of the reference points. [Gu, Chen and Zhang (2011)] applied the singular boundary method to two-dimensional (2D) elasticity problems, in which they use an inverse interpolation technique to regularize the singularity of the fundamental solution of the equation governing the problem of interest. [Chen, Lin and Wang (2011)] developed the regularized meshless method also for the nonhomogeneous problems in conjunction with the dual reciprocity technique in the evaluation of the particular solution. [Liu (2010)] recently presented a new boundary meshless approach based on the modified MFS that has no fictitious boundaries and singularities. In the new approach, the concentrated point sources are replaced with area-distributed sources covering the source points for 2D problems. These area-distributed sources represent analytical integration of the original singular fundamental solution, so that they preserve the advantage of diagonal dominance for the system of equations, while they have no troublesome singularity issues. [Liu (2010)] called the method boundary distributed source (BDS) method. [Liu (2010)] used the approach of [Šarler (2009)] to determine the diagonal coefficients of the derivatives of the fundamental solution. Liu's approach has been recently extended to solve porous media problems with moving boundaries [Perne, Šarler and Gabrovšek (2012)]. But the BDS can't at the present solve the void, elastic inclusions and rigid inclusion micromechanics problems

[Dong and Atluri (2011a); Dong and Atluri (2011b); Dong and Atluri (2012); Dong and Atluri (2013)]. [Kim (2013)] very recently improved the BDS for Laplace equation by using the fact that the boundary integration of the normal gradient of the potential should vanish to determine the diagonal element for the Neumann boundary conditions.

1.3 The Goals of the Dissertation

The dissertation deals with the improvements of the MFS for solid mechanics problems and its use in micromechanics. The main idea through all the work is to remove the fictitious boundary of the MFS. However, main aspects of the method development, which should be met to the largest possible extents, are the accuracy and the stability. In this work, two new method formulations, Non-Singular Method of Fundamental Solutions (NMFS) and Improved Non-Singular Method of Fundamental Solutions (INMFS) are originally developed and presented. In order to assess the proposed methods, a detailed analysis regarding to all newly introduced features is done. From the analysis of the results it is evident that not all method configurations are suitable for all problems and regimes and so the optimal ranges of all numerical free parameters are proposed based on the numerical experiments. Application of this novel method to industrial micromechanics problems is very important and promising, since the method reduces the amount of discretisation, needed in classical mesh based methods. It will most probably evolve into a new powerful tool for engineering design, fabrication, and analysis of a wide range of materials including polycrystalline, composite, geotechnical, biological, and electronic materials. Optimum microstructures can be, by use of modelling, forecasted rather than found by trial and error. Fracture and fatigue of solids and structures, martensitic transformations, interphases in composites, and dispersion hardening of alloys are examples of the phenomena that might be tackled by the developed method in the future.

Chapter 2, that follows the present introduction, describes the physical background of the dissertation with basic definitions of stress, strain, traction, displacement, and the relationship of these elements in the linear elasticity theory in Cartesian coordinate system. The equations of equilibrium are derived from the balance of the stresses. The Hooke's law in an elastic material is elaborated through stiffness and compliance matrices. Different material behaviour reflects in the number of independent elastic constants. Anisotropic triclinic materials have 21 independent coefficients; monoclinic materials have 13 independent coefficients; orthotropic materials have 9 independent coefficients; hexagonal materials have 7 independent coefficients; cubic materials have only 3 independent coefficients. For isotropic materials, the coefficients only depend on the Young's modulus and the Poisson's ratio. When a two-dimensional anisotropic deformation is considered in plane stress and plane strain cases, the number of elastic constants is reduced to a maximum of 9.

Chapter 3 introduces the classical MFS for isotropic and anisotropic elastic problems. Each of the fundamental solutions contains two points, the field point and the source point. In order to avoid the singularity, the source point should be put outside of the

physical domain to avoid the coincidence with the collocation points. Fundamental tractions are calculated from the relationships involving displacement, strain and stress. An approximate solution of the governing equation is obtained by a linear combination of fundamental solutions. At the same time, the corresponding approximating traction was obtained from a linear combination of fundamental tractions. The coefficients in the linear combination of fundamental solutions and fundamental tractions are obtained from the systems of algebraic equations based on satisfaction of the the known Dirichlet, Neumann or mixed boundary conditions at the boundary. The fundamental solution for isotropic elastic problems is given in an exact expression with Young's modulus and Poisson's ratio. The fundamental solution of anisotropic elastic problems is given as a real part of a first order complex polynomial. The coefficients of polynomial are determined by solving a six-order equation, originating from a zero determinant of a six-order matrix. The elements of the matrix stem from the elements of the stiffness metrix. There are three pairs of complex roots for the six-order equation. The three roots with positive imaginary parts are the coefficients of the complex polynomial. Two of the three roots are used for analysis of the plain strain deformation.

Chapters 4 and 5 represent the formulation of NMFS for isotropic and anisotropic elastic problems, respectively. It is based on the classical MFS with regularization of the singularities. This is achieved by replacement of the concentrated point sources by distributed sources over circular discs around the singularity, as originally suggested by [Liu (2010)] for potential problems. The desingularisation for isotropic problems can be calculated analytically. But the disingularisation for anisotropic problems can't be obtained in a closed form. The numerical evaluation is performed respectively. In case of the displacement boundary conditions, the values of distributed sources are calculated directly and analytically. In case of traction boundary conditions, the respective desingularized values of the derivatives of the fundamental solution in the coordinate directions, as required in the calculations, are calculated indirectly from the considerations of two reference solutions of a linearly varying simple displacement fields. Respectively, the system of algebraic equations has to be solved three times. This novel method modifies MFS in such a way that the fictitious boundary is not needed any more. Two examples for isotropic problems are divided into four cases and presented in Chapter 4. Two examples for anisotropic problems are divided into five cases and presented in Chapter 5.

Chapter 6 is focused on the Improved Method of Fundamental Solutions (INMFS) for isotropic and anisotropic elastic problems. Because of the limitations of NMFS, that does not perform well for inclusions and voids problems and because of the computational effort needed for solving the three systems of algebraic equations, the INMFS is developed. This method is based on the idea of [Kim (2013)] for potential problems. In steady state potential problems, the balance of the derivatives of the potential field values at the boundary should be zero. However, in the present solid mechanics problems, the balance of the tractions on the boundary should be zero. This idea, together with the assumption of the constant value of the traction near the boundary node allowed for a simple calculation of the diagonal elements of the matrix of fundamental tractions for the Neumann boundary conditions. From this consideration, the values of the fundamental tractions in singular points are obtained.

This novel INMFS represents an effective upgrade of NMFS for problems with inclusions and voids. INMFS method reduces the computation time of NMFS method since the system of equations has to be solved only once instead of three times. Five examples for isotropic and anisotropic problems are divided into fourteen cases and represented in Chapter 6.

Chapter 7 demonstrates the use of the NMFS and the INMFS in multi-body problems in contact. Both methods turn out to give similar results than the MFS in all spectra of performed tests except in the void/inclusion problem for NMFS. The lack of the artificial boundary is particularly advantageous when using both novel methods in multi-body problems. A micromechanics simulation of a deformation of a peace of a realistic microstructure is shown in this chapter. Five examples for isotropic and anisotropic problems are divided into twelve cases and represented in Chapter 7.

In the final chapter with the conclusions, an overview of the performed work is given, together with: (I) advantages of research given in the dissertation, of which the most important is the lack of artificial boundary, (II) originality of the dissertation, of which the most important scientific aspect is the development and the application of NMFS and INMFS for isotropic and anisotropic elastic problems, (III) engineering impact of dissertation, of which the most important aspect is the application to micromechanics, and (III) plans for future work of which the most important is the upgrade of the method to plasticity.

2. Elements of Elasticity Theory

2.1 Introduction

This chapter introduces the physical background of the dissertation with basic definitions of stress, strain, traction, displacement, and the relationship of these elements in the linear elasticity theory in Cartesian coordinate system. The equations of equilibrium are derived from the balance of the stresses. The Hooke's law in an elastic material is elaborated through stiffness and compliance matrices. Different material behaviour reflects in the number of independent elastic constants. Anisotropic triclinic materials have 21 independent coefficients; monoclinic materials have 13 independent coefficients; orthotropic materials have 9 independent coefficients; hexagonal materials have 7 independent coefficients; cubic materials have only 3 independent coefficients. For isotropic materials, the coefficients only depend on the Young's modulus and the Poisson's ratio. When a two-dimensional anisotropic deformation is considered in plane stress and plane strain cases, the number of elastic constants is reduced to a maximum of 9. At last, anti-plan deformation is described and compared with in-plane situations.

2.2 Basic Definitions and Comments

In this section, stress, displacement and strain are introduced. The equations of equilibrium for stress are presented in Cartesian coordinate system.

2.2.1 Cartesian Coordinate System

In this dissertation, we will exclusively use Cartesian coordinate system x, y, z with orthonormal base vectors $\mathbf{i}_x$, $\mathbf{i}_y$ and $\mathbf{i}_z$ and coordinates p_x, p_y and p_z of point P with position vector $\mathbf{p}$. We consider a solid in domain Ω with boundary Γ. See Figure 2.1.

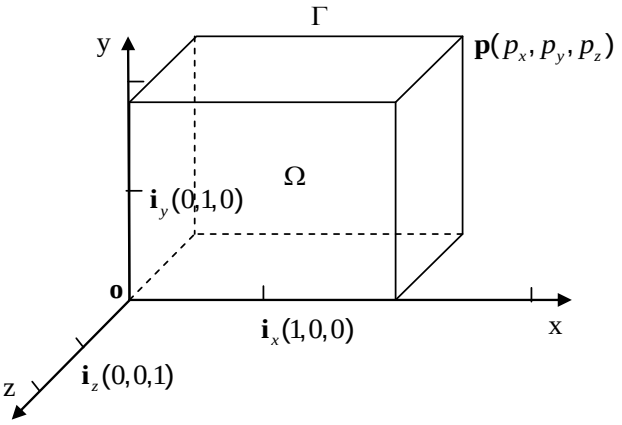

Figure 2.1: Cartesian coordinate system.

2.2.2 Stress

Consider an arbitrary shaped body, as illustrated in Figure 2.2. The body is in equilibrium under the action of externally applied forces $F_1, F_2, \cdots$. It is assumed that the body is continuously deformable so that the forces are transmitted throughout its volume. At an internal point with position vector $\mathbf{o}$, there is a resultant force δF, which may be considered as being uniformly distributed over a small area δA. The internal force per unit area is called stress σ, and is given by

$$\sigma = \frac{\delta F}{\delta A}. \tag{2.1}$$

In the limit,

$$\sigma = \lim_{\delta A \to 0}\left(\frac{\delta F}{\delta A}\right) = \frac{dF}{dA}. \tag{2.2}$$

Generally, the force can be resolved into normal δF_n and tangential δF_t components as shown in Figure 2.3. The normal of direct stress associated with these components is defined as

$$\sigma_n = \lim_{\delta A \to 0}\left(\frac{\delta F_n}{\delta A}\right) = \frac{dF_n}{dA}, \tag{2.3}$$

and a shear stress is defined by

$$\sigma_t = \lim_{\delta A \to 0}\left(\frac{\delta F_t}{\delta A}\right) = \frac{dF_t}{dA}. \tag{2.4}$$

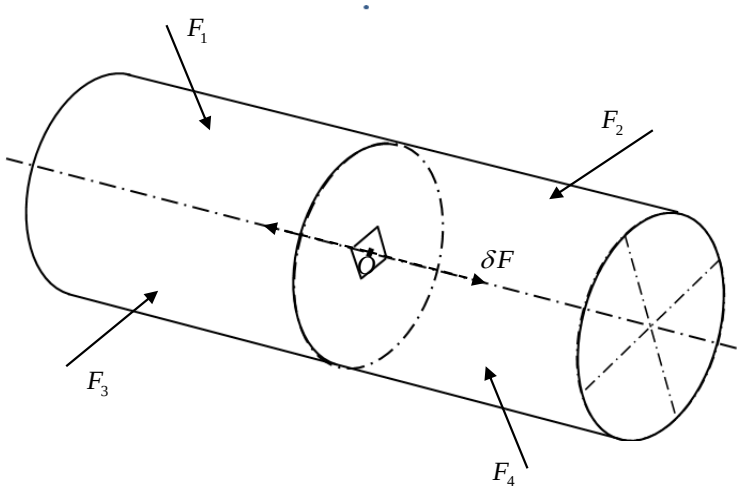

Figure 2.2: Internal force δF at a point in a body.

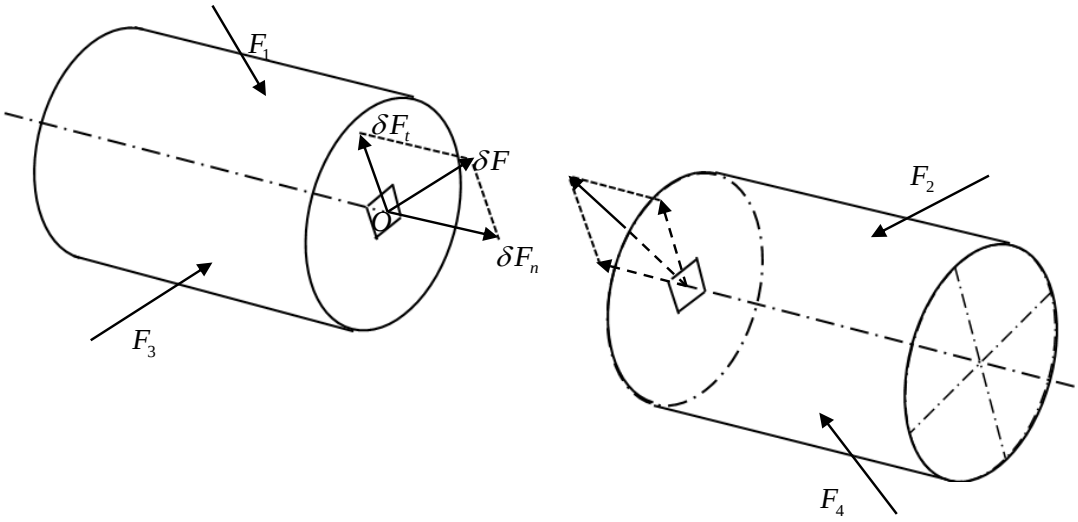

Figure 2.3: Internal force components at a point.

2.2.3 Tractions

Equilibrium must be satisfied at all locations on the boundary of the body where the components of tractions (surface forces per unit area) are t_x and t_y. For the triangular element of Figure 2.4 at the boundary of a two-dimensional body of unit thickness, the tractions on element AB of the boundary must be in equilibrium with internal forces on internal faces AC and CB.

Summing up the forces in the $x-$ direction, we have

$$t_x \delta s - \sigma_{xx} \delta y - \sigma_{yx} \delta x = 0. \qquad (2.5)$$

Taking the limit as δx approaches zero gives

$$t_x = \sigma_{xx}\frac{dy}{ds} + \sigma_{yx}\frac{dx}{ds}. \tag{2.6}$$

The derivatives $\frac{dy}{ds}$ and $\frac{dx}{ds}$ are the directional cosines m_x and m_y of the angles which a normal to AB makes with x and y axes, respectively. Hence

$$t_x = \sigma_{xx}m_x + \sigma_{yx}m_y, \tag{2.7}$$

and by similarly considering the summation of forces in the $y-$ direction it can be shown that

$$t_y = \sigma_{xy}m_x + \sigma_{yy}m_y. \tag{2.8}$$

The extension to three-dimensional bodies is relatively simple and can be shown to give

$$t_x = \sigma_{xx}m_x + \sigma_{yx}m_y + \sigma_{zx}m_z, \tag{2.9}$$

$$t_y = \sigma_{xy}m_x + \sigma_{yy}m_y + \sigma_{zy}m_z, \tag{2.10}$$

$$t_z = \sigma_{xz}m_x + \sigma_{yz}m_y + \sigma_{zz}m_z, \tag{2.11}$$

where m_x, m_y and m_z are the directional cosines of the angles (m_x, m_y, m_z are components of the outward unit normal) that a normal to the surface makes with the x, y and z axes, respectively. The expression for stresses on inclined planes can be derived by considering a corner cut off element by the plane AB inclined at angle θ to the $y-$ axes (see Figure 2.5).

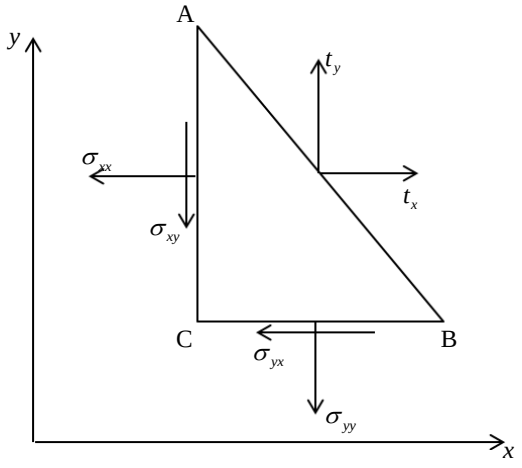

Figure 2.4: Stresses on the faces of a triangular element.

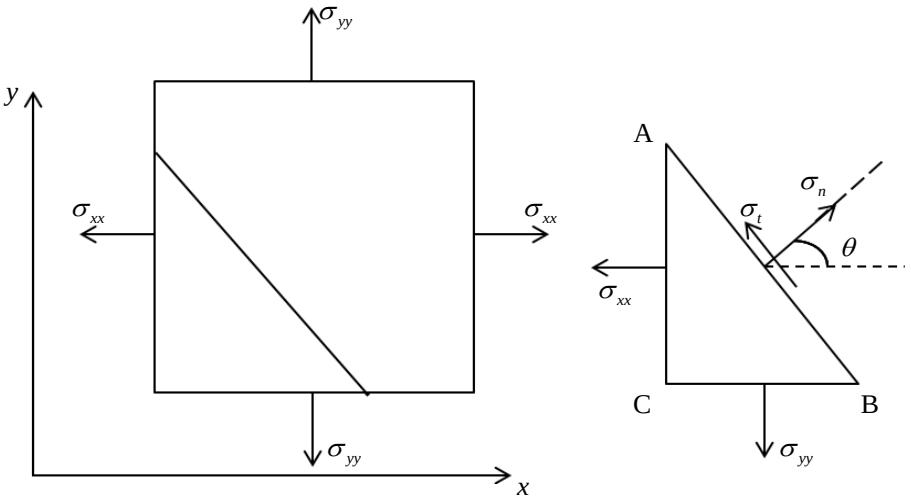

Figure 2.5: Stresses on an inclined plane at a point.

2.2.4 Equilibrium

The state of stress at a point can be described by stress components formed on an element with sides $\delta x, \delta y, \delta z$ formed at point with position vector $\mathbf{o}$ by cutting planes, shown in Figure 2.6.

The state of stress in an elemental volume of a loaded three-dimensional body, shown in Figure 2.6, can be defined in terms of six components of stress ($\sigma_{xx}, \sigma_{yy}, \sigma_{zz}, \sigma_{xy}, \sigma_{xz}, \sigma_{yz}$); because of the equilibrium of an infinitesimal element of the body, they have a symmetry such that $\sigma_{xy} = \sigma_{yx}, \sigma_{xz} = \sigma_{zx}$ and $\sigma_{yz} = \sigma_{zy}$. The first suffix indicates the direction of normal to the plane on which the stress acts, and the second suffix indicates the direction in which it acts.

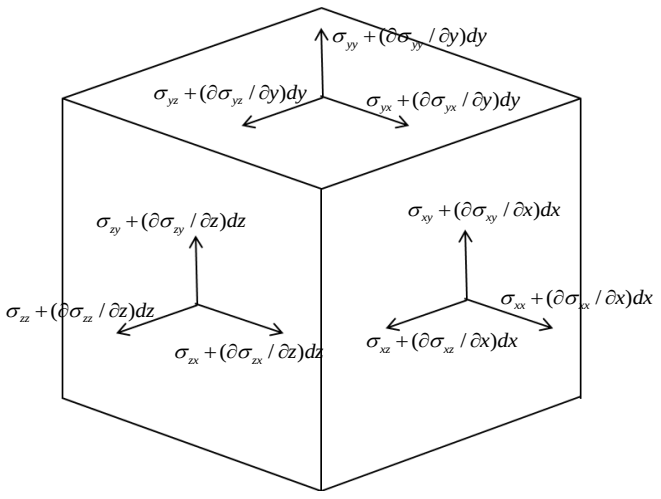

Figure 2.6: Stresses on the faces of an infinitesimal element of Ω.

The equations of equilibrium for a three-dimensional system subjected to external forces acting on the surface of the body and body forces b_x, b_y and b_z, acting on the domain of the body, are given by

$$\frac{\partial \sigma_{xx}}{\partial x} + \frac{\partial \sigma_{xy}}{\partial y} + \frac{\partial \sigma_{xz}}{\partial z} + b_x = 0, \tag{2.12}$$

$$\frac{\partial \sigma_{yx}}{\partial x} + \frac{\partial \sigma_{yy}}{\partial y} + \frac{\partial \sigma_{yz}}{\partial z} + b_y = 0, \tag{2.13}$$

$$\frac{\partial \sigma_{zx}}{\partial x} + \frac{\partial \sigma_{zy}}{\partial y} + \frac{\partial \sigma_{zz}}{\partial z} + b_z = 0. \tag{2.14}$$

2.2.5 Displacement

Displacement $\mathbf{u}$ is the difference between the final position $\mathbf{p}_{fin}$ and initial position $\mathbf{p}_{ini}$ of a point. The actual path covered to reach the final position is irrelevant. It can simply be defined as the shortest path between the final point and the initial point of a body.

$$\mathbf{u} = \mathbf{p}_{fin} - \mathbf{p}_{ini}. \tag{2.15}$$

2.2.6 Strain

The external and internal forces described earlier result in linear and angular displacements in a deformable body. These displacements are generally defined in terms of strain. Direct longitudinal strains are associated with direct stresses and related to changes in length. If a line element of length L at a point in the body undergoes an extension in length $\triangle L$, then the longitudinal strains at that point are defined as

$$\varepsilon = \lim_{L \to 0} \frac{\triangle L}{L}. \tag{2.16}$$

The six strain components corresponding to the components of the stress can be written in Cartesian directions as $\varepsilon_{\varsigma\xi} = \varepsilon_{\xi\varsigma}, \xi, \varsigma = x, y, z$. $\varepsilon_{xx}, \varepsilon_{yy}$ and ε_{zz} are direct strains and $\varepsilon_{xy}, \varepsilon_{yz}$ and ε_{xz} are shear strains, respectively. Denoting the displacements u_x, u_y and u_z, the strains are related to the displacements via

$$\varepsilon_{xx} = \frac{\partial u_x}{\partial x}, \tag{2.17}$$

$$\varepsilon_{yy} = \frac{\partial u_y}{\partial y}, \tag{2.18}$$

$$\varepsilon_{zz} = \frac{\partial u_z}{\partial z}, \tag{2.19}$$

for direct strains, and

$$\varepsilon_{xy} = \frac{1}{2}\left(\frac{\partial u_y}{\partial x} + \frac{\partial u_x}{\partial y} \right), \tag{2.20}$$

$$\varepsilon_{xz} = \frac{1}{2}\left(\frac{\partial u_z}{\partial x} + \frac{\partial u_x}{\partial z} \right), \tag{2.21}$$

$$\varepsilon_{yz} = \frac{1}{2}\left(\frac{\partial u_z}{\partial y} + \frac{\partial u_y}{\partial z} \right), \tag{2.22}$$

for shear strains.

2.3 Boundary Conditions

There are two principal kinds of boundary conditions, Dirichlet (displacement) boundary condition and Neumann (traction) boundary condition. The Dirichlet boundary condition specifies the values of displacement that a solution needs to take on along a part of the boundary of the domain

$$u_\varsigma = \bar{u}_\varsigma, \quad \varsigma = x, y. \tag{2.23}$$

The Neumann boundary condition specifies the values of traction that the derivative of a solution is to take on the boundary of the domain

$$t_\varsigma = \bar{t}_\varsigma, \quad \varsigma = x, y. \tag{2.24}$$

When an elastic inclusion is to be considered, the boundary conditions at the interface between two materials $\Gamma^{\mathrm{I}\cap\mathrm{II}}$ are given in the form that represents the continuity of displacements and equilibrium of forces [Braccini and Dupeux (2012)]

$$u_\varsigma^{\mathrm{I}} - u_\varsigma^{\mathrm{II}} = 0, \quad \varsigma = x, y, \tag{2.25}$$

$$t_\varsigma^{\mathrm{I}} + t_\varsigma^{\mathrm{II}} = 0, \quad \varsigma = x, y. \tag{2.26}$$

When the inclusion is rigid, the boundary conditions at the interface between two materials $\Gamma^{\mathrm{I}\cap\mathrm{II}}$ are given in the form

$$u_\varsigma^{\mathrm{I}} = u_\varsigma^{\mathrm{II}} = 0, \quad \varsigma = x, y. \tag{2.27}$$

Neumann boundary conditions are not needed in this case.
When the inclusion is in the type of a void instead of an elastic/rigid inclusion, the boundary conditions for the boundary of the inclusion are given in the form

$$t_\varsigma = 0, \quad \varsigma = x, y, \tag{2.28}$$

and the Dirichlet boundary conditions are not needed.

2.4 Hooke's Law

The relations between stresses and strain are presented in this section. Referring to a fixed Cartesian coordinate system x, y, z. The Hooke's law can be written as

$$\boldsymbol{\sigma} = \mathbf{C}\boldsymbol{\varepsilon}, \tag{2.29}$$

in which

$$\sigma_{\varsigma\xi} = C_{\varsigma\xi\upsilon\tau}\varepsilon_{\upsilon\tau}, \quad \varsigma, \xi, \upsilon, \tau = x, y, z, \tag{2.30}$$

where $C_{\varsigma\xi\upsilon\tau}$ are the elastic stiffnesses which are the components of a fourth rank tensor. They satisfy the symmetry conditions

$$C_{\varsigma\xi\upsilon\tau} = C_{\xi\varsigma\upsilon\tau}, \quad C_{\varsigma\xi\upsilon\tau} = C_{\xi\varsigma\tau\upsilon}, \quad C_{\varsigma\xi\upsilon\tau} = C_{\upsilon\tau\xi\varsigma}. \tag{2.31}$$

The inverse of Eq. (2.29) is written as

$$\boldsymbol{\varepsilon} = \mathbf{S}\boldsymbol{\sigma}, \tag{2.32}$$

in which

$$\varepsilon_{\varsigma\xi} = S_{\varsigma\xi\upsilon\tau}\sigma_{\upsilon\tau}, \quad \varsigma, \xi, \upsilon, \tau = x, y, z, \tag{2.33}$$

where $S_{\varsigma\xi\upsilon\tau}$ are the elastic compliances which are the components of a fourth rank tensor too. They also possess the symmetry

$$S_{\varsigma\xi\upsilon\tau} = S_{\xi\varsigma\upsilon\tau}, \quad S_{\varsigma\xi\upsilon\tau} = S_{\xi\varsigma\tau\upsilon}, \quad S_{\varsigma\xi\upsilon\tau} = S_{\upsilon\tau\xi\varsigma}. \tag{2.34}$$

2.4.1 Hooke's Law for Isotropic Materials

Isotropic materials have identical values of a property in all directions. In a matrix form, the Hooke's law for isotropic material can be written as

$$\begin{bmatrix} \varepsilon_{xx} \\ \varepsilon_{yy} \\ \varepsilon_{zz} \\ 2\varepsilon_{yz} \\ 2\varepsilon_{xz} \\ 2\varepsilon_{xy} \end{bmatrix} = \frac{1}{E}\begin{bmatrix} 1 & -\nu & -\nu & 0 & 0 & 0 \\ -\nu & 1 & -\nu & 0 & 0 & 0 \\ -\nu & -\nu & 1 & 0 & 0 & 0 \\ 0 & 0 & 0 & 2(1+\nu) & 0 & 0 \\ 0 & 0 & 0 & 0 & 2(1+\nu) & 0 \\ 0 & 0 & 0 & 0 & 0 & 2(1+\nu) \end{bmatrix}\begin{bmatrix} \sigma_{xx} \\ \sigma_{yy} \\ \sigma_{zz} \\ \sigma_{yz} \\ \sigma_{xz} \\ \sigma_{xy} \end{bmatrix}, \tag{2.35}$$

where E stands for Young's modulus and ν for Poisson's ratio. In the matrix form, the inverse relation may be written as

$$\begin{bmatrix}\sigma_{xx}\\ \sigma_{yy}\\ \sigma_{zz}\\ \sigma_{yz}\\ \sigma_{xz}\\ \sigma_{xy}\end{bmatrix}=\frac{E}{(1+\nu)(1-2\nu)}\begin{bmatrix}1-\nu & \nu & \nu & 0 & 0 & 0\\ \nu & 1-\nu & \nu & 0 & 0 & 0\\ \nu & \nu & 1-\nu & 0 & 0 & 0\\ 0 & 0 & 0 & \frac{(1-2\nu)}{2} & 0 & 0\\ 0 & 0 & 0 & 0 & \frac{(1-2\nu)}{2} & 0\\ 0 & 0 & 0 & 0 & 0 & \frac{(1-2\nu)}{2}\end{bmatrix}\begin{bmatrix}\varepsilon_{xx}\\ \varepsilon_{yy}\\ \varepsilon_{zz}\\ 2\varepsilon_{yz}\\ 2\varepsilon_{xz}\\ 2\varepsilon_{xy}\end{bmatrix}. \quad (2.36)$$

Many problems in elasticity may be treated satisfactorily by a two-dimensional, or plane theory of elasticity. There are two general types of problems involved in this plane analysis, the plane stress and the plane strain problems. These two types are defined by setting certain restrictions and assumptions on the stress and displacement fields. They are introduced descriptively in terms of their physical prototypes.

2.4.1.1 Plane Stress

The plane stress problem is defined to be a state of stress in which the normal stresses σ_{zz} and the shear stresses σ_{xz} and σ_{yz}, directed perpendicular to the $x-y$ plane are assumed to be zero.
The geometry of the body is essentially that of a plate with one dimension (thickness) much smaller than the other two, see Figur 2.7. The loads are applied uniformly over the thickness of the plate and act in the plane of the plate. The plane stress condition is the simplest form of behaviour for continuum structures and represents situations frequently encountered in practice.

Typical loading and boundary conditions for plane stress problems in two-dimensional elasticity

a. Loadings may be point forces or distributed forces applied over the thickness of the plate.
b. Supports may be fixed points or fixed edges or roller supports.

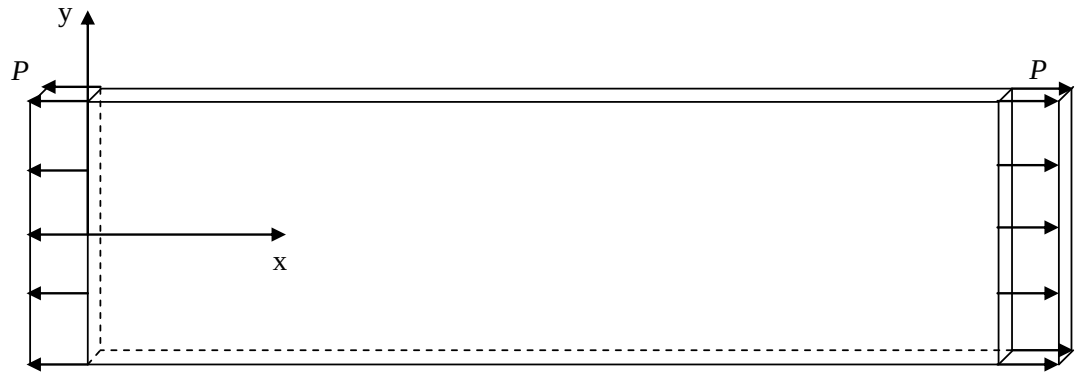

Figure 2.7: Scheme of a plane stress problem.

Plane stress situation implies

$$\sigma_{zz} = \sigma_{xz} = \sigma_{yz} = 0, \tag{2.37}$$

and

$$\varepsilon_{xz} = \varepsilon_{yz} = 0, \tag{2.38}$$

which yields

$$\begin{bmatrix} \sigma_{xx} \\ \sigma_{yy} \\ \sigma_{xy} \end{bmatrix} = \frac{E}{1-\nu^2} \begin{bmatrix} 1 & \nu & 0 \\ \nu & 1 & 0 \\ 0 & 0 & \dfrac{1-\nu}{2} \end{bmatrix} \begin{bmatrix} \varepsilon_{xx} \\ \varepsilon_{yy} \\ 2\varepsilon_{xy} \end{bmatrix}. \tag{2.39}$$

The strains in plane stress situation are

$$\begin{bmatrix} \varepsilon_{xx} \\ \varepsilon_{yy} \\ 2\varepsilon_{xy} \end{bmatrix} = \frac{1}{E} \begin{bmatrix} 1 & -\nu & 0 \\ -\nu & 1 & 0 \\ 0 & 0 & 2(1+\nu) \end{bmatrix} \begin{bmatrix} \sigma_{xx} \\ \sigma_{yy} \\ \sigma_{xy} \end{bmatrix}. \tag{2.40}$$

The following relation is valid as well

$$\varepsilon_{zz} = \frac{1}{E}(-\nu)(\sigma_{xx} + \sigma_{yy}). \tag{2.41}$$

2.4.1.2 Plane Strain

The plane strain problem is defined to be a state of strain in which the strain normal to the $x-y$ plane ε_{zz} and the shear strains ε_{xz} and ε_{yz} are assumed to be zero.

In plane strain problem, one deals with a situation in which the dimension of the structure in one direction, say the $z-$ coordinate direction, is very large in comparison with the dimensions of the structure in the other two directions ($x-$ and $y-$ coordinate axes). The geometry of the body is essentially that of a prismatic cylinder with one dimension much larger than the others, see Figure 2.8. The applied forces act in $x-y$ plane and do not vary in the $z-$ direction, i. e. the loads are uniformly distributed with respect to the large dimension and act perpendicular to it. Some important practical applications of this representation occur in the analysis of dams, tunnels, and other geotechnical works. Also such small scale problems as bars and rollers compressed by forces normal to their cross section are amenable to analysis in this way.

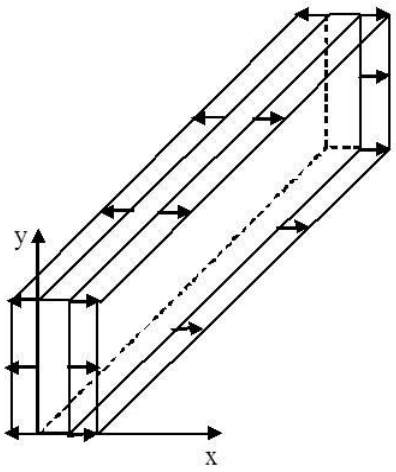

Figure 2.8: Scheme of a plane strain problem.

The plane strain relation for isotropic materials are

$$\varepsilon_{zz} = \varepsilon_{xz} = \varepsilon_{yz} = 0, \tag{2.42}$$

and

$$\sigma_{xz} = \sigma_{yz} = 0. \tag{2.43}$$

This yields

$$\begin{bmatrix} \sigma_{xx} \\ \sigma_{yy} \\ \sigma_{xy} \end{bmatrix} = \frac{E}{(1+\nu)(1-2\nu)} \begin{bmatrix} 1-\nu & \nu & 0 \\ \nu & 1-\nu & 0 \\ 0 & 0 & \dfrac{1-2\nu}{2} \end{bmatrix} \begin{bmatrix} \varepsilon_{xx} \\ \varepsilon_{yy} \\ 2\varepsilon_{xy} \end{bmatrix}, \tag{2.44}$$

with

$$\sigma_{zz} = \frac{E}{1+\nu}\left[\frac{\nu}{1-2\nu}(\varepsilon_{xx} + \varepsilon_{yy})\right]. \tag{2.45}$$

2.4.2 Hooke's Law for Anisotropic Materials

An anisotropic material is a material which does not behave in the same way in all directions. The compliance matrix for a completely anisotropic material subjected to a traixial stress system can be written as

$$\begin{bmatrix} \varepsilon_{xx} \\ \varepsilon_{yy} \\ \varepsilon_{zz} \\ 2\varepsilon_{yz} \\ 2\varepsilon_{xz} \\ 2\varepsilon_{xy} \end{bmatrix} = \begin{bmatrix} s_{11} & s_{12} & s_{13} & s_{14} & s_{15} & s_{16} \\ s_{12} & s_{22} & s_{23} & s_{24} & s_{25} & s_{26} \\ s_{13} & s_{23} & s_{33} & s_{34} & s_{35} & s_{36} \\ s_{14} & s_{24} & s_{34} & s_{44} & s_{45} & s_{46} \\ s_{15} & s_{25} & s_{35} & s_{45} & s_{55} & s_{56} \\ s_{16} & s_{26} & s_{36} & s_{46} & s_{56} & s_{66} \end{bmatrix} \begin{bmatrix} \sigma_{xx} \\ \sigma_{yy} \\ \sigma_{zz} \\ \sigma_{yz} \\ \sigma_{xz} \\ \sigma_{xy} \end{bmatrix}, \tag{2.46}$$

with the coefficients matrix defined as

$$\mathbf{S} \equiv S_{ijkl} = \begin{bmatrix} S_{xxxx} & S_{xxyy} & S_{xxzz} & S_{xxyz} & S_{xxxz} & S_{xxxy} \\ S_{xxyy} & S_{yyyy} & S_{yyzz} & S_{yyyz} & S_{xzyy} & S_{xyyy} \\ S_{xxzz} & S_{yyzz} & S_{zzzz} & S_{yzzz} & S_{xzzz} & S_{xyzz} \\ S_{xxyz} & S_{yyyz} & S_{yzzz} & S_{yzyz} & S_{xzyz} & S_{xyyz} \\ S_{xxxz} & S_{xzyy} & S_{xzzz} & S_{xzyz} & S_{xzxz} & S_{xyxz} \\ S_{xxxy} & S_{xyyy} & S_{xyzz} & S_{xyyz} & S_{xyxz} & S_{xyxy} \end{bmatrix} = \begin{bmatrix} s_{11} & s_{12} & s_{13} & s_{14} & s_{15} & s_{16} \\ s_{12} & s_{22} & s_{23} & s_{24} & s_{25} & s_{26} \\ s_{13} & s_{23} & s_{33} & s_{34} & s_{35} & s_{36} \\ s_{14} & s_{24} & s_{34} & s_{44} & s_{45} & s_{46} \\ s_{15} & s_{25} & s_{35} & s_{45} & s_{55} & s_{56} \\ s_{16} & s_{26} & s_{36} & s_{46} & s_{56} & s_{66} \end{bmatrix}, \tag{2.47}$$

and

$$\mathbf{S} = \begin{bmatrix} \frac{1}{E_{xx}} & \frac{-\nu_{yx}}{E_{yy}} & \frac{-\nu_{zx}}{E_{zz}} & \frac{\eta_{yz,x}}{G_{yz}} & \frac{\eta_{xz,x}}{G_{xz}} & \frac{\eta_{xy,x}}{G_{xy}} \\ \frac{-\nu_{xy}}{E_{xx}} & \frac{1}{E_{yy}} & \frac{-\nu_{zy}}{E_{zz}} & \frac{\eta_{yz,y}}{G_{yz}} & \frac{\eta_{xz,y}}{G_{xz}} & \frac{\eta_{xy,y}}{G_{xy}} \\ \frac{-\nu_{xz}}{E_{xx}} & \frac{-\nu_{yz}}{E_{yy}} & \frac{1}{E_{zz}} & \frac{\eta_{yz,z}}{G_{yz}} & \frac{\eta_{xz,z}}{G_{xz}} & \frac{\eta_{xy,z}}{G_{xy}} \\ \frac{\eta_{x,yz}}{E_{xx}} & \frac{\eta_{y,yz}}{E_{yy}} & \frac{\eta_{z,yz}}{E_{zz}} & \frac{1}{G_{yz}} & \frac{\mu_{xz,yz}}{G_{xz}} & \frac{\mu_{xy,yz}}{G_{xy}} \\ \frac{\eta_{x,xz}}{E_{xx}} & \frac{\eta_{y,xz}}{E_{yy}} & \frac{\eta_{z,xz}}{E_{zz}} & \frac{\mu_{yz,xz}}{G_{yz}} & \frac{1}{G_{xz}} & \frac{\mu_{xy,xz}}{G_{xy}} \\ \frac{\eta_{x,xy}}{E_{xx}} & \frac{\eta_{y,xy}}{E_{yy}} & \frac{\eta_{z,xy}}{E_{zz}} & \frac{\mu_{yz,xy}}{G_{yz}} & \frac{\mu_{xz,xy}}{G_{xz}} & \frac{1}{G_{xy}} \end{bmatrix}, \tag{2.48}$$

where

$$\frac{-\nu_{yx}}{E_{yy}}=\frac{-\nu_{xy}}{E_{xx}};\quad \frac{-\nu_{zx}}{E_{zz}}=\frac{-\nu_{xz}}{E_{xx}};\quad \frac{-\nu_{zy}}{E_{zz}}=\frac{-\nu_{yz}}{E_{yy}};\quad \frac{\eta_{yz,x}}{G_{yz}}=\frac{\eta_{x,yz}}{E_{xx}};\quad \frac{\eta_{yz,y}}{G_{yz}}=\frac{\eta_{y,yz}}{E_{yy}};$$
$$\frac{\eta_{yz,z}}{G_{yz}}=\frac{\eta_{z,yz}}{E_{zz}};\quad \frac{\eta_{xz,x}}{G_{xz}}=\frac{\eta_{x,xz}}{E_{xx}};\quad \frac{\eta_{xz,y}}{G_{xz}}=\frac{\eta_{y,xz}}{E_{yy}};\quad \frac{\eta_{xz,z}}{G_{xz}}=\frac{\eta_{z,xz}}{E_{zz}};\quad \frac{\mu_{xz,yz}}{G_{xz}}=\frac{\mu_{yz,xz}}{G_{yz}};\qquad (2.49)$$
$$\frac{\eta_{xy,x}}{G_{xy}}=\frac{\eta_{x,xy}}{E_{xx}};\quad \frac{\eta_{xy,y}}{G_{xy}}=\frac{\eta_{y,xy}}{E_{yy}};\quad \frac{\eta_{xy,z}}{G_{xy}}=\frac{\eta_{z,xy}}{E_{zz}};\quad \frac{\mu_{xy,yz}}{G_{xy}}=\frac{\mu_{yz,xy}}{G_{yz}};\quad \frac{\mu_{xy,xz}}{G_{xy}}=\frac{\mu_{xz,xy}}{G_{xz}},$$

E_{xx}, E_{yy}, E_{zz} are Young's moduli in tension-compression in the directions of the x, y, z axes, G_{yz}, G_{xz}, G_{xy} are the shear moduli for planes parallel to the coordinate plates, ν_{yx}, ν_{zx}, ν_{xy}, ν_{zy}, ν_{xz}, ν_{yz} are Poisson's ratios characterizing the contraction in the direction of one axis when tension is applied in the direction of another axis. The coefficients $\mu_{xz,yz}$, $\mu_{xy,yz}$, $\mu_{yz,xz}$, $\mu_{xy,xz}$, $\mu_{yz,xy}$, $\mu_{xz,xy}$ are termed Chentsov's coefficients; they characterize shears in planes parallel to the coordinate planes produced by shearing stresses acting in other planes parallel to the coordinate planes. The constants $\eta_{yz,x}$, $\eta_{xz,x}$, $\eta_{xy,x}$, $\eta_{yz,y}$, $\eta_{xz,y}$, $\eta_{xy,y}$, $\eta_{yz,z}$, $\eta_{xz,z}$, $\eta_{xy,z}$ are the mutual influence coefficients of the first kind; they characterize extensions in the directions of the coordinate axes produced by shearing stresses acting in the coordinate planes. $\eta_{x,yz}$, $\eta_{y,yz}$, $\eta_{z,yz}$, $\eta_{x,xz}$, $\eta_{y,xz}$, $\eta_{z,xz}$, $\eta_{x,xy}$, $\eta_{y,xy}$, $\eta_{z,xy}$ express shears in the coordinate planes due to the normal stresses acting in the directions of the coordinate axes; they are termed the mutual influence coefficients of the second kind. The inverse relation to Eq. (2.46) may be written as

$$\begin{bmatrix}\sigma_{xx}\\ \sigma_{yy}\\ \sigma_{zz}\\ \sigma_{yz}\\ \sigma_{xz}\\ \sigma_{xy}\end{bmatrix}=\begin{bmatrix}c_{11} & c_{12} & c_{13} & c_{14} & c_{15} & c_{16}\\ c_{12} & c_{22} & c_{23} & c_{24} & c_{25} & c_{26}\\ c_{13} & c_{23} & c_{33} & c_{34} & c_{35} & c_{36}\\ c_{14} & c_{24} & c_{34} & c_{44} & c_{45} & c_{46}\\ c_{15} & c_{25} & c_{35} & c_{45} & c_{55} & c_{56}\\ c_{16} & c_{26} & c_{36} & c_{46} & c_{56} & c_{66}\end{bmatrix}\begin{bmatrix}\varepsilon_{xx}\\ \varepsilon_{yy}\\ \varepsilon_{zz}\\ 2\varepsilon_{yz}\\ 2\varepsilon_{xz}\\ 2\varepsilon_{xy}\end{bmatrix},\qquad (2.50)$$

with the stiffness matrix defined as

$$\mathbf{C}\equiv C_{ijkl}=\begin{bmatrix}C_{xxxx} & C_{xxyy} & C_{xxzz} & C_{xxyz} & C_{xxxz} & C_{xxxy}\\ C_{xxyy} & C_{yyyy} & C_{yyzz} & C_{yyyz} & C_{xzyy} & C_{xyyy}\\ C_{xxzz} & C_{yyzz} & C_{zzzz} & C_{yzzz} & C_{xzzz} & C_{xyzz}\\ C_{xxyz} & C_{yyyz} & C_{yzzz} & C_{yzyz} & C_{xzyz} & C_{xyyz}\\ C_{xxxz} & C_{xzyy} & C_{xzzz} & C_{xzyz} & C_{xzxz} & C_{xyxz}\\ C_{xxxy} & C_{xyyy} & C_{xyzz} & C_{xyyz} & C_{xyxz} & C_{xyxy}\end{bmatrix}=\begin{bmatrix}c_{11} & c_{12} & c_{13} & c_{14} & c_{15} & c_{16}\\ c_{12} & c_{22} & c_{23} & c_{24} & c_{25} & c_{26}\\ c_{13} & c_{23} & c_{33} & c_{34} & c_{35} & c_{36}\\ c_{14} & c_{24} & c_{34} & c_{44} & c_{45} & c_{46}\\ c_{15} & c_{25} & c_{35} & c_{45} & c_{55} & c_{56}\\ c_{16} & c_{26} & c_{36} & c_{46} & c_{56} & c_{66}\end{bmatrix}.\qquad (2.51)$$

2.4.2.1 Plane Stress

For plane stress problems, **S** is composed of the elements of the first, second and third rows and columns of Eq. (2.47).

$$\mathbf{S} = \begin{bmatrix} s_{11} & s_{12} & s_{16} \\ s_{12} & s_{22} & s_{26} \\ s_{16} & s_{26} & s_{66} \end{bmatrix}. \tag{2.52}$$

C is the inverse of **S**.

For plane strain problems,

$$s_{ij}^{strain} = s_{ij} - \frac{s_{i3}s_{3j}}{s_{33}}, \quad j \neq 3,4,5. \tag{2.53}$$

2.4.2.2 Plane strain

For plane strain problems, **C** is composed of the elements of the first, second and third rows and columns of Eq. (2.51).

$$\mathbf{C} = \begin{bmatrix} c_{11} & c_{12} & c_{16} \\ c_{12} & c_{22} & c_{26} \\ c_{16} & c_{26} & c_{66} \end{bmatrix}. \tag{2.54}$$

S is the inverse of **C**. For plane stress problems,

$$c_{ij}^{stress} = c_{ij} - \frac{c_{i3}c_{3j}}{c_{33}}, \quad j \neq 3,4,5. \tag{2.55}$$

2.4.2.3 No Plane of Elastic Symmetry (Triclinic Materials)

No reflection planes or axes of rotational symmetry are prescribed to impose restrictions on the structure of stiffness matrix, which remains full populated by 21 independent coefficients $C_{\varsigma\xi\upsilon\tau}$

$$\mathbf{C} = \begin{bmatrix} c_{11} & c_{12} & c_{13} & c_{14} & c_{15} & c_{16} \\ c_{12} & c_{22} & c_{23} & c_{24} & c_{25} & c_{26} \\ c_{13} & c_{23} & c_{33} & c_{34} & c_{35} & c_{36} \\ c_{14} & c_{24} & c_{34} & c_{44} & c_{45} & c_{46} \\ c_{15} & c_{25} & c_{35} & c_{45} & c_{55} & c_{56} \\ c_{16} & c_{26} & c_{36} & c_{46} & c_{56} & c_{66} \end{bmatrix}. \tag{2.56}$$

2.4.2.4 Plane of Elastic Symmetry (Monoclinic Materials)

Suppose that through each point of a body there passes a plane possessing the following property: every two directions that are symmetrical with respect to this plane are equivalent regarding the elastic properties. A direction normal to the plane of elastic symmetry will be termed the principal direction of elasticity (or simply the principal direction, in case no other principal directions, e.g. those of the stress and strain tensors, are considered at the same time). In this case only one principal direction passes through a point of a body.
If the z axis is taken normal to the plane of elastic symmetry and the other two axes lie in this plane, we conclude that eight elastic constants must be zero, and the number of elastic constants c_{ij} reduces to 13

$$\mathbf{C} = \begin{bmatrix} c_{11} & c_{12} & c_{13} & 0 & 0 & c_{16} \\ c_{12} & c_{22} & c_{23} & 0 & 0 & c_{26} \\ c_{13} & c_{23} & c_{33} & 0 & 0 & c_{36} \\ 0 & 0 & 0 & c_{44} & c_{45} & 0 \\ 0 & 0 & 0 & c_{45} & c_{55} & 0 \\ c_{16} & c_{26} & c_{36} & 0 & 0 & c_{66} \end{bmatrix}. \tag{2.57}$$

2.4.2.5 Three Planes of Elastic Symmetry (Orthotropic Materials)

If through each point of a body there pass three mutually perpendicular (orthogonal) planes of elastic symmetry, and the planes of elastic symmetry are parallel at all points, then, taking the coordinate axes normal to the planes of elastic symmetry (along the principal directions), we find that, in addition to the eight elastic constants of the preceding case, there are four more constants equal to zero

$$\mathbf{C} = \begin{bmatrix} c_{11} & c_{12} & c_{13} & 0 & 0 & 0 \\ c_{12} & c_{22} & c_{23} & 0 & 0 & 0 \\ c_{13} & c_{23} & c_{33} & 0 & 0 & 0 \\ 0 & 0 & 0 & c_{44} & 0 & 0 \\ 0 & 0 & 0 & 0 & c_{55} & 0 \\ 0 & 0 & 0 & 0 & 0 & c_{66} \end{bmatrix}. \tag{2.58}$$

The compliance matrix for orthotropic materials is

$$\mathbf{S}=\begin{bmatrix} \frac{1}{E_{xx}} & \frac{-\nu_{yx}}{E_{yy}} & \frac{-\nu_{zx}}{E_{zz}} & 0 & 0 & 0 \\ \frac{-\nu_{xy}}{E_{xx}} & \frac{1}{E_{yy}} & \frac{-\nu_{zy}}{E_{zz}} & 0 & 0 & 0 \\ \frac{-\nu_{xz}}{E_{xx}} & \frac{-\nu_{yz}}{E_{yy}} & \frac{1}{E_{zz}} & 0 & 0 & 0 \\ 0 & 0 & 0 & \frac{1}{G_{yz}} & 0 & 0 \\ 0 & 0 & 0 & 0 & \frac{1}{G_{xz}} & 0 \\ 0 & 0 & 0 & 0 & 0 & \frac{1}{G_{xy}} \end{bmatrix}. \tag{2.59}$$

The stiffness matrix for orthotropic materials, found from the inverse of the compliance matrix, is given by

$$\mathbf{C}=\begin{bmatrix} \frac{1-\nu_{yz}\nu_{zy}}{E_{yy}E_{zz}\triangle} & \frac{\nu_{yx}+\nu_{zx}\nu_{yz}}{E_{yy}E_{zz}\triangle} & \frac{\nu_{zx}+\nu_{yx}\nu_{zy}}{E_{yy}E_{zz}\triangle} & 0 & 0 & 0 \\ \frac{\nu_{xy}+\nu_{xz}\nu_{yz}}{E_{zz}E_{xx}\triangle} & \frac{1-\nu_{zx}\nu_{xz}}{E_{zz}E_{xx}\triangle} & \frac{\nu_{zy}+\nu_{zx}\nu_{xy}}{E_{zz}E_{xx}\triangle} & 0 & 0 & 0 \\ \frac{\nu_{xz}+\nu_{xy}\nu_{yz}}{E_{xx}E_{yy}\triangle} & \frac{\nu_{yz}+\nu_{xz}\nu_{yx}}{E_{xx}E_{yy}\triangle} & \frac{1-\nu_{xy}\nu_{yx}}{E_{xx}E_{yy}\triangle} & 0 & 0 & 0 \\ 0 & 0 & 0 & G_{yz} & 0 & 0 \\ 0 & 0 & 0 & 0 & G_{xz} & 0 \\ 0 & 0 & 0 & 0 & 0 & G_{xy} \end{bmatrix}, \tag{2.60}$$

where

$$\triangle=\frac{1-\nu_{xy}\nu_{yx}-\nu_{yz}\nu_{zy}-\nu_{zx}\nu_{xz}-2\nu_{xy}\nu_{yz}\nu_{zx}}{E_{xx}E_{yy}E_{zz}}. \tag{2.61}$$

2.4.2.6 Plane of Isotropy (Axis of Rotational Symmetry, Transversely Isotropic or Hexagonal Materials)

Consider a body possessing the following properties: through all points there pass parallel planes of elastic symmetry in which all directions are elastically equivalent (plane of isotropy). In other words, at each point there is one principal direction and an infinite number of principal directions in a plane normal to the first direction. Such a body may also be regarded as a body through each point of which there passes an axis of elastic symmetry of infinitely high order, i.e., a rotational axis.

Let z axis be taken normal to a plane of isotropy, with the x and y axes directed arbitrarily in this plane. The stiffnesses are then written as

$$\mathbf{C} = \begin{bmatrix} c_{11} & c_{12} & c_{13} & 0 & 0 & 0 \\ c_{12} & c_{22} & c_{23} & 0 & 0 & 0 \\ c_{13} & c_{23} & c_{33} & 0 & 0 & 0 \\ 0 & 0 & 0 & c_{44} & 0 & 0 \\ 0 & 0 & 0 & 0 & c_{44} & 0 \\ 0 & 0 & 0 & 0 & 0 & 2(c_{11} - c_{12}) \end{bmatrix}. \tag{2.62}$$

2.4.2.7 Nine Planes of Elastic Symmetry (Cubic Material)

Nine planes of symmetry whose normals are on the three coordinate axes and on the coordinate planes making an angle $\frac{\pi}{4}$ with the coordinate axes. The stiffnesses are then written as

$$\mathbf{C} = \begin{bmatrix} c_{11} & c_{12} & c_{12} & 0 & 0 & 0 \\ c_{12} & c_{11} & c_{12} & 0 & 0 & 0 \\ c_{12} & c_{12} & c_{11} & 0 & 0 & 0 \\ 0 & 0 & 0 & c_{44} & 0 & 0 \\ 0 & 0 & 0 & 0 & c_{44} & 0 \\ 0 & 0 & 0 & 0 & 0 & c_{44} \end{bmatrix}. \tag{2.63}$$

Besides above cases of elastic symmetry there exist a number of others. Typical kinds of symmetry here are those of single crystals of various elements and compounds. It has been proven that there are altogether 32 kinds of geometrical crystal symmetry. However, the number of classes of elastic crystal symmetry is much fewer (nine) since the same form of the generalized Hooke's law equations for crystals applies to several cases of their geometrical symmetry.

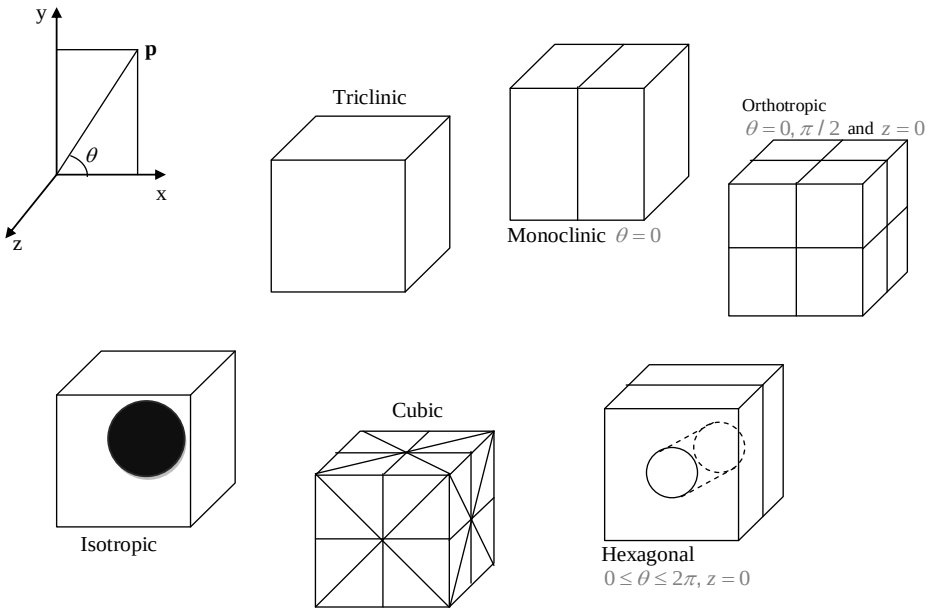

Figure 2.9: Evolution of material symmetries by addition of planes and axes of symmetry.

2.4.3 Transformation of Elastic Constants to New Coordinate System

In solving a specific elasticity problem, we have to use the generalized Hooke's law equations, which involve the elastic constants s_{ij} or c_{ij}. In case of an anisotropic body these quantities depend on the directions of the axes of a coordinate system, and if the directions of the axes change, so do the values of the elastic constants. An exception is an isotropic body for which the generalized Hookee's law equations retain the same form in any orthogonal coordinate system, and the corresponding elastic constants remain unchanged (invariant). In studying a state of stress the following question often arises: the constants s_{ij} and c_{ij} are known for a coordinate system x, y, z, but it is more convenient to use another orthogonal system x', y', z' (see Figure 2.10). It is required to find the constants s'_{ij}, c'_{ij} for the second system. We assign the cosines of the angles between the axes of the old and new coordinate system by Table 2.1. Thus, $l_{xx} = \cos(x', x)$, $l_{xy} = \cos(x', y)$, etc.

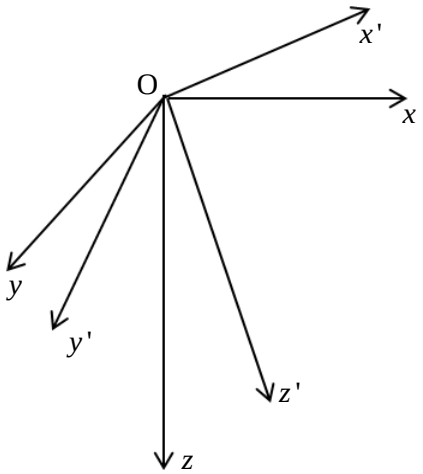

Figure 2.10: Old coordinate system and new coordinate system.

Table 2.1: The cosines of the angles between the axes of the old and new coordinate system.

	x	y	z
x'	l_{xx}	l_{xy}	l_{xz}
y'	l_{yx}	l_{yy}	l_{yz}
z'	l_{zx}	l_{zy}	l_{zz}

The transformation formulas between two coordinate systems can be written as

$$s'_{ij} = \sum_{m=1}^{6}\sum_{n=1}^{6} s_{mn} q_{im} q_{jn}, \tag{2.64}$$

where q_{ij} are defined in Table 2.2.

Table 2.2: Symbols q_{ij} in transformation formulas for s_{ij}.

	1	2	3	4	5	6
1	l_{xx}^2	l_{xy}^2	l_{xz}^2	$l_{xy}l_{xz}$	$l_{xz}l_{xx}$	$l_{xy}l_{xx}$
2	l_{yx}^2	l_{yy}^2	l_{yz}^2	$l_{yz}l_{yy}$	$l_{yz}l_{yx}$	$l_{yy}l_{yx}$
3	l_{zx}^2	l_{zy}^2	l_{zz}^2	$l_{zz}l_{zy}$	$l_{zz}l_{zx}$	$l_{zy}l_{zx}$
4	$2l_{zx}l_{yx}$	$2l_{zy}l_{yy}$	$2l_{zz}l_{yz}$	$l_{zz}l_{yy}-l_{zy}l_{yz}$	$l_{zz}l_{yx}-l_{zx}l_{yz}$	$l_{zx}l_{yy}-l_{zy}l_{yx}$
5	$2l_{zx}l_{xx}$	$2l_{zy}l_{xy}$	$2l_{zz}l_{xz}$	$l_{zz}l_{xy}-l_{zy}l_{xz}$	$l_{yz}l_{xx}-l_{zx}l_{xz}$	$l_{zx}l_{xy}-l_{zy}l_{xx}$
6	$2l_{yx}l_{xx}$	$2l_{xy}l_{yy}$	$2l_{xz}l_{yz}$	$l_{xz}l_{yy}-l_{xy}l_{yz}$	$l_{xz}l_{yx}-l_{xx}l_{yz}$	$l_{xx}l_{yy}-l_{xy}l_{yx}$

The first subscript in the symbols q_{ij} indicates a line number in Table 2.2, and the second subscript a column number. $q_{11} = l_{xx}^2$, $q_{14} = l_{xy}l_{xz}$, $q_{44} = l_{zz}l_{yy} - l_{zy}l_{yz}$, etc.

2.4.4 Transformation of Elastic Constants when the Coordinate System is Rotated

Consider a special case when a new coordinate system x', y', z' is obtained from the old system x, y, z by a rotation for a certain angle θ about the common axis $z = z'$ (see Figure 2.11). In this case, q_{ij} is defined by Table 2.3.

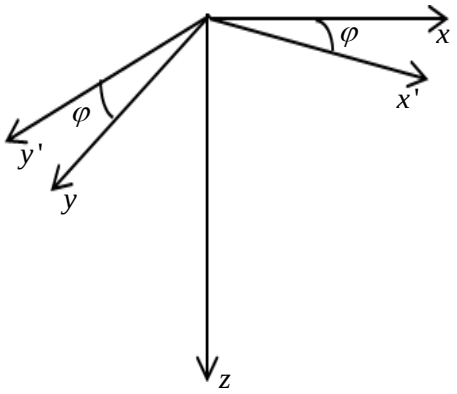

Figure 2.11: New coordinate system obtained by rotation of the old system.

Table 2.3: Symbols q_{ij} in transformation formulas for s_{ij} in rotated coordinate system.

	1	2	3	4	5	6
1	$\cos^2\varphi$	$\sin^2\varphi$	0	0	0	$\sin\varphi\cos\varphi$
2	$\sin^2\varphi$	$\cos^2\varphi$	0	0	0	$-\sin\varphi\cos\varphi$
3	0	0	1	0	0	0
4	0	0	0	$\cos\varphi$	$-\sin\varphi$	0
5	0	0	0	$\sin\varphi$	$\cos\varphi$	0
6	$-2\sin\varphi\cos\varphi$	$2\sin\varphi\cos\varphi$	0	0	0	$\cos^2\varphi-\sin^2\varphi$

2.4.5 Transformation of the Boundary Conditions if there are Two Arbitrary Oriented Anisotropic Crystals in Contact

For the boundary condition, we change all the stresses into the same coordinate system. The formulas for the transformation of stress components to new axes are

$$\sigma'_{\varsigma\xi} = \sum_{\varsigma}\sum_{\xi}\sigma_{\varsigma\xi}l_{\tau\varsigma}l_{\upsilon\xi}, \quad \varsigma,\xi,\tau,\upsilon = x,y,z, \tag{2.65}$$

where $l_{\varsigma\xi}$ are defined in Table 2.1. $l_{\varsigma\xi}$ were defined in Table 2.4 for the transformation between stresses in a Cartesian coordinate system and stresses in a cylindrical system r, θ, z (the z axes of both system are coincident).

Table 2.4: The transformation between stresses in a Cartesian coordinate system and stresses in a cylindrical system.

	x	y	z
x'	$\cos\theta$	$-\sin\theta$	0
y'	$\sin\theta$	$\cos\theta$	0
z'	0	0	1

2.5 Anti-plane Deformation

Anti-plane deformation denotes a special class of deformation where the displacements in the body are zero in the plane of interest but non-zero in the direction perpendicular to that plane. For small strains, the strain tensor under anti-plane strain can be written as

$$\boldsymbol{\varepsilon} = \begin{bmatrix} 0 \\ 0 \\ 0 \\ \varepsilon_{yz} \\ \varepsilon_{xz} \\ 0 \end{bmatrix}. \tag{2.66}$$

The stress tensor that results from a state of anti-plane strain can be expressed as

$$\boldsymbol{\sigma} = \begin{bmatrix} 0 \\ 0 \\ 0 \\ \sigma_{yz} \\ \sigma_{xz} \\ 0 \end{bmatrix}. \tag{2.67}$$

The displacement field that leads to a state of anti-plane strain is

$$u_x = 0, u_y = 0. \tag{2.68}$$

3. Method of Fundamental Solutions

3.1 Introduction

The purpose of this chapter is to introduce the MFS [Chen, Karageorghis and Smyrils (2008)] to solve the isotropic and anisotropic elastic problems in 2D.
The main idea of MFS consists of approximating the solution of the partial differential equation by a linear combination of fundamental solutions, defined in source points. In order to avoid the singularity, the source point should be put outside of the physical domain to avoid the coincidence with the collocation points. At the same time, the corresponding approximating traction was obtained from a linear combination of fundamental tractions. The expansion coefficients of the solution in MFS are determined so that the solution satisfies the boundary condition. The fundamental solution for isotropic elastic problems is given in an exact expression with Young's modulus and Poisson's ratio. The fundamental solution of anisotropic elastic problems is given as a real part of a first order complex polynomial. The coefficients of polynomial are determined by solving a six-order equation, originating from a zero determinant of a six-order matrix. The elements of the matrix stem from the elements of the stiffness matrix. There are three pairs of complex roots for the six-order equation. The three roots with positive imaginary parts are the coefficients of the complex polynomial. Two of the three roots are used for analysis of the plain strain deformation.

3.2 Governing Equations

We begin our discussion with three dimensional (3D) problems and afterwards reduce it to 2D problems of interest. In order to simplify the discussion, we shall assume: (i) the solid is free of body forces, (ii) the thermal strains can be neglected. Under these conditions the general equation of elasticity [Bower (2009)] is

$$C_{\varsigma\xi\upsilon\tau}\frac{\partial^2 u_\upsilon(\mathbf{p})}{\partial p_\varsigma \partial p_\tau}=0,\quad \varsigma,\xi,\upsilon,\tau=x,y,z. \tag{3.1}$$

The matrix form of the three equilibrium equations (3.1) are

$$\begin{bmatrix} \frac{\partial}{\partial p_x} & 0 & 0 & \frac{\partial}{\partial p_y} & \frac{\partial}{\partial p_z} & 0 \\ 0 & \frac{\partial}{\partial p_y} & 0 & \frac{\partial}{\partial p_x} & 0 & \frac{\partial}{\partial p_z} \\ 0 & 0 & \frac{\partial}{\partial p_z} & 0 & \frac{\partial}{\partial p_x} & \frac{\partial}{\partial p_y} \end{bmatrix} \begin{bmatrix} c_{11} & c_{12} & c_{13} & c_{14} & c_{15} & c_{16} \\ c_{12} & c_{22} & c_{23} & c_{24} & c_{25} & c_{26} \\ c_{13} & c_{23} & c_{33} & c_{34} & c_{35} & c_{36} \\ c_{14} & c_{24} & c_{34} & c_{44} & c_{45} & c_{46} \\ c_{15} & c_{25} & c_{35} & c_{45} & c_{55} & c_{56} \\ c_{16} & c_{26} & c_{36} & c_{46} & c_{56} & c_{66} \end{bmatrix} \begin{bmatrix} \partial u_x / \partial p_x \\ \partial u_y / \partial p_y \\ \partial u_z / \partial p_z \\ \partial u_y / \partial p_z + \partial u_z / \partial p_y \\ \partial u_x / \partial p_z + \partial u_z / \partial p_x \\ \partial u_x / \partial p_y + \partial u_y / \partial p_x \end{bmatrix} = 0. \tag{3.2}$$

3.2.1 Governing Equations for Isotropic Elastic Material

Consider a two-dimensional solid in domain Ω with boundary Γ. The solid behaves ideally isotropic elastic. The solid is governed by Navier's equations for plane strain problems, which are the conditions for equilibrium equations (3.2) by using the stiffness matrix $\mathbf{C}$ in Eq. (2.44), expressed with the displacement $\mathbf{u}$.

$$\frac{2(1-\nu)}{1-2\nu}\frac{\partial^2 u_x(\mathbf{p})}{\partial {p_x}^2}+\frac{\partial^2 u_x(\mathbf{p})}{\partial {p_y}^2}+\frac{1}{1-2\nu}\frac{\partial^2 u_y(\mathbf{p})}{\partial p_x \partial p_y}=0, \tag{3.3}$$

$$\frac{2(1-\nu)}{1-2\nu}\frac{\partial^2 u_y(\mathbf{p})}{\partial p_y^2}+\frac{\partial^2 u_y(\mathbf{p})}{\partial p_x^2}+\frac{1}{1-2\nu}\frac{\partial^2 u_x(\mathbf{p})}{\partial p_x \partial p_y}=0, \mathbf{p}\in\Omega. \tag{3.4}$$

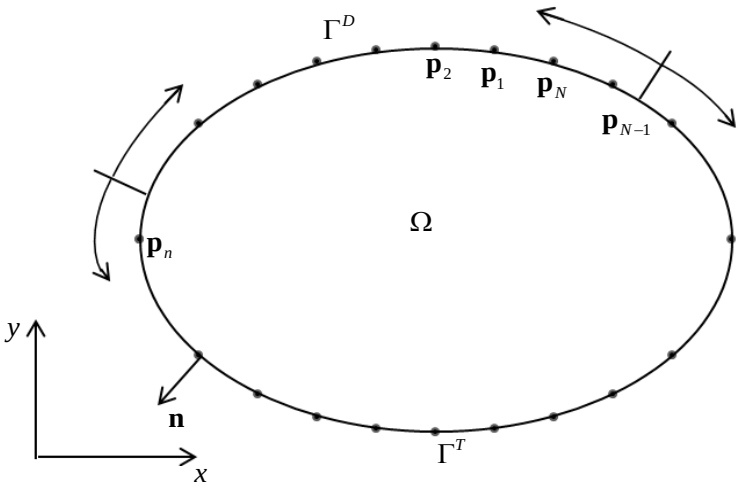

Figure 3.1: Problem domain Ω with Dirichlet Γ^D and Neumann Γ^T parts of the boundary.

The boundary is divided into two not necessarily connected parts $\Gamma=\Gamma^D+\Gamma^T$. On the part Γ^D the Dirichlet (displacement) boundary conditions are given, and on the part Γ^T the Neumann (traction) boundary conditions are given. (see Figure 3.1)

3.2.2 Governing Equations for Anisotropic Elastic Material

For plane strain deformations the displacement field has the form $\mathbf{u} = u_x(p_x, p_y)\mathbf{i}_x + u_y(p_x, p_y)\mathbf{i}_y$. Under these conditions the equilibrium equations (3.2) reduce to

$$c_{11}\frac{\partial^2 u_x}{\partial p_x^2} + c_{66}\frac{\partial^2 u_x}{\partial p_y^2} + 2c_{16}\frac{\partial^2 u_x}{\partial p_x \partial p_y} + c_{16}\frac{\partial^2 u_y}{\partial p_x^2} + c_{26}\frac{\partial^2 u_y}{\partial p_y^2} + (c_{12}+c_{66})\frac{\partial^2 u_y}{\partial p_x \partial p_y} = 0, \quad (3.5)$$

$$c_{16}\frac{\partial^2 u_x}{\partial p_x^2} + c_{26}\frac{\partial^2 u_x}{\partial p_y^2} + (c_{12}+c_{66})\frac{\partial^2 u_x}{\partial p_x \partial p_y} + c_{66}\frac{\partial^2 u_y}{\partial p_x^2} + c_{22}\frac{\partial^2 u_y}{\partial p_y^2} + 2c_{26}\frac{\partial^2 u_y}{\partial p_x \partial p_y} = 0, \quad (3.6)$$

$$c_{15}\frac{\partial^2 u_x}{\partial p_x^2} + c_{46}\frac{\partial^2 u_x}{\partial p_y^2} + (c_{56}+c_{14})\frac{\partial^2 u_x}{\partial p_x \partial p_y} + c_{56}\frac{\partial^2 u_y}{\partial p_x^2} + c_{24}\frac{\partial^2 u_y}{\partial p_y^2} + (c_{25}+c_{46})\frac{\partial^2 u_y}{\partial p_x \partial p_y} = 0. \quad (3.7)$$

u_x and u_y can be chosen to satisfy two, but not all three, of the three equations, because of 2 unknowns. The elastic constants must satisfy $c_{11} > 0,\ c_{22} > 0,\ c_{66} > 0.$ Consequently, the third equation can only be satisfied by setting $c_{15} = c_{46} = c_{14} = c_{56} = c_{24} = c_{25} = 0.$

The formulas for plane stress problems can be obtained from formulas of plane strain problems by replacing the components c_{ij} by

$$c'_{ij} = c_{ij} - \frac{c_{i3}c_{3j}}{c_{33}},\ j \neq 3,4,5, \quad (3.8)$$

and setting $c'_{14} = c'_{15} = c'_{24} = c'_{25} = c'_{34} = c'_{35} = c'_{46} = c'_{56} = 0$ in the stiffness tensor.

3.3 Fundamental Solution

3.3.1 Fundamental Solution for Isotropic Elastic Material

Kelvin's fundamental solution of elasticity is given (see [Beskos (1987), Aliabadi (2002)]) in two dimensional plane strain situation by

$$U_{\varsigma\xi}(\mathbf{p},\mathbf{s}) = \frac{1}{8\pi\mu(1-\nu)}\left\{(3-4\nu)\log\left(\frac{1}{r}\right)\delta_{\varsigma\xi} + \frac{(p_\varsigma - s_\varsigma)(p_\xi - s_\xi)}{r^2}\right\}, \varsigma, \xi = x, y, \quad (3.9)$$

where $U_{\varsigma\xi}(\mathbf{p},\mathbf{s})$ represents the displacement in the direction ς at point $\mathbf{p}$ due to a unit point force acting in the direction ξ at point $\mathbf{s}$. $r = \sqrt{(p_x - s_x)^2 + (p_y - s_y)^2}$ is

the distance between the point $\mathbf{p}$ and the source point $\mathbf{s}$. $\mu = E/2(1+\nu)$ is the shear modulus of elasticity. The solution (3.9) is expanded as follows

$$U_{xx}(\mathbf{p},\mathbf{s}) = \frac{1}{8\pi\mu(1-\nu)}\left\{(3-4\nu)\log\left(\frac{1}{r}\right)+\frac{(p_x-s_x)^2}{r^2}\right\}, \tag{3.10}$$

$$U_{xy}(\mathbf{p},\mathbf{s}) = U_{yx}(\mathbf{p},\mathbf{s}) = \frac{1}{8\pi\mu(1-\nu)}\frac{(p_x-s_x)(p_y-s_y)}{r^2}, \tag{3.11}$$

$$U_{yy}(\mathbf{p},\mathbf{s}) = \frac{1}{8\pi\mu(1-\nu)}\left\{(3-4\nu)\log\left(\frac{1}{r}\right)+\frac{(p_y-s_y)^2}{r^2}\right\}. \tag{3.12}$$

It can be shown that the following u_x and u_y satisfy the governing Eqs. (3.3)(3.4)

$$u_x(\mathbf{p}) = U_{xx}(\mathbf{p},\mathbf{s})\alpha + U_{xy}(\mathbf{p},\mathbf{s})\beta, \tag{3.13}$$

$$u_y(\mathbf{p}) = U_{yx}(\mathbf{p},\mathbf{s})\alpha + U_{yy}(\mathbf{p},\mathbf{s})\beta, \tag{3.14}$$

where α and β represent arbitrary constants.

The explicit expressions for isotropic problems, used in calculation of the traction boundary conditions, are

$$\frac{\partial U_{xx}(\mathbf{p},\mathbf{s})}{\partial p_x} = \frac{1}{8\pi\mu(1-\nu)}\left[(4\nu-3)\frac{p_x-s_x}{r^2}+\frac{2(p_x-s_x)(p_y-s_y)^2}{r^4}\right], \tag{3.15}$$

$$\frac{\partial U_{xx}(\mathbf{p},\mathbf{s})}{\partial p_y} = \frac{1}{8\pi\mu(1-\nu)}\left[(4\nu-3)\frac{p_y-s_y}{r^2}-\frac{2(p_y-s_y)(p_x-s_x)^2}{r^4}\right], \tag{3.16}$$

$$\frac{\partial U_{xy}(\mathbf{p},\mathbf{s})}{\partial p_x} = \frac{\partial U_{yx}(\mathbf{p},\mathbf{s})}{\partial p_x} = \frac{1}{8\pi\mu(1-\nu)}\frac{(p_y-s_y)[(p_y-s_y)^2-(p_x-s_x)^2]}{r^4}, \tag{3.17}$$

$$\frac{\partial U_{yy}(\mathbf{p},\mathbf{s})}{\partial p_x} = \frac{1}{8\pi\mu(1-\nu)}\left[(4\nu-3)\frac{(p_x-s_x)}{r^2}-\frac{2(p_x-s_x)(p_y-s_y)^2}{r^4}\right], \tag{3.18}$$

$$\frac{\partial U_{yy}(\mathbf{p},\mathbf{s})}{\partial p_y} = \frac{1}{8\pi\mu(1-\nu)}\left[(4\nu-3)\frac{(p_y-s_y)}{r^2}+\frac{2(p_y-s_y)(p_x-s_x)^2}{r^4}\right], \tag{3.19}$$

$$\frac{\partial U_{xy}(\mathbf{p},\mathbf{s})}{\partial p_y} = \frac{\partial U_{yx}(\mathbf{p},\mathbf{s})}{\partial p_y} = \frac{1}{8\pi\mu(1-\nu)}\frac{(p_x-s_x)[(p_x-s_x)^2-(p_y-s_y)^2]}{r^4}. \tag{3.20}$$

3.3.2 Fundamental Solution for Anisotropic Elastic Material

A fundamental solution for the system (3.1) is obtained from the Green function in [Teway, Wagoner and Hirth (1989)]

$$U_{\varsigma\xi}(\mathbf{p},\mathbf{s}) = -\frac{1}{\pi}\mathrm{Re}\sum_{m=1}^{3}\gamma_{\varsigma\xi}^{m}\log\left(z_m(\mathbf{p})-z_m(\mathbf{s})\right), \tag{3.21}$$

in which $\gamma_{\varsigma\xi}^{m}$ and z_m are variables.

We introduce the complex variable $z_m, m=1,2,3,$ as in [Stroh (1958)]

$$z_m(\mathbf{p}) = p_x + \rho_m p_y. \tag{3.22}$$

The complex constants $\rho_m, m=1,2,3$ are the roots with positive imaginary parts of the sixth-order determinant [Ting (1996)]

$$|\mathbf{Q} + \rho(\mathbf{R} + \mathbf{R}^{\mathrm{T}}) + \rho^2 \mathbf{T}| = 0, \tag{3.23}$$

where $|\bullet|$ represents determinant of matrix, and the matrices $\mathbf{Q}$, $\mathbf{R}$ and $\mathbf{T}$ are defined through the elements of the stiffness tensor as

$$Q_{kl} = C_{k1l1}, \quad R_{kl} = C_{k1l2}, \quad T_{kl} = C_{k2l2}. \tag{3.24}$$

For a general anisotropic material, the sixtic equation in ρ from Eq. (3.23) is then

$$\begin{vmatrix} c_{11}+2\rho c_{16}+\rho^2 c_{66} & c_{16}+\rho(c_{12}+c_{66})+\rho^2 c_{26} & c_{15}+\rho(c_{14}+c_{56})+\rho^2 c_{46} \\ c_{16}+\rho(c_{12}+c_{66})+\rho^2 c_{26} & c_{66}+2\rho c_{26}+\rho^2 c_{22} & c_{56}+\rho(c_{46}+c_{25})+\rho^2 c_{24} \\ c_{15}+\rho(c_{14}+c_{56})+\rho^2 c_{46} & c_{56}+\rho(c_{46}+c_{25})+\rho^2 c_{24} & c_{55}+2\rho c_{45}+\rho^2 c_{44} \end{vmatrix} = 0. \tag{3.25}$$

Here, our interest is focused on anisotropic materials under plane strain deformation. As shown in [Ting (1996)], in-plane and anti-plane deformations are uncoupled only for anisotropic materials, which satisfy

$$c_{14} = c_{15} = c_{24} = c_{25} = c_{46} = c_{56} = 0. \tag{3.26}$$

Under these conditions, Eq. (3.25) is

$$(c_{55}+2\rho c_{45}+\rho^2 c_{44}) \begin{vmatrix} c_{11}+2\rho c_{16}+\rho^2 c_{66} & c_{16}+\rho(c_{12}+c_{66})+\rho^2 c_{26} \\ c_{16}+\rho(c_{12}+c_{66})+\rho^2 c_{26} & c_{66}+2\rho c_{26}+\rho^2 c_{22} \end{vmatrix} = 0. \tag{3.27}$$

The roots of Eq. (3.27) with positive imaginary parts, ρ_1 and ρ_2, are those needed for the analysis of plane strain deformations. The root with positive imaginary part of the quadratic term multiplying the determinant in Eq. (3.27) is given by

$$\rho_3 = \frac{-c_{45} + \iota\sqrt{c_{44}c_{55} - c_{45}^2}}{c_{44}}, \tag{3.28}$$

where $\iota = \sqrt{-1}$. This root is needed for problems of anti-plane strain. We emphasize again that the deformations studied here are plane strain deformations since we have

assumed that the elastic state is independent of p_z. This assumes that the anisotropic material being analyzed can support plane strain deformation. Anisotropic materials that do not satisfy (3.26), such as triclinic materials, cannot support a state of plane strain. For cubic material

$$\rho_1 = \frac{1}{2}(\sqrt{2-\eta} + \imath\sqrt{2+\eta}) \ , \quad \rho_2 = \frac{1}{2}(-\sqrt{2-\eta} + \imath\sqrt{2+\eta}) \ , \quad \rho_3 = \imath, \tag{3.29}$$

where

$$\eta = \frac{c_{11}^2 - c_{12}^2 - 2c_{12}c_{44}}{c_{11}c_{44}}. \tag{3.30}$$

We define the elements of the matrix $\boldsymbol{\gamma}$, written using the standard reduction scheme in Eq. (2.51) for the elastic constants [Lekhnitskii (1981)], by

$$\gamma_{\varsigma\xi}^m = \frac{\imath\Gamma_{\varsigma\xi}}{(c_{11}c_{66} - c_{16}^2)(\rho_m - \bar{\rho}_m)\prod_{m\neq n}(\rho_m - \rho_n)(\rho_m - \bar{\rho}_n)}, \quad m,n = 1,2,3, \tag{3.31}$$

where $\bar{\rho}_m$ is the conjugate complex of ρ_m, and

$$\begin{aligned} \Gamma_{xx} &= c_{44} + c_{11}\rho_m^2, \\ \Gamma_{xy} &= \Gamma_{yx} = -(c_{44} + c_{12})\rho_m, \\ \Gamma_{yy} &= c_{11} + c_{44}\rho_m^2. \end{aligned} \tag{3.32}$$

3.4 Solution Procedure

The solution of the problem is sought in the form

$$u_x(\mathbf{p}) = \sum_{n=1}^{N^\Gamma} U_{xx}(\mathbf{p},\mathbf{s})\,\alpha_n + \sum_{n=1}^{N^\Gamma} U_{xy}(\mathbf{p},\mathbf{s})\beta_n, \tag{3.33}$$

$$u_y(\mathbf{p}) = \sum_{n=1}^{N^\Gamma} U_{yx}(\mathbf{p},\mathbf{s})\,\alpha_n + \sum_{n=1}^{N^\Gamma} U_{yy}(\mathbf{p},\mathbf{s})\beta_n. \tag{3.34}$$

Because of Eqs. (2.7)(2.8)(2.17)(2.18)(2.20)(2.21) and (2.29), the traction can be expressed as

$$t_x(\mathbf{p}) = \sum_{n=1}^{N^\Gamma} T_{xx}(\mathbf{p},\mathbf{s})\alpha_n + \sum_{n=1}^{N^\Gamma} T_{xy}(\mathbf{p},\mathbf{s})\beta_n, \tag{3.35}$$

$$t_y(\mathbf{p}) = \sum_{n=1}^{N^\Gamma} T_{yx}(\mathbf{p},\mathbf{s})\alpha_n + \sum_{n=1}^{N^\Gamma} T_{yy}(\mathbf{p},\mathbf{s})\beta_n, \tag{3.36}$$

where

$$T_{xx}(\mathbf{p},\mathbf{s})=\left[c_{11}\frac{\partial U_{xx}(\mathbf{p},\mathbf{s})}{\partial p_x}+c_{12}\frac{\partial U_{yx}(\mathbf{p},\mathbf{s})}{\partial p_y}+c_{16}\frac{\partial U_{xx}(\mathbf{p},\mathbf{s})}{\partial p_y}+c_{16}\frac{\partial U_{yx}(\mathbf{p},\mathbf{s})}{\partial p_x}\right]n_{nx}$$
$$+\left[c_{16}\frac{\partial U_{xx}(\mathbf{p},\mathbf{s})}{\partial p_x}+c_{26}\frac{\partial U_{yx}(\mathbf{p},\mathbf{s})}{\partial p_y}+c_{66}\frac{\partial U_{xx}(\mathbf{p},\mathbf{s})}{\partial p_y}+c_{66}\frac{\partial U_{yx}(\mathbf{p},\mathbf{s})}{\partial p_x}\right]n_{ny}, \tag{3.37}$$

$$T_{xy}(\mathbf{p},\mathbf{s})=\left[c_{11}\frac{\partial U_{xy}(\mathbf{p},\mathbf{s})}{\partial p_x}+c_{12}\frac{\partial U_{yy}(\mathbf{p},\mathbf{s})}{\partial p_y}+c_{16}\frac{\partial U_{xy}(\mathbf{p},\mathbf{s})}{\partial p_y}+c_{16}\frac{\partial U_{yy}(\mathbf{p},\mathbf{s})}{\partial p_x}\right]n_{nx}$$
$$+\left[c_{16}\frac{\partial U_{xy}(\mathbf{p},\mathbf{s})}{\partial p_x}+c_{26}\frac{\partial U_{yy}(\mathbf{p},\mathbf{s})}{\partial p_y}+c_{66}\frac{\partial U_{xy}(\mathbf{p},\mathbf{s})}{\partial p_y}+c_{66}\frac{\partial U_{yy}(\mathbf{p},\mathbf{s})}{\partial p_x}\right]n_{ny}, \tag{3.38}$$

$$T_{yx}(\mathbf{p},\mathbf{s})=\left[c_{16}\frac{\partial U_{xx}(\mathbf{p},\mathbf{s})}{\partial p_x}+c_{26}\frac{\partial U_{yx}(\mathbf{p},\mathbf{s})}{\partial p_y}+c_{66}\frac{\partial U_{xx}(\mathbf{p},\mathbf{s})}{\partial p_y}+c_{66}\frac{\partial U_{yx}(\mathbf{p},\mathbf{s})}{\partial p_x}\right]n_{nx}$$
$$+\left[c_{21}\frac{\partial U_{xx}(\mathbf{p},\mathbf{s})}{\partial p_x}+c_{22}\frac{\partial U_{yx}(\mathbf{p},\mathbf{s})}{\partial p_y}+c_{26}\frac{\partial U_{xx}(\mathbf{p},\mathbf{s})}{\partial p_y}+c_{26}\frac{\partial U_{yx}(\mathbf{p},\mathbf{s})}{\partial p_x}\right]n_{ny}, \tag{3.39}$$

$$T_{yy}(\mathbf{p},\mathbf{s})=\left[c_{16}\frac{\partial U_{xy}(\mathbf{p},\mathbf{s})}{\partial p_x}+c_{26}\frac{\partial U_{yy}(\mathbf{p},\mathbf{s})}{\partial p_y}+c_{66}\frac{\partial U_{xy}(\mathbf{p},\mathbf{s})}{\partial p_y}+c_{66}\frac{\partial U_{yy}(\mathbf{p},\mathbf{s})}{\partial p_x}\right]n_{nx}$$
$$+\left[c_{21}\frac{\partial U_{xy}(\mathbf{p},\mathbf{s})}{\partial p_x}+c_{22}\frac{\partial U_{yy}(\mathbf{p},\mathbf{s})}{\partial p_y}+c_{26}\frac{\partial U_{xy}(\mathbf{p},\mathbf{s})}{\partial p_y}+c_{26}\frac{\partial U_{yy}(\mathbf{p},\mathbf{s})}{\partial p_x}\right]n_{ny}. \tag{3.40}$$

The coefficients α_n and β_n are calculated from a system of $2N^{\Gamma}$ algebraic equations

$$\mathbf{A}\mathbf{x}=\mathbf{g}, \tag{3.41}$$

where $\mathbf{A}$ stands for a $2N^{\Gamma}\times 2N^{\Gamma}$ matrix with the entries A_{ij}, $\mathbf{x}$ is a $2N^{\Gamma}\times 1$ vector with the entries x_i, and $\mathbf{g}$ is a $2N^{\Gamma}\times 1$ vector with entries g_i,

$$\begin{aligned}
&A_{ij}=\chi_x^D(\mathbf{p}_i)U_{xx}(\mathbf{p}_i,\mathbf{s}_j)+\chi_x^T(\mathbf{p}_i)T_{xx}(\mathbf{p}_i,\mathbf{s}_j),\\
&A_{i(N^{\Gamma}+j)}=\chi_x^D(\mathbf{p}_i)U_{xy}(\mathbf{p}_i,\mathbf{s}_j)+\chi_x^T(\mathbf{p}_i)T_{xy}(\mathbf{p}_i,\mathbf{s}_j),\\
&A_{(N^{\Gamma}+i)j}=\chi_y^D(\mathbf{p}_i)U_{yx}(\mathbf{p}_i,\mathbf{s}_j)+\chi_y^T(\mathbf{p}_i)T_{yx}(\mathbf{p}_i,\mathbf{s}_j),\\
&A_{(N^{\Gamma}+i)(N^{\Gamma}+j)}=\chi_y^D(\mathbf{p}_i)U_{yy}(\mathbf{p}_i,\mathbf{s}_j)+\chi_y^T(\mathbf{p}_i)T_{yy}(\mathbf{p}_i,\mathbf{s}_j),\quad i,j=1,2,\cdots,N^{\Gamma}.
\end{aligned} \tag{3.42}$$

$$x_i=\alpha_i,\ x_{(N^{\Gamma}+i)}=\beta_i,\quad i=1,2,\cdots,N^{\Gamma}, \tag{3.43}$$

$$\begin{aligned} g_i &= \chi^D(\mathbf{p}_i)u_x(\mathbf{p}_i) + \chi^T(\mathbf{p}_i)t_x(\mathbf{p}_i), \\ g_{(N^\Gamma+i)} &= \chi^D(\mathbf{p}_i)u_y(\mathbf{p}_i) + \chi^T(\mathbf{p}_i)t_y(\mathbf{p}_i), \end{aligned} \quad i = 1, 2, \cdots, N^\Gamma, \tag{3.44}$$

where the Dirichlet $\chi^D_\varsigma, \varsigma = x, y$ and the Neumann $\chi^T_\varsigma, \varsigma = x, y$ type of boundary conditions indicators are

$$\chi^D_\varsigma(\mathbf{p}) = \begin{cases} 1; & \mathbf{p} \in \Gamma^D \text{ in } \mathbf{i}_\varsigma \text{ direction}, \\ 0; & \mathbf{p} \notin \Gamma^D \text{ in } \mathbf{i}_\varsigma \text{ direction}, \end{cases} \quad \chi^T_\varsigma(\mathbf{p}) = \begin{cases} 1; & \mathbf{p} \in \Gamma^T \text{ in } \mathbf{i}_\varsigma \text{ direction}, \\ 0; & \mathbf{p} \notin \Gamma^T \text{ in } \mathbf{i}_\varsigma \text{ direction}. \end{cases} \tag{3.45}$$

3.5 Solution Procedure for a Bi-material

We generalize the previous discussion for a bi-material problem. Consider that the domain Ω is split into two parts, Ω^{I} and Ω^{II}, bounded by boundaries Γ^{I} and Γ^{II}, and a common interface boundary $\Gamma^{\mathrm{I}\cap\mathrm{II}}$, as shown in Figure 3.2. The material properties in both domains can be different in general. The governing equations are formally the same as Eqs. (3.3) (3.4) for isotropic materials and Eqs. (3.5) (3.6) for anisotropic materials with

$$\nu = \begin{cases} \nu^{\mathrm{I}} & \mathbf{p} \in \Omega^{\mathrm{I}}, \\ \nu^{\mathrm{II}} & \mathbf{p} \in \Omega^{\mathrm{II}}, \end{cases} \quad u_\varsigma = \begin{cases} u_\varsigma{}^{\mathrm{I}} & \mathbf{p} \in \Omega^{\mathrm{I}}, \\ u_\varsigma{}^{\mathrm{II}} & \mathbf{p} \in \Omega^{\mathrm{II}}, \end{cases} \quad \varsigma = x, y, \tag{3.46}$$

or

$$c_{ij} = \begin{cases} c_{ij}^{\mathrm{I}} & \mathbf{p} \in \Omega^{\mathrm{I}}, \\ c_{ij}^{\mathrm{II}} & \mathbf{p} \in \Omega^{\mathrm{II}}, \end{cases} \tag{3.47}$$

where indexes I and II denote material properties in the domains Ω^{I} and Ω^{II}, respectively. The boundary conditions at the outer boundaries are given in the form, given by the Eqs. (2.23) (2.24). The boundary conditions at the interface between two materials $\Gamma^{\mathrm{I}\cap\mathrm{II}}$ are given by the Eqs.(2.25) (2.26)

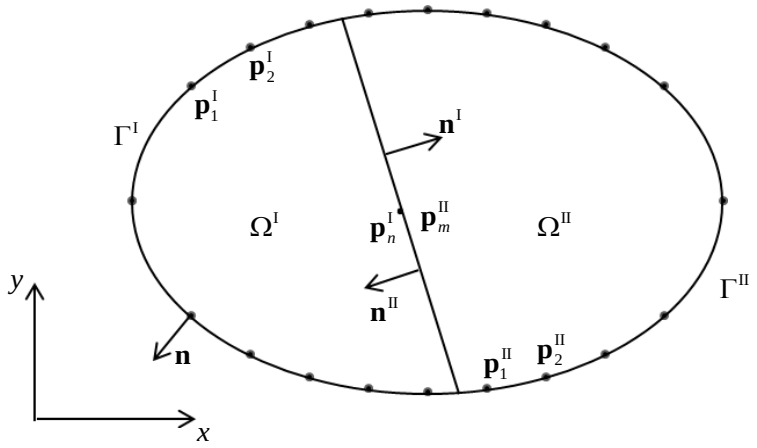

Figure 3.2**:** A bi-material with isotropic elastic or anisotropic elastic, however in general different, material properties in domains Ω^{I} and Ω^{II}.

The boundary $\Gamma^{\mathrm{I}} \bigcup \Gamma^{\mathrm{I} \cap \mathrm{II}}$ is discretized in $N^{\Gamma^{\mathrm{I}}} + N^{\Gamma^{\mathrm{I} \cap \mathrm{II}}}$ collocation points, and the boundary $\Gamma^{\mathrm{II}} \bigcup \Gamma^{\mathrm{I} \cap \mathrm{II}}$ into $N^{\Gamma^{\mathrm{II}}} + N^{\Gamma^{\mathrm{I} \cap \mathrm{II}}}$ collocation points, where $N^{\Gamma} = N^{\Gamma^{\mathrm{I}}} + N^{\Gamma^{\mathrm{II}}}$, and the number of collocation points on the interphase between two materials is $N^{\Gamma^{\mathrm{I} \cap \mathrm{II}}}$. The system (3.41) has in the bi-material problem a dimension of $2(N^{\Gamma} + N^{\Gamma^{\mathrm{I} \cap \mathrm{II}}})$, respectively.

4. Non-singular Method of Fundamental Solutions for Isotropic Problems

4.1 Introduction

The purpose of this chapter is development of a Non-singular Method of Fundamental Solutions (NMFS) for two-dimensional isotropic linear elasticity problems. The NMFS is based on the classical MFS with regularization of the singularities. This is achieved by replacement of the concentrated point sources by distributed sources over circular discs around the singularity, as originally suggested by [Liu (2010)] for potential problems. The Kelvin's fundamental solution is employed in collocation of the governing plane strain force balance equations. In case of the Dirichlet boundary conditions, the values of distributed sources are calculated directly and analytically. In case of Neumann boundary conditions, the respective desingularized values of the derivatives of the fundamental solution in the coordinate directions, as required in the calculations, are calculated indirectly from the considerations of two reference solutions of the linearly varying simple displacement fields. The developments represent a first use of NMFS for solid mechanics problems. With this, the main drawback of MFS for these types of problems is removed, since the artificial boundary is not present.

Two examples are used to demonstrate the feasibility and accuracy of the newly developed method. First one is about a single domain problem in two cases with a unit uniform normal load and a bending laod, respectively. In these two cases, the NMFS solutions are compared to the MFS solution and analytical solutions. The second example with two cases is about the bi-material problems with the normal stress and the shear stress. It shows a good agreement with the MFS.

4.2 Solution Procedure

The governing equations of the isotropic elastic problems are showin in Chapter 3 as Eqs. (3.3) (3.4) and Kelvin's fundamental solution in Eqs.(3.9) is used to solve the governing equations.

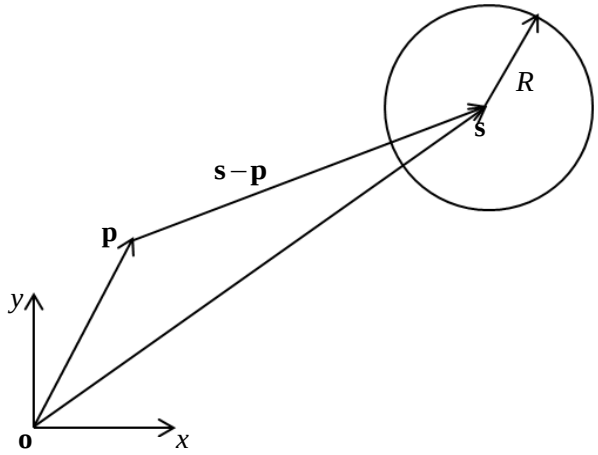

Figure 4.1: Distributed source on a disk $A(\mathbf{s},R)$ with radius R.

It can be shown that the following u_x and u_y satisfy the governing Eqs. (3.3)(3.4)

$$u_x(\mathbf{p}) = U_{xx}(\mathbf{p},\mathbf{s})\alpha + U_{xy}(\mathbf{p},\mathbf{s})\beta, \tag{4.1}$$

$$u_y(\mathbf{p}) = U_{yx}(\mathbf{p},\mathbf{s})\alpha + U_{yy}(\mathbf{p},\mathbf{s})\beta, \tag{4.2}$$

where α and β represent arbitrary constants. The fundamental solution $U_{\varsigma\xi}(\mathbf{p},\mathbf{s})$ is singular when $\mathbf{p}=\mathbf{s}$. We use the desingularization technique, proposed by Liu (2010), for evaluating the singular values. We modify his approach in the sense of preserving the original fundamental solution in all points except near the singularity, and by scaling the singularity with the area of the circle over which the desingularization integration is performed (see Figure 4.1). This allows us to treat the MFS and the NMFS in a formally same way. The desingularization (transformation of $U_{\varsigma\xi}(\mathbf{p},\mathbf{s})$ into $\tilde{U}_{\varsigma\xi}(\mathbf{p},\mathbf{s})$) is performed as follows

$$U'_{\varsigma\xi}(\mathbf{p},\mathbf{s}) = \begin{cases} U_{\varsigma\xi}(\mathbf{p},\mathbf{s}); & r > R, \\ \dfrac{1}{\pi R^2}\displaystyle\int_{A(\mathbf{s},R)} U_{\varsigma\xi}(\mathbf{p},\mathbf{s})\, dA; & r \le R, \end{cases} \tag{4.3}$$

where $A(\mathbf{s},R)$ represents a circle with radius R, centered around $\mathbf{s}$. The involved integrals can be calculated as follows (by using the integration in polar coordinates $p_x - s_x = r\cos\theta,\ \ p_y - s_y = r\sin\theta$)

$$\frac{1}{\pi R^2}\int_{A(\mathbf{s},R)} U_{\varsigma\xi}(\mathbf{p},\mathbf{s})dA = \frac{1}{\pi R^2}\int_0^{2\pi}\int_0^R U_{\varsigma\xi}(\mathbf{p},\mathbf{s})\, r\, d\theta dr, \tag{4.4}$$

$$\frac{1}{\pi R^2}\int\limits_{A(\mathbf{s},R)} U_{xx}(\mathbf{p},\mathbf{s})dA=\frac{1}{\pi R^2}\int\limits_{A(\mathbf{s},R)} U_{yy}(\mathbf{p},\mathbf{s})dA=\frac{1}{8\pi\mu(1-\nu)}\left((3-4\nu)\log\left(\frac{1}{R}\right)+2(1-\nu)\right), \tag{4.5}$$

$$\frac{1}{\pi R^2}\int\limits_{A(\mathbf{s},R)} U_{xy}(\mathbf{p},\mathbf{s})dA=\frac{1}{\pi R^2}\int\limits_{A(\mathbf{s},R)} U_{yx}(\mathbf{p},\mathbf{s})dA=0. \tag{4.6}$$

In order to impose smoothness of the desingularized value of the fundamental solution and its derivatives at point $r=R$, Liu (2010) used an additional term $-\frac{r^2}{4}$ inside the circular disc, with a remark in the discussion, that the desingularized fundamental solution inside the disc does not satisfy the governing equation. This is acceptable, since the dimension of R is usually much smaller than a typical distance between the boundary nodes. However, the values inside the disc, except at $r=0$ have never been used in his calculations. In a similar way, in order to match $U_{\varsigma\xi}(\mathbf{p},\mathbf{s})=U'_{\varsigma\xi}(\mathbf{p},\mathbf{s})$ and $\frac{\partial}{\partial p_\varsigma}U_{\varsigma\xi}(\mathbf{p},\mathbf{s})=\frac{\partial}{\partial p_\varsigma}U'_{\varsigma\xi}(\mathbf{p},\mathbf{s})$, when $r=R$, we modify

$$\tilde{U}_{\varsigma\xi}(\mathbf{p},\mathbf{s})=\begin{cases}U_{\varsigma\xi}(\mathbf{p},\mathbf{s}); & r>R,\\ \underset{\sim}{U}_{\varsigma\xi}(\mathbf{p},\mathbf{s}); & r\le R,\end{cases} \tag{4.7}$$

where

$$\begin{aligned}\underset{\sim}{U}_{xx}(\mathbf{p},\mathbf{s})=\frac{1}{8\pi\mu(1-\nu)}\Bigg((3-4\nu)\log\left(\frac{1}{R}\right)+2(1-\nu)\frac{R^2-r^2}{R^2}+\frac{(p_x-s_x)^2r^2}{R^4}\\ +\frac{\left[3(p_x-s_x)^2-(p_y-s_y)^2\right]\left[(R^2-r^2)r^2\right]}{2R^6}\Bigg),\end{aligned} \tag{4.8}$$

$$\begin{aligned}\underset{\sim}{U}_{yy}(\mathbf{p},\mathbf{s})=\frac{1}{8\pi\mu(1-\nu)}\Bigg((3-4\nu)\log\left(\frac{1}{R}\right)+2(1-\nu)\frac{R^2-r^2}{R^2}+\frac{(p_y-s_y)^2r^2}{R^4}\\ +\frac{\left[3(p_y-s_y)^2-(p_x-s_x)^2\right]\left[(R^2-r^2)r^2\right]}{2R^6}\Bigg),\end{aligned} \tag{4.9}$$

$$\begin{aligned}\underset{\sim}{U}_{xy}(\mathbf{p},\mathbf{s})&=\underset{\sim}{U}_{yx}(\mathbf{p},\mathbf{s})\\ &=\frac{1}{8\pi\mu(1-\nu)}\left[\frac{(p_x-s_x)(p_y-s_y)r^2}{R^4}+\frac{\left[2(p_x-s_x)(p_y-s_y)\right]\left[(R^2-r^2)r^2\right]}{R^6}\right].\end{aligned} \tag{4.10}$$

This forms than give smoothness of the desingularized and singular fundamental solution and their derivatives at $r=R$ and at the same time preserve the desingularized value at $r=0$. It can also be shown that the following u_x and u_y satisfy the governing Eqs. (3.3)(3.4)

$$u_x(\mathbf{p}) = \tilde{U}_{xx}(\mathbf{p},\mathbf{s})\alpha + \tilde{U}_{xy}(\mathbf{p},\mathbf{s})\beta, \tag{4.11}$$

$$u_y(\mathbf{p}) = \tilde{U}_{yx}(\mathbf{p},\mathbf{s})\alpha + \tilde{U}_{yy}(\mathbf{p},\mathbf{s})\beta, \quad \mathbf{p} \notin A(\mathbf{s}, R). \tag{4.12}$$

4.3 Discretisation

The solution of the problem is sought in the form

$$u_x(\mathbf{p}) = \sum_{n=1}^{N^\Gamma} \tilde{U}_{xx}(\mathbf{p},\mathbf{p}_n)\,\alpha_n + \sum_{n=1}^{N^\Gamma} \tilde{U}_{xy}(\mathbf{p},\mathbf{p}_n)\beta_n, \tag{4.13}$$

$$u_y(\mathbf{p}) = \sum_{n=1}^{N^\Gamma} \tilde{U}_{yx}(\mathbf{p},\mathbf{p}_n)\,\alpha_n + \sum_{n=1}^{N^\Gamma} \tilde{U}_{yy}(\mathbf{p},\mathbf{p}_n)\beta_n, \quad \mathbf{p} \notin \bigcup_{n=1}^{N^\Gamma} A(\mathbf{p}_n, R). \tag{4.14}$$

where N^Γ number of boundary nodes. Because of Eqs. (2.7)(2.8)(2.17)(2.18)(2.20) (2.21)(2.29), the traction can be expressed as

$$t_x(\mathbf{p}) = \sum_{n=1}^{N^\Gamma} \tilde{T}_{xx}(\mathbf{p},\mathbf{p}_n)\alpha_n + \sum_{n=1}^{N^\Gamma} \tilde{T}_{xy}(\mathbf{p},\mathbf{p}_n)\beta_n, \tag{4.15}$$

$$t_y(\mathbf{p}) = \sum_{n=1}^{N^\Gamma} \tilde{T}_{yx}(\mathbf{p},\mathbf{p}_n)\alpha_n + \sum_{n=1}^{N^\Gamma} \tilde{T}_{yy}(\mathbf{p},\mathbf{p}_n)\beta_n, \quad \mathbf{p} \notin \bigcup_{n=1}^{N^\Gamma} A(\mathbf{p}_n, R), \tag{4.16}$$

where

$$\begin{aligned}\tilde{T}_{xx}(\mathbf{p},\mathbf{p}_n) = &\left[\frac{2\mu(1-\nu)}{1-2\nu}\frac{\partial \tilde{U}_{xx}(\mathbf{p},\mathbf{p}_n)}{\partial p_x} + \frac{2\mu\nu}{1-2\nu}\frac{\partial \tilde{U}_{yx}(\mathbf{p},\mathbf{p}_n)}{\partial p_y}\right] n_{nx} \\ &+ \left[\mu\frac{\partial \tilde{U}_{xx}(\mathbf{p},\mathbf{p}_n)}{\partial p_y} + \mu\frac{\partial \tilde{U}_{yx}(\mathbf{p},\mathbf{p}_n)}{\partial p_x}\right] n_{ny},\end{aligned} \tag{4.17}$$

$$\begin{aligned}\tilde{T}_{xy}(\mathbf{p},\mathbf{p}_n) = &\left[\frac{2\mu(1-\nu)}{1-2\nu}\frac{\partial \tilde{U}_{xy}(\mathbf{p},\mathbf{p}_n)}{\partial p_x} + \frac{2\mu\nu}{1-2\nu}\frac{\partial \tilde{U}_{yy}(\mathbf{p},\mathbf{p}_n)}{\partial p_y}\right] n_{nx} \\ &+ \left[\mu\frac{\partial \tilde{U}_{xy}(\mathbf{p},\mathbf{p}_n)}{\partial p_y} + \mu\frac{\partial \tilde{U}_{yy}(\mathbf{p},\mathbf{p}_n)}{\partial p_x}\right] n_{ny},\end{aligned} \tag{4.18}$$

$$\begin{aligned}\tilde{T}_{yx}(\mathbf{p},\mathbf{p}_n) = &\left[\mu\frac{\partial \tilde{U}_{yx}(\mathbf{p},\mathbf{p}_n)}{\partial p_x} + \mu\frac{\partial \tilde{U}_{xx}(\mathbf{p},\mathbf{p}_n)}{\partial p_y}\right] n_{nx} \\ &+ \left[\frac{2\mu(1-\nu)}{1-2\nu}\frac{\partial \tilde{U}_{yx}(\mathbf{p},\mathbf{p}_n)}{\partial p_y} + \frac{2\mu\nu}{1-2\nu}\frac{\partial \tilde{U}_{xx}(\mathbf{p},\mathbf{p}_n)}{\partial p_x}\right] n_{ny},\end{aligned} \tag{4.19}$$

$$\tilde{T}_{yy}(\mathbf{p},\mathbf{p}_n)=\left[\mu\frac{\partial\tilde{U}_{yy}(\mathbf{p},\mathbf{p}_n)}{\partial p_x}+\mu\frac{\partial\tilde{U}_{xy}(\mathbf{p},\mathbf{p}_n)}{\partial p_y}\right]n_{nx} + \left[\frac{2\mu(1-\nu)}{1-2\nu}\frac{\partial\tilde{U}_{yy}(\mathbf{p},\mathbf{p}_n)}{\partial p_y}+\frac{2\mu\nu}{1-2\nu}\frac{\partial\tilde{U}_{xy}(\mathbf{p},\mathbf{p}_n)}{\partial p_x}\right]n_{ny}, \tag{4.20}$$

where $\mathbf{p}_n$ represent N^Γ points, placed on the physical boundary. The explicit expressions, used in calculation of the traction boundary conditions, are

$$\frac{\partial\tilde{U}_{xx}(\mathbf{p},\mathbf{p}_n)}{\partial p_x}=\frac{1}{8\pi\mu(1-\nu)}\left[(4\nu-3)\frac{p_x-p_{nx}}{r^2}+\frac{2(p_x-p_{nx})(p_y-p_{ny})^2}{r^4}\right], \tag{4.21}$$

$$\frac{\partial\tilde{U}_{xx}(\mathbf{p},\mathbf{p}_n)}{\partial p_y}=\frac{1}{8\pi\mu(1-\nu)}\left[(4\nu-3)\frac{p_y-p_{ny}}{r^2}-\frac{2(p_y-p_{ny})(p_x-p_{nx})^2}{r^4}\right], \tag{4.22}$$

$$\frac{\partial\tilde{U}_{xy}(\mathbf{p},\mathbf{p}_n)}{\partial p_x}=\frac{\partial\tilde{U}_{yx}(\mathbf{p},\mathbf{p}_n)}{\partial p_x}=\frac{1}{8\pi\mu(1-\nu)}\frac{(p_y-p_{ny})[(p_y-p_{ny})^2-(p_x-p_{nx})^2]}{r^4}, \tag{4.23}$$

$$\frac{\partial\tilde{U}_{yy}(\mathbf{p},\mathbf{p}_n)}{\partial p_x}=\frac{1}{8\pi\mu(1-\nu)}\left[(4\nu-3)\frac{(p_x-p_{nx})}{r^2}-\frac{2(p_x-p_{nx})(p_y-p_{ny})^2}{r^4}\right], \tag{4.24}$$

$$\frac{\partial\tilde{U}_{yy}(\mathbf{p},\mathbf{p}_n)}{\partial p_y}=\frac{1}{8\pi\mu(1-\nu)}\left[(4\nu-3)\frac{(p_y-p_{ny})}{r^2}+\frac{2(p_y-p_{ny})(p_x-p_{nx})^2}{r^4}\right], \tag{4.25}$$

$$\frac{\partial\tilde{U}_{xy}(\mathbf{p},\mathbf{p}_n)}{\partial p_y}=\frac{\partial\tilde{U}_{yx}(\mathbf{p},\mathbf{p}_n)}{\partial p_y}=\frac{1}{8\pi\mu(1-\nu)}\frac{(p_x-p_{nx})[(p_x-p_{nx})^2-(p_y-p_{ny})^2]}{r^4}. \tag{4.26}$$

except at $\mathbf{p}=\mathbf{s}$, where the derivatives are calculated in an indirect way. The coefficients α_n and β_n are calculated from a system of $2N^\Gamma$ algebraic equations

$$\mathbf{A}\mathbf{x}=\mathbf{g}, \tag{4.27}$$

where $\mathbf{A}$ stands for a $2N^\Gamma\times 2N^\Gamma$ matrix with the entries A_{ij}, $\mathbf{x}$ is a $2N^\Gamma\times 1$ vector with the entries x_i, and $\mathbf{g}$ is a $2N^\Gamma\times 1$ vector with entries g_i,

$$\begin{aligned}
A_{ij}&=\chi_x^D(\mathbf{p}_i)\tilde{U}_{xx}(\mathbf{p}_i,\mathbf{p}_j)+\chi_x^T(\mathbf{p}_i)\tilde{T}_{xx}(\mathbf{p}_i,\mathbf{p}_j),\\
A_{i(N^\Gamma+j)}&=\chi_x^D(\mathbf{p}_i)\tilde{U}_{xy}(\mathbf{p}_i,\mathbf{p}_j)+\chi_x^T(\mathbf{p}_i)\tilde{T}_{xy}(\mathbf{p}_i,\mathbf{p}_j),\\
A_{(N^\Gamma+i)j}&=\chi_y^D(\mathbf{p}_i)\tilde{U}_{yx}(\mathbf{p}_i,\mathbf{p}_j)+\chi_y^T(\mathbf{p}_i)\tilde{T}_{yx}(\mathbf{p}_i,\mathbf{p}_j),\\
A_{(N^\Gamma+i)(N^\Gamma+j)}&=\chi_y^D(\mathbf{p}_i)\tilde{U}_{yy}(\mathbf{p}_i,\mathbf{p}_j)+\chi_y^T(\mathbf{p}_i)\tilde{T}_{yy}(\mathbf{p}_i,\mathbf{p}_j),\qquad i,j=1,2,\cdots,N^\Gamma.
\end{aligned} \tag{4.28}$$

$$x_i=\alpha_i,\ x_{(N^\Gamma+i)}=\beta_i,\qquad i=1,2,\cdots,N^\Gamma, \tag{4.29}$$

$$\begin{aligned}
g_i&=\chi^D(\mathbf{p}_i)u_x(\mathbf{p}_i)+\chi^T(\mathbf{p}_i)t_x(\mathbf{p}_i),\\
g_{(N^\Gamma+i)}&=\chi^D(\mathbf{p}_i)u_y(\mathbf{p}_i)+\chi^T(\mathbf{p}_i)t_y(\mathbf{p}_i),\qquad i=1,2,\cdots,N^\Gamma,
\end{aligned} \tag{4.30}$$

where the Dirichlet $\chi_\varsigma^D, \varsigma = x, y$ and the Neumann $\chi_\varsigma^T, \varsigma = x, y$ type of boundary conditions indicators are

$$\chi_\varsigma^D(\mathbf{p}) = \begin{cases} 1; & \mathbf{p} \in \Gamma^D \text{ in } \mathbf{i}_\varsigma \text{ direction}, \\ 0; & \mathbf{p} \notin \Gamma^D \text{ in } \mathbf{i}_\varsigma \text{ direction}, \end{cases} \quad \chi_\varsigma^T(\mathbf{p}) = \begin{cases} 1; & \mathbf{p} \in \Gamma^T \text{ in } \mathbf{i}_\varsigma \text{ direction}, \\ 0; & \mathbf{p} \notin \Gamma^T \text{ in } \mathbf{i}_\varsigma \text{ direction}. \end{cases} \tag{4.31}$$

The diagonal terms $\tilde{T}_{\varsigma\xi}(\mathbf{p}_m, \mathbf{p}_m)$, $\varsigma, \xi = x, y, m = 1, ..., N^\Gamma$ in Eqs. (4.15)(4.16) are in case of NMFS determined indirectly for collocation points on Γ^T. For this purpose, the method proposed by Šarler (2009) for potential problems, is applied to determine the diagonal terms in these equations. We assume two simple solutions in this approach, modified to cope with elasticity problems. The first simple solution is $\bar{u}_x(\mathbf{p}) = p_x + c_x, \bar{u}_y(\mathbf{p}) = 0,$ everywhere, and c_x denotes a constant. It follows from the first solution

$$\frac{\partial u_x(\mathbf{p})}{\partial p_x} = 1, \quad \frac{\partial u_x(\mathbf{p})}{\partial p_y} = \frac{\partial u_y(\mathbf{p})}{\partial p_x} = \frac{\partial u_y(\mathbf{p})}{\partial p_y} = 0. \tag{4.32}$$

It follows from Eq. (4.13) for the first solution

$$\frac{\partial \bar{u}_x(\mathbf{p})}{\partial p_x} = \sum_{n=1}^{N^\Gamma} \frac{\partial \tilde{U}_{xx}(\mathbf{p}, \mathbf{p}_n)}{\partial p_x} \alpha_n^1 + \sum_{n=1}^{N^\Gamma} \frac{\partial \tilde{U}_{xy}(\mathbf{p}, \mathbf{p}_n)}{\partial p_x} \beta_n^1 = 1, \tag{4.33}$$

$$\frac{\partial \bar{u}_x(\mathbf{p})}{\partial p_y} = \sum_{n=1}^{N^\Gamma} \frac{\partial \tilde{U}_{xx}(\mathbf{p}, \mathbf{p}_n)}{\partial p_y} \alpha_n^1 + \sum_{n=1}^{N^\Gamma} \frac{\partial \tilde{U}_{xy}(\mathbf{p}, \mathbf{p}_n)}{\partial p_y} \beta_n^1 = 0. \tag{4.34}$$

It follows from Eq. (4.14) for the first solution

$$\frac{\partial \bar{u}_y(\mathbf{p})}{\partial p_x} = \sum_{n=1}^{N^\Gamma} \frac{\partial \tilde{U}_{yx}(\mathbf{p}, \mathbf{p}_n)}{\partial p_x} \alpha_n^1 + \sum_{n=1}^{N^\Gamma} \frac{\partial \tilde{U}_{yy}(\mathbf{p}, \mathbf{p}_n)}{\partial p_x} \beta_n^1 = 0, \tag{4.35}$$

$$\frac{\partial \bar{u}_y(\mathbf{p})}{\partial p_y} = \sum_{n=1}^{N^\Gamma} \frac{\partial \tilde{U}_{yx}(\mathbf{p}, \mathbf{p}_n)}{\partial p_y} \alpha_n^1 + \sum_{n=1}^{N^\Gamma} \frac{\partial \tilde{U}_{yy}(\mathbf{p}, \mathbf{p}_n)}{\partial p_y} \beta_n^1 = 0. \tag{4.36}$$

We solve these equations for the corresponding α_n^1 and β_n^1. The second simple solution is $\bar{u}_x(\mathbf{p}) = 0, \bar{u}_y(\mathbf{p}) = p_y + c_y,$ everywhere, and c_y denotes a constant. It follows from the second solution

$$\frac{\partial u_x(\mathbf{p})}{\partial p_x} = \frac{\partial u_x(\mathbf{p})}{\partial p_y} = \frac{\partial u_y(\mathbf{p})}{\partial p_x} = 0, \quad \frac{\partial u_y(\mathbf{p})}{\partial p_y} = 1. \tag{4.37}$$

It follows from Eq. (4.13) for the second solution

$$\frac{\partial \overline{u}_x(\mathbf{p})}{\partial p_x} = \sum_{n=1}^{N^\Gamma} \frac{\partial \tilde{U}_{xx}(\mathbf{p},\mathbf{p}_n)}{\partial p_x} \alpha_n^2 + \sum_{n=1}^{N^\Gamma} \frac{\partial \tilde{U}_{xy}(\mathbf{p},\mathbf{p}_n)}{\partial p_x} \beta_n^2 = 0, \tag{4.38}$$

$$\frac{\partial \overline{u}_x(\mathbf{p})}{\partial p_y} = \sum_{n=1}^{N^\Gamma} \frac{\partial \tilde{U}_{xx}(\mathbf{p},\mathbf{p}_n)}{\partial p_y} \alpha_n^2 + \sum_{n=1}^{N^\Gamma} \frac{\partial \tilde{U}_{xy}(\mathbf{p},\mathbf{p}_n)}{\partial p_y} \beta_n^2 = 0. \tag{4.39}$$

It follows from Eq. (4.14) for the second solution

$$\frac{\partial \overline{u}_y(\mathbf{p})}{\partial p_x} = \sum_{n=1}^{N^\Gamma} \frac{\partial \tilde{U}_{yx}(\mathbf{p},\mathbf{p}_n)}{\partial p_x} \alpha_n^2 + \sum_{n=1}^{N^\Gamma} \frac{\partial \tilde{U}_{yy}(\mathbf{p},\mathbf{p}_n)}{\partial p_x} \beta_n^2 = 0, \tag{4.40}$$

$$\frac{\partial \overline{u}_y(\mathbf{p})}{\partial p_y} = \sum_{n=1}^{N^\Gamma} \frac{\partial \tilde{U}_{yx}(\mathbf{p},\mathbf{p}_n)}{\partial p_y} \alpha_n^2 + \sum_{n=1}^{N^\Gamma} \frac{\partial \tilde{U}_{yy}(\mathbf{p},\mathbf{p}_n)}{\partial p_y} \beta_n^2 = 1. \tag{4.41}$$

We solve them for the corresponding α_n^2 and β_n^2. The unknown 8 values of the derivatives of the fundamental solutions can respectively be calculated as follows. Eqs. (4.33)(4.38) are used to obtain

$$\frac{\partial \tilde{U}_{xx}(\mathbf{p}_m,\mathbf{p}_m)}{\partial p_x} = \frac{1}{\alpha_m^1\beta_m^2 - \alpha_m^2\beta_m^1}\Bigg[\beta_m^2 - \sum_{n=1,n\neq m}^{N^\Gamma}\left(\left(\alpha_n^1\beta_m^2 - \alpha_n^2\beta_m^1\right)\frac{\partial \tilde{U}_{xx}(\mathbf{p}_m,\mathbf{p}_n)}{\partial p_x} + \left(\beta_n^1\beta_m^2 - \beta_n^2\beta_m^1\right)\frac{\partial \tilde{U}_{xy}(\mathbf{p}_m,\mathbf{p}_n)}{\partial p_x}\right)\Bigg], \tag{4.42}$$

$$\frac{\partial \tilde{U}_{xy}(\mathbf{p}_m,\mathbf{p}_m)}{\partial p_x} = \frac{1}{\alpha_m^2\beta_m^1 - \alpha_m^1\beta_m^2}\Bigg[\alpha_m^2 - \sum_{n=1,n\neq m}^{N^\Gamma}\left(\left(\alpha_n^1\alpha_m^2 - \alpha_n^2\alpha_m^1\right)\frac{\partial \tilde{U}_{xx}(\mathbf{p}_m,\mathbf{p}_n)}{\partial p_x} + \left(\beta_n^1\alpha_m^2 - \beta_n^2\alpha_m^1\right)\frac{\partial \tilde{U}_{xy}(\mathbf{p}_m,\mathbf{p}_n)}{\partial p_x}\right)\Bigg]. \tag{4.43}$$

Eqs. (4.34)(4.39) are used to obtain

$$\frac{\partial \tilde{U}_{xx}(\mathbf{p}_m,\mathbf{p}_m)}{\partial p_y} = \frac{1}{\alpha_m^1\beta_m^2 - \alpha_m^2\beta_m^1}\Bigg[-\sum_{n=1,n\neq m}^{N^\Gamma}\left(\left(\alpha_n^1\beta_m^2 - \alpha_n^2\beta_m^1\right)\frac{\partial \tilde{U}_{xx}(\mathbf{p}_m,\mathbf{p}_n)}{\partial p_y} + \left(\beta_n^1\beta_m^2 - \beta_n^2\beta_m^1\right)\frac{\partial \tilde{U}_{xy}(\mathbf{p}_m,\mathbf{p}_n)}{\partial p_y}\right)\Bigg], \tag{4.44}$$

$$\frac{\partial \tilde{U}_{xy}(\mathbf{p}_m,\mathbf{p}_m)}{\partial p_y} = \frac{1}{\alpha_m^2\beta_m^1-\alpha_m^1\beta_m^2}\left[-\sum_{n=1,n\neq m}^{N^\Gamma}\left(\left(\alpha_n^1\alpha_m^2-\alpha_n^2\alpha_m^1\right)\frac{\partial \tilde{U}_{xx}(\mathbf{p}_m,\mathbf{p}_n)}{\partial p_y}+\left(\beta_n^1\alpha_m^2-\beta_n^2\alpha_m^1\right)\frac{\partial \tilde{U}_{xy}(\mathbf{p}_m,\mathbf{p}_n)}{\partial p_y}\right)\right]. \tag{4.45}$$

The Eqs. (4.35)(4.40) are used to obtain

$$\frac{\partial \tilde{U}_{yx}(\mathbf{p}_m,\mathbf{p}_m)}{\partial p_x} = \frac{1}{\alpha_m^1\beta_m^2-\alpha_m^2\beta_m^1}\left[-\sum_{n=1,n\neq m}^{N^\Gamma}\left(\left(\alpha_n^1\beta_m^2-\alpha_n^2\beta_m^1\right)\frac{\partial \tilde{U}_{yx}(\mathbf{p}_m,\mathbf{p}_n)}{\partial p_x}+\left(\beta_n^1\beta_m^2-\beta_n^2\beta_m^1\right)\frac{\partial \tilde{U}_{yy}(\mathbf{p}_m,\mathbf{p}_n)}{\partial p_x}\right)\right], \tag{4.46}$$

$$\frac{\partial \tilde{U}_{yy}(\mathbf{p}_m,\mathbf{p}_m)}{\partial p_x} = \frac{1}{\alpha_m^2\beta_m^1-\alpha_m^1\beta_m^2}\left[-\sum_{n=1,n\neq m}^{N^\Gamma}\left(\left(\alpha_n^1\alpha_m^2-\alpha_n^2\alpha_m^1\right)\frac{\partial \tilde{U}_{yx}(\mathbf{p}_m,\mathbf{p}_n)}{\partial p_x}+\left(\beta_n^1\alpha_m^2-\beta_n^2\alpha_m^1\right)\frac{\partial \tilde{U}_{yy}(\mathbf{p}_m,\mathbf{p}_n)}{\partial p_x}\right)\right]. \tag{4.47}$$

The Eqs. (4.36)(4.41) are used to obtain

$$\frac{\partial \tilde{U}_{yx}(\mathbf{p}_m,\mathbf{p}_m)}{\partial p_y} = \frac{1}{\alpha_m^1\beta_m^2-\alpha_m^2\beta_m^1}\left[-\beta_m^1 - \sum_{n=1,n\neq m}^{N^\Gamma}\left(\left(\alpha_n^1\beta_m^2-\alpha_n^2\beta_m^1\right)\frac{\partial \tilde{U}_{yx}(\mathbf{p}_m,\mathbf{p}_n)}{\partial p_y}+\left(\beta_n^1\beta_m^2-\beta_n^2\beta_m^1\right)\frac{\partial \tilde{U}_{yy}(\mathbf{p}_m,\mathbf{p}_n)}{\partial p_y}\right)\right], \tag{4.48}$$

$$\frac{\partial \tilde{U}_{yy}(\mathbf{p}_m,\mathbf{p}_m)}{\partial p_y} = \frac{1}{\alpha_m^2\beta_m^1-\alpha_m^1\beta_m^2}\left[-\alpha_m^1 - \sum_{n=1,n\neq m}^{N^\Gamma}\left(\left(\alpha_n^1\alpha_m^2-\alpha_n^2\alpha_m^1\right)\frac{\partial \tilde{U}_{yx}(\mathbf{p}_m,\mathbf{p}_n)}{\partial p_y}+\left(\beta_n^1\alpha_m^2-\beta_n^2\alpha_m^1\right)\frac{\partial \tilde{U}_{yy}(\mathbf{p}_m,\mathbf{p}_n)}{\partial p_y}\right)\right]. \tag{4.49}$$

The selection of the constants c_x and c_y in reference solutions need some care. They should be selected in such a way that the denominators in the fractions on the right hand side of Eqs. (4.42)-(4.49) are non-zero. By knowing all the elements A_{ij} and g_i

of the system (4.27), we can determine the values of x_i. (i.e. α_n and β_n). Afterwards, we can calculate the solution of the governing equation from

$$u_\varsigma(\mathbf{p}) = \sum_{n=1}^{N^\Gamma} \tilde{U}_{\varsigma x}(\mathbf{p},\mathbf{p}_n)\alpha_n + \sum_{n=1}^{N^\Gamma} \tilde{U}_{\varsigma y}(\mathbf{p},\mathbf{p}_n)\beta_n, \quad \varsigma = x, y, \tag{4.50}$$

where $\mathbf{p}$ is any point inside the domain or on the boundary. Solution procedure for a bi-material is the same as described in Chapter 3.5.

4.4 Numerical Examples

4.4.1 Example 4.1: Single Domain Problem

In the Example 4.1, we consider a square with the side length $a = 2$ m centered around $p_x = 0$ m, $p_y = 0$ m. Elastic media is defined by $E = 1\ \mathrm{N/m^2}$, $\nu = 0.3$.

Case 4.1.1: a Unit Uniform Normal Load Case

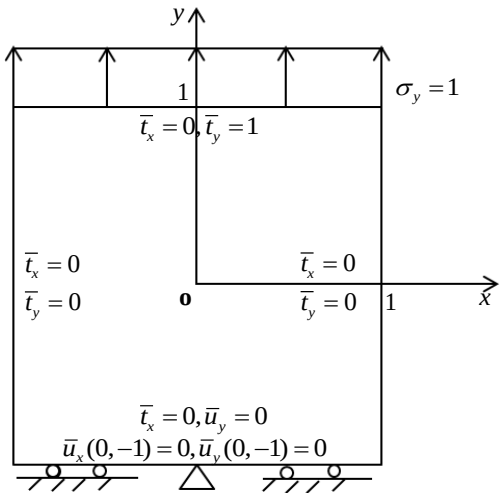

Figure 4.2: Case 4.1.1. Scheme of square subject to a unit uniform normal load.

We consider a solution of the Navier's equations in this square subject to the boundary conditions $\bar{u}_x = 0$ m, $\bar{u}_y = 0$ m at point $p_x = 0$ m, $p_y = -1$ m, and $\bar{t}_x = 0\ \mathrm{N/m^2}$, $\bar{u}_y = 0$ m on all other points of the south side of the square with $p_y = -1$ m. On the north side of the square with $p_y = 1$ m, uniform traction is prescribed $\bar{t}_x = 0\ \mathrm{N/m^2}$, $\bar{t}_y = 1\ \mathrm{N/m^2}$, and on the east $p_x = 1$ m and west $p_x = -1$ m sides $\bar{t}_x = 0\ \mathrm{N/m^2}$, $\bar{t}_y = 0\ \mathrm{N/m^2}$ is set (see Figure 4.2). Such a unit uniform normal (in-plane) load acting along a single side of the square, was previously studied by Huang and Cruse (1994) when developing non-singular traction boundary integral equations in elasticity, and Panzeca, Fujita Yashima and Salerno (2001) by developing symmetric boundary element Galerkin method. The analytical solution is

$$u_x = -0.39\,p_x, \quad u_y = 0.91(p_y + 1), \tag{4.51}$$

$$\sigma_x = 0, \quad \sigma_y = 1, \quad \sigma_{xy} = 0. \tag{4.52}$$

A plot of the deformation, obtained with the analytical solution and the numerical solutions with MFS and NMFS is shown in Figure 4.3 for the case with 100 nodes. The distance of the fictitious boundary from the true boundary for the MFS is set $R_M = 5d$, where d is the smallest distance between two nodes on the boundary. The radius of the circular disk for the distributed area source covering each node is set to $R = d/5$. The simple solution constants used in calculation of the diagonal coefficients are defined as $c_x = c_y = 4\,\mathrm{m}$ (see Figure A in Appendix). When selecting $c_x = c_y = 0\,\mathrm{m}$ (see Figure B in Appendix), we obtain for $\alpha_m^1\beta_m^2 - \alpha_m^2\beta_m^1$ a numerical value -7.8413×10^{-18} for point $p_x = 0\,\mathrm{m}$, $p_y = 1\,\mathrm{m}$ (both solutions have $\bar{u}_x(\mathbf{p}) = 0\,\mathrm{m}$ in this point) and the solution obtained in this way is wrong (see Figure C in Appendix). So the two reference solutions should be selected in such a way that $\alpha_m^1\beta_m^2 - \alpha_m^2\beta_m^1 \neq 0,\ \alpha_m^2\beta_m^1 - \alpha_m^1\beta_m^2 \neq 0, m = 1,2,...,N$.

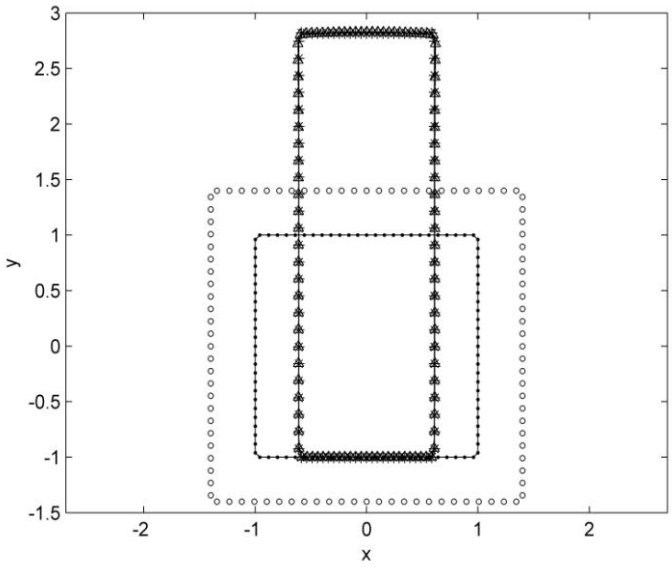

Figure 4.3: Case 4.1.1. The analytical solution and the numerical solution of MFS and NMFS with $N^{\Gamma} = 100$ ($\bullet$: collocation points; $\circ$: source points in MFS; $+$: analytical solution; $\times$: MFS solution; $\triangle$: NMFS solution).

The solution on boundary points are computed and compared with the analytical solutions. The root mean square (RMS) errors of the numerical solution are defined as

$$e_\varsigma = \sqrt{\frac{1}{N}\sum_{n=1}^{N}(u_{\varsigma n} - u_{\varsigma n})^2}, \quad \varsigma = x, y. \tag{4.53}$$

where $\underline{u}_{\varsigma n}$ and $u_{\varsigma n}, (\varsigma = x, y)$ is the analytical and the numerical solution, respectively. The number of boundary nodes used is from 100 to 1924 (Odd-number of points should be used on the side in uniform discretization, since the middle point is fixed at $p_y = -1\,\mathrm{m}$).

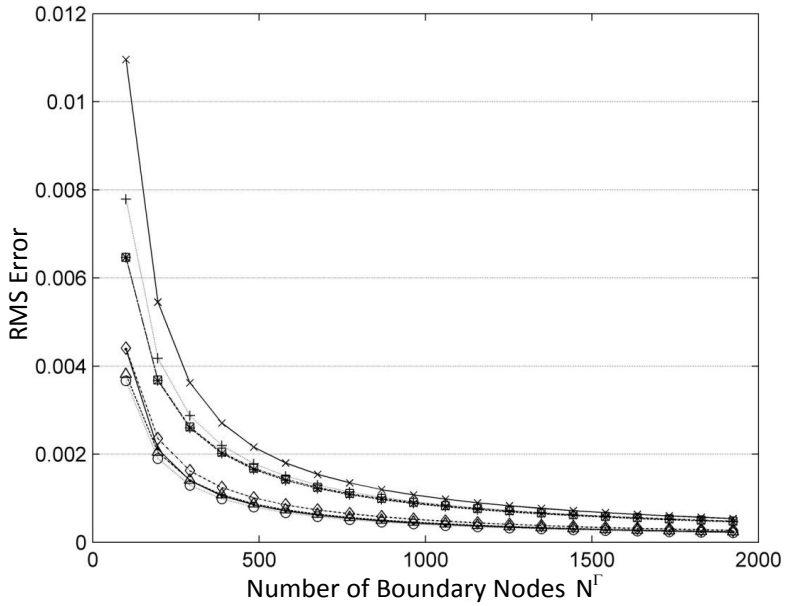

Figure 4.4: Case 4.1.1. The relationship between the RMS errors and the number of boundary nodes for different R, calculated by NMFS (e_x: • $R = d/3$, ◦ $R = d/4$, △ $R = d/5$, ◊ $R = d/6$; e_y: × $R = d/3$, + $R = d/4$, * $R = d/5$, □ $R = d/6$).

Figure 4.4 shows RMS errors of the results obtained using the NMFS with different R. The errors are already less than 10^{-2} with $N^{\Gamma} = 196$ and the solution converges to the analytical solution with the increasing number of the nodes. The e_x and e_y are increasing with the decreasing R when $R < d/5$ (see Table 4.1). A comparison of the NMFS results with the MFS results is shown in 2 for $R = d/5$. Here it should be noted, that the MFS solution error is rather small, however the convergence is not uniform. This fact is due to the choice of the artificial boundary position, that was for all node arrangements $R_M = 5d$, and thus most probably not optimally varying.

Table 4.1**:** Case 4.1.1. RMS errors of NMFS solution as a function of different R.

Number of boundary nodes (N^{Γ})	$R = d/3$		$R = d/4$		$R = d/5$		$R = d/6$	
	e_x ($\times 10^{-2}$)	e_y ($\times 10^{-2}$)	e_x ($\times 10^{-2}$)	e_y ($\times 10^{-2}$)	e_x ($\times 10^{-2}$)	e_y ($\times 10^{-2}$)	e_x ($\times 10^{-2}$)	e_y ($\times 10^{-2}$)
100	0.4384	1.0959	0.3664	0.7791	0.3812	0.6467	0.4404	0.6466
196	0.2116	0.5453	0.1902	0.4175	0.2044	0.3672	0.2355	0.3681
292	0.1401	0.3620	0.1295	0.2873	0.1408	0.2595	0.1622	0.2616
388	0.1054	0.2707	0.0986	0.2197	0.1078	0.2017	0.1241	0.2042
484	0.0848	0.2162	0.0798	0.1782	0.0875	0.1654	0.1007	0.1681
580	0.0712	0.1799	0.0672	0.1500	0.0737	0.1405	0.0848	0.1431
676	0.0614	0.1541	0.0581	0.1297	0.0638	0.1222	0.0733	0.1247
772	0.0542	0.1347	0.0513	0.1142	0.0562	0.1082	0.0646	0.1107
868	0.0485	0.1197	0.0459	0.1021	0.0503	0.0972	0.0578	0.0995
964	0.0439	0.1077	0.0416	0.0924	0.0455	0.0882	0.0523	0.0905
1060	0.0402	0.0979	0.0380	0.0844	0.0416	0.0808	0.0477	0.0830
1156	0.0371	0.0897	0.0350	0.0776	0.0383	0.0746	0.0439	0.0767
1252	0.0344	0.0828	0.0325	0.0719	0.0355	0.0693	0.0407	0.0712
1348	0.0322	0.0769	0.0303	0.0670	0.0331	0.0647	0.0379	0.0666
1444	0.0302	0.0718	0.0284	0.0627	0.0310	0.0606	0.0355	0.0625
1540	0.0285	0.0673	0.0268	0.0589	0.0292	0.0571	0.0334	0.0589
1636	0.0269	0.0633	0.0253	0.0556	0.0275	0.0540	0.0315	0.0557
1732	0.0255	0.0598	0.0240	0.0526	0.0261	0.0512	0.0298	0.0528
1828	0.0243	0.0567	0.0228	0.0500	0.0248	0.0486	0.0283	0.0502
1924	0.0232	0.0538	0.0217	0.0476	0.0236	0.0464	0.0269	0.0479

Table 4.2: Case 4.1.1. RMS errors of MFS and NMFS solutions with $R_M = 5d$, $R = d/5$.

Number of boundary nodes (N^Γ)	MFS		NMFS	
	$e_x(\times 10^{-2})$	$e_y(\times 10^{-2})$	$e_x(\times 10^{-2})$	$e_y(\times 10^{-2})$
100	0.0001	0.0001	0.3812	0.6467
196	0.0000	0.0000	0.2044	0.3672
292	0.0000	0.0000	0.1408	0.2595
388	0.0067	0.0073	0.1078	0.2017
484	0.0086	0.0055	0.0875	0.1654
580	0.0001	0.0001	0.0737	0.1405
676	0.0000	0.0000	0.0638	0.1222
772	0.0005	0.0002	0.0562	0.1082
868	0.0007	0.0003	0.0503	0.0972
964	0.0181	0.0139	0.0455	0.0882
1060	0.0849	0.0556	0.0416	0.0808
1156	0.0002	0.0004	0.0383	0.0746
1252	0.0004	0.0005	0.0355	0.0693
1348	0.1234	0.0840	0.0331	0.0647
1444	0.0003	0.0003	0.0310	0.0606
1540	0.0003	0.0004	0.0292	0.0571
1636	0.0001	0.0002	0.0275	0.0540
1732	0.0000	0.0001	0.0261	0.0512
1828	0.0001	0.0001	0.0248	0.0486
1924	0.3393	0.2868	0.0236	0.0464

Case 4.1.2: A Bending Load Case

In the case 4.1.2, the boundary conditions on east, west, and south sides of the square are also the same as in the first example. On the north side of the square with $p_y = 1\,\text{m}$, bending traction is prescribed $\bar{t}_x = 0\ \text{N/m}^2$, $\bar{t}_y = (p_x/\text{m})\ \text{N/m}^2$ (see Figure 4.5). Such a bending load, acting along a single side of the plate, was previously studied (like Case 4.1.1) by Huang and Cruse (1994) and Panzeca, Fujita Yashima and Salerno (2001). The analytical solution is

$$u_x = -0.195 p_x^{\,2} - 0.445(p_y + 1)^2, \quad u_y = 0.91 p_x (p_y + 1), \tag{4.54}$$

$$\sigma_x = 0, \quad \sigma_y = p_x, \quad \sigma_{xy} = 0. \tag{4.55}$$

A plot of the deformation, obtained with the analytical solution and the numerical solutions with MFS and NMFS is shown in Figure 4.6 for the case with 100 nodes. R_M, R, c_x, c_y, are set the same as in Case 4.1. The number of boundary nodes used is from 100 to 1924 and the results are shown in Table 4.4.

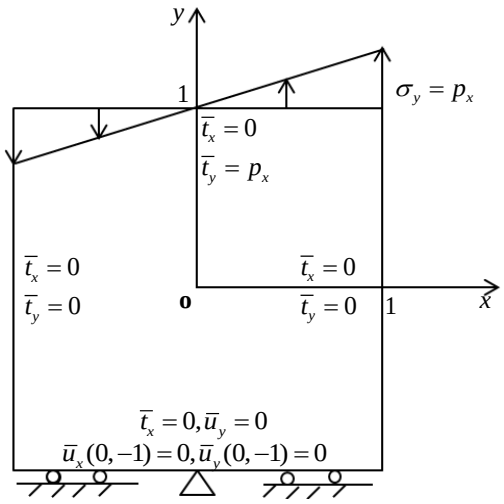

Figure 4.5: Case 4.1.2. A square plate subjected to a bending load.

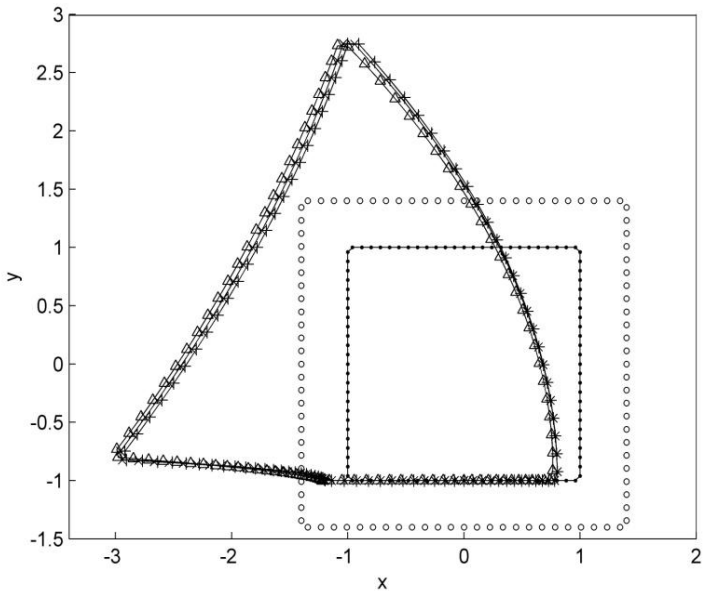

Figure 4.6: Case 4.1.2. The analytical solution and the numerical solution of MFS and NMFS with $N^{\Gamma} = 100$ ($\bullet$: collocation points; $\circ$: source points in MFS; $+$: analytical solution; $\times$: MFS solution; $\triangle$: NMFS solution).

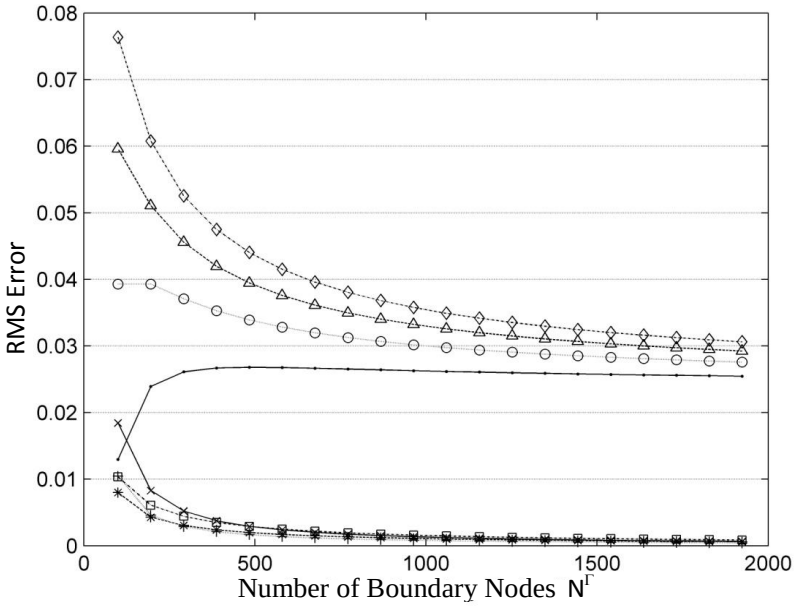

Figure 4.7: Case 4.1.2. The relationship between the RMS and the number of boundary nodes for different R, calculated by NMFS (e_x: • $R = d/3$, ◦ $R = d/4$, △ $R = d/5$, ◊ $R = d/6$; e_y: × $R = d/3$, + $R = d/4$, * $R = d/5$, □ $R = d/6$).

Figure 4.7 shows RMS errors of the results obtained by using the NMFS for different R. The solution converges to the analytical solution with the increasing number of the nodes, except in case with $R = d/3$. The e_x and e_y are increasing with the decreasing of R when $R < d/5$ (see Table 4.3). A comparison of the NMFS results with the MFS results is shown in Table 4.4 for $R = d/5$. Here it should be noted, that the MFS solution error is rather small, however the convergence is not uniform. This fact it is due to the choice of the artificial boundary position, that was for all node arrangement $R_M = 5d$, and thus most probably not optimally varying.

Table 4.3: Case 4.1.2. RMS errors of NMFS solution as a function of different R.

Number of boundary nodes (N^{Γ})	$R = d/3$		$R = d/4$		$R = d/5$		$R = d/6$	
	e_x ($\times 10^{-2}$)	e_y ($\times 10^{-2}$)	e_x ($\times 10^{-2}$)	e_y ($\times 10^{-2}$)	e_x ($\times 10^{-2}$)	e_y ($\times 10^{-2}$)	e_x ($\times 10^{-2}$)	e_y ($\times 10^{-2}$)
100	1.2966	1.8427	3.9306	1.0462	5.9593	0.7990	7.6367	1.0348
196	2.3923	0.8280	3.9301	0.4572	5.1065	0.4276	6.0761	0.6090
292	2.6117	0.5201	3.7094	0.2878	4.5558	0.3037	5.2546	0.4415
388	2.6686	0.3751	3.5290	0.2097	4.1962	0.2388	4.7481	0.3491
484	2.6797	0.2917	3.3904	0.1651	3.9439	0.1980	4.4024	0.2898
580	2.6751	0.2379	3.2824	0.1364	3.7568	0.1697	4.1503	0.2484
676	2.6649	0.2004	3.1961	0.1163	3.6121	0.1489	3.9575	0.2178
772	2.6528	0.1729	3.1257	0.1015	3.4967	0.1328	3.8049	0.1940
868	2.6406	0.1518	3.0672	0.0901	3.4023	0.1200	3.6810	0.1751
964	2.6287	0.1353	3.0176	0.0810	3.3236	0.1095	3.5781	0.1597
1060	2.6175	0.1219	2.9752	0.0737	3.2568	0.1008	3.4912	0.1469
1156	2.6071	0.1109	2.9384	0.0676	3.1994	0.0934	3.4168	0.1360
1252	2.5974	0.1016	2.9061	0.0624	3.1495	0.0871	3.3522	0.1266
1348	2.5885	0.0938	2.8776	0.0581	3.1057	0.0816	3.2957	0.1185
1444	2.5802	0.0870	2.8522	0.0543	3.0669	0.0768	3.2458	0.1115
1540	2.5725	0.0812	2.8294	0.0509	3.0323	0.0725	3.2013	0.1052
1636	2.5654	0.0760	2.8088	0.0480	3.0011	0.0687	3.1614	0.0996
1732	2.5588	0.0715	2.7902	0.0454	2.9730	0.0653	3.1254	0.0946
1828	2.5526	0.0675	2.7731	0.0431	2.9475	0.0623	3.0928	0.0901
1924	2.5468	0.0639	2.7575	0.0410	2.9241	0.0595	3.0630	0.0860

Table 4.4: Case 4.1.2. RMS errors of MFS and NMFS solutions with $R_M = 5d$, $R = d/5$.

Number of boundary nodes (N^{Γ})	MFS		NMFS	
	$e_x(\times 10^{-2})$	$e_y(\times 10^{-2})$	$e_x(\times 10^{-2})$	$e_x(\times 10^{-2})$
100	2.3656	0.0002	5.9593	0.7990
196	4.5717	5.3138	5.1065	0.4276
292	3.5939	1.4795	4.5558	0.3037
388	2.3657	0.0037	4.1962	0.2388
484	2.3710	0.0038	3.9439	0.1980
580	2.0706	1.1063	3.7568	0.1697
676	1.3096	1.1845	3.6121	0.1489
772	1.8889	2.4678	3.4967	0.1328
868	0.8536	0.4878	3.4023	0.1200
964	2.4082	0.0282	3.3236	0.1095
1060	2.3126	0.0347	3.2568	0.1008
1156	2.3640	0.0016	3.1994	0.0934
1252	2.3620	0.0196	3.1495	0.0871
1348	2.3589	0.0055	3.1057	0.0816
1444	2.3638	0.0016	3.0669	0.0768
1540	2.3654	0.0008	3.0323	0.0725
1636	2.4276	0.3268	3.0011	0.0687
1732	1.8726	2.3862	2.9730	0.0653
1828	1.6583	1.7767	2.9475	0.0623
1924	2.3374	0.0267	2.9241	0.0595

4.4.2 Numerical Example 4.2: Bi-material Problem

We consider a square with the side length $a = 2$ m in Example 4.2. It is divided into two cases and each case is distinguishes three sub-cases. In the first sub-case, the whole square is occupied by one material, with the material properties $E = 1\ \mathrm{N/m^2}$, $\nu = 0.3$. In the second sub-case, the square is split into upper and lower parts with the same material properties as in the first example $E^{\mathrm{I}} = E^{\mathrm{II}} = 1\ \mathrm{N/m^2}$, $\nu^{\mathrm{I}} = \nu^{\mathrm{II}} = 0.3$, and in the third sub-case, the square is split as in the second one, but with more rigid material on the top, i.e. $E^{\mathrm{I}} = 5\ \mathrm{N/m^2}$, $E^{\mathrm{II}} = 1\ \mathrm{N/m^2}$, $\nu^{\mathrm{I}} = \nu^{\mathrm{II}} = 0.3$.

Case 4.2.1: Normal Stress Problem

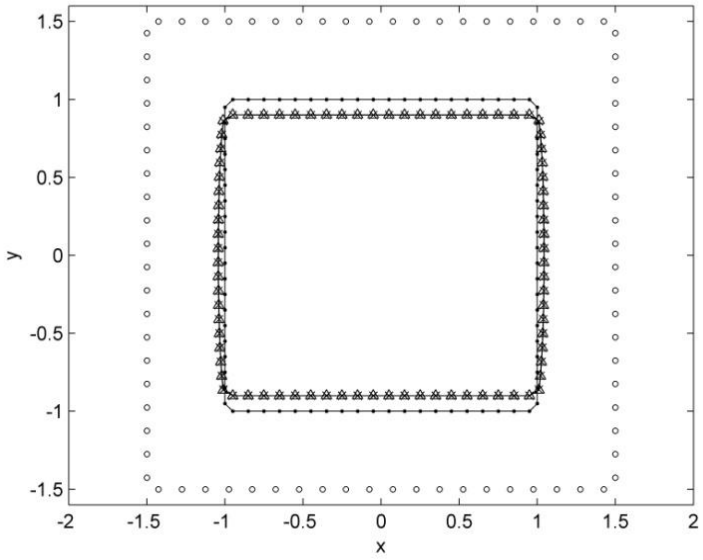

Figure 4.8: Case 4.2.1. The deformation, calculated with MFS and NMFS, for a one-domain case with $E = 1\text{N/m}^2$, $\nu = 0.3$ and $N^{\Gamma} = 80$ ($\bullet$: collocation points; $\circ$: source points in MFS; $\times$: MFS solution; $\triangle$: NMFS solution).

We consider the solution of the Navier's equations in this square subject to the boundary conditions $\bar{u}_x = 0\,\text{m}$, $\bar{u}_y = -0.1\,\text{m}$ on the north side with $p_y = 1\,\text{m}$, and $\bar{u}_x = 0\,\text{m}$, $\bar{u}_y = 0.1\,\text{m}$ on the south side with $p_y = -1\,\text{m}$, and $\bar{t}_x = 0\ \text{N/m}$, $\bar{t}_y = 0\ \text{N/m}^2$ on the east and west sides of the square with $p_x = -1\,\text{m}$ and $p_x = 1\,\text{m}$, respectively. A plot of the deformation, calculated with the defined three sub-cases is shown in Figure 4.8, Figure 4.9 and Figure 4.10, respectively. The following parameters have been used $R = d/5$, $R^{\text{I}} = d^{\text{I}}/5$, $R^{\text{II}} = d^{\text{II}}/5$, $c_x = c_y = c_x^{\text{I}} = c_y^{\text{I}} = c_x^{\text{II}} = c_y^{\text{II}} = 4\,\text{m}$. The distance of the fictitious boundary from the true boundary in case of MFS is $R_M = 5d$, $R_M^{\text{I}} = 5d^{\text{I}}$, $R_M^{\text{II}} = 5d^{\text{II}}$.

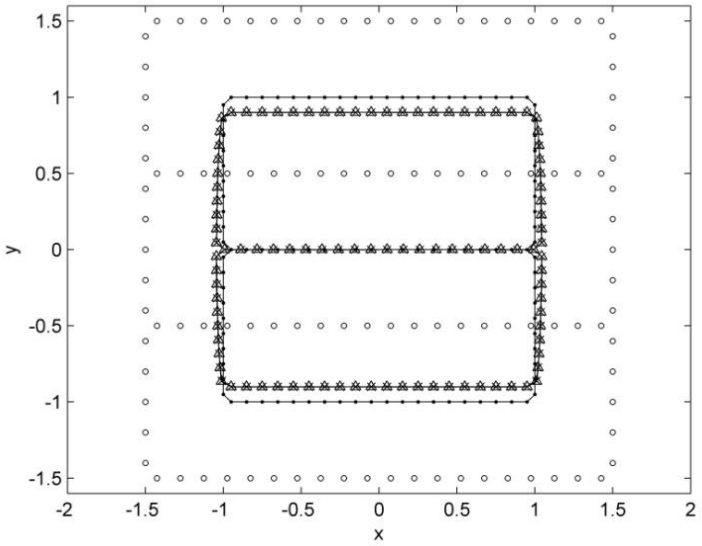

Figure 4.9: Case 4.2.1. The deformation, calculated with MFS and NMFS, for a bi-material case with material properties $E^{\mathrm{I}} = E^{\mathrm{II}} = 1\ \mathrm{N/m^2}$, $\nu^{\mathrm{I}} = \nu^{\mathrm{II}} = 0.3$, and $N^{\Gamma} = 80$ and $N^{\Gamma^{\mathrm{I}} \cap \mathrm{II}} = 20$ ($\bullet$: collocation points; $\circ$: source points in MFS; $\times$: MFS solution; $\triangle$: NMFS solution) .

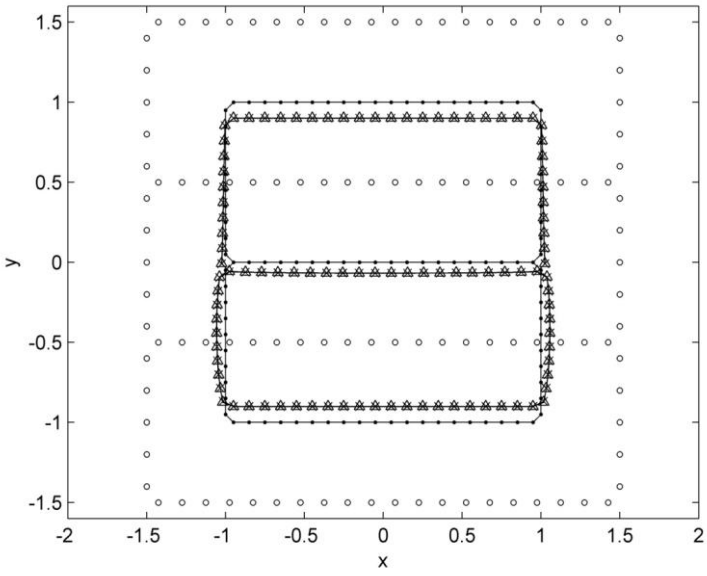

Figure 4.10: Case 4.2.1. The deformation, calculated with MFS and NMFS, for a bi-material case with material properties $E^{\mathrm{I}} = 5\ \mathrm{N/m^2}$, $E^{\mathrm{II}} = 1\ \mathrm{N/m^2}$, $\nu^{\mathrm{I}} = \nu^{\mathrm{II}} = 0.3$ and $N^{\Gamma} = 80$ and $N^{\Gamma^{\mathrm{I}} \cap \mathrm{II}} = 20$ ($\bullet$: collocation points; $\circ$: source points in MFS; $\times$: MFS solution; $\triangle$: NMFS solution) .

Table 4.5: Case 4.2.1. The results of MFS and NMFS for example from Figure 4.10.

p_x	p_z	MFS		NMFS	
		$u_x(\times 10^{-2})$	$u_y(\times 10^{-2})$	$u_x(\times 10^{-2})$	$u_y(\times 10^{-2})$
0	0.9000	0.0000	-9.7508	0.0006	-9.5376
0	0.7000	0.0000	-9.2060	0.0027	-9.0131
0	0.5000	0.0000	-8.5927	0.0056	-8.4228
0	0.3000	0.0000	-7.9061	0.0089	-7.7673
0	0.1000	0.0000	-7.1430	0.0125	-7.0381
0	-0.1000	0.0000	-5.0788	0.0142	-4.8667
0	-0.3000	0.0000	-1.6275	0.0119	-1.5403
0	-0.5000	0.0000	1.8972	0.0085	1.8589
0	-0.7000	0.0000	5.3340	0.0050	5.1709
0	-0.9000	0.0000	8.5295	0.0018	8.2406

Case 4.2.2: Shear Stress Problem

We consider the solution of the Navier's equations subject to the boundary conditions $\bar{u}_x = -0.1\,\mathrm{m}$, $\bar{u}_y = 0\,\mathrm{m}$ on the north side with $p_y = 1\,\mathrm{m}$, and $\bar{u}_x = 0.1\,\mathrm{m}$, $\bar{u}_y = 0\,\mathrm{m}$ on the south side with $p_y = -1\,\mathrm{m}$, and $\bar{t}_x = 0\ \mathrm{N/m^2}$, $\bar{t}_y = 0\ \mathrm{N/m^2}$ on the east and west sides of the square with $p_x = -1\,\mathrm{m}$ and $p_x = 1\,\mathrm{m}$, respectively. A plot of the deformation, calculated with the three sub-cases is shown in Figure 4.11 to Figure 4.145, respectively.

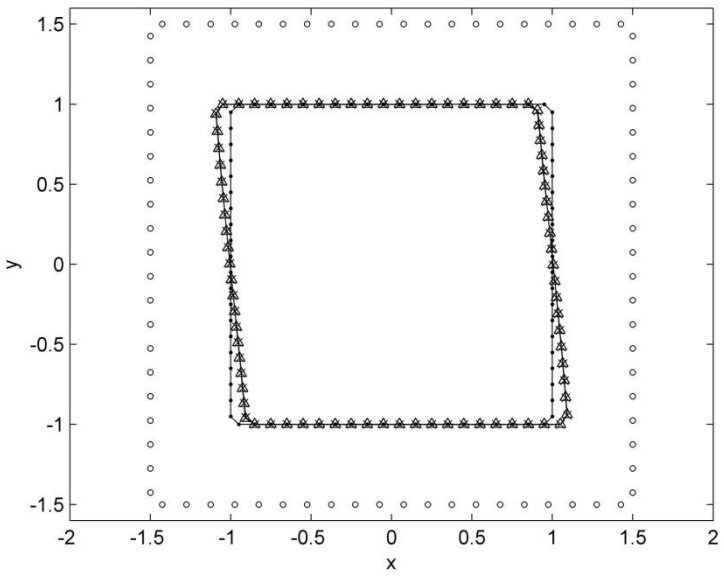

Figure 4.11: Case 4.2.2. The deformation, calculated with MFS and NMFS, for a one-domain case with material properties $E = 1\ \mathrm{N/m^2}$, $\nu = 0.3$ and $N^{\Gamma} = 80$ ($\bullet$: collocation points; $\circ$: source points in MFS; $\times$: MFS solution; $\triangle$: NMFS solution).

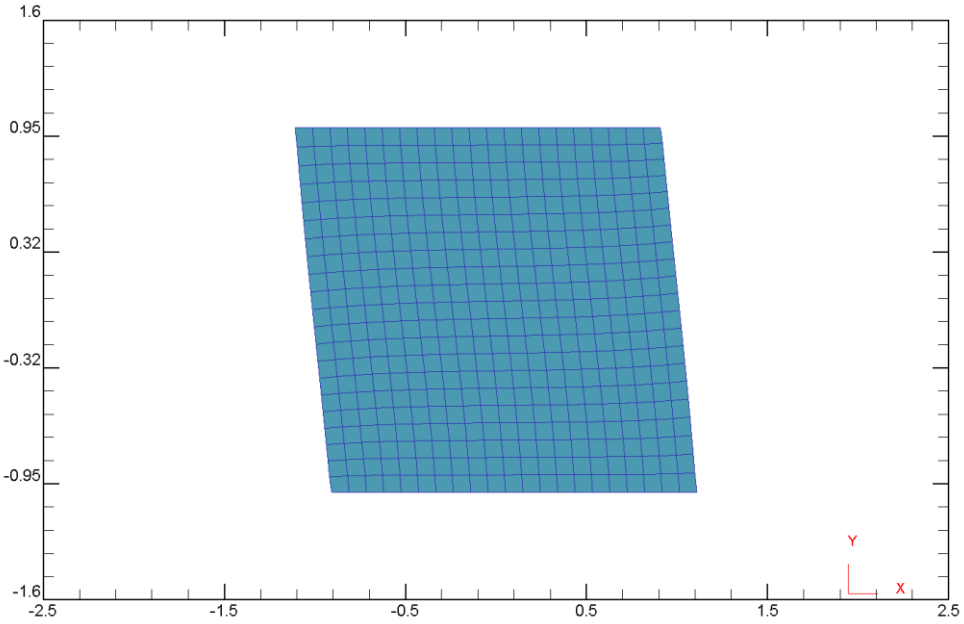

Figure 4.12：Case 4.2.2. The deformation, calculated with FEM by Deform code for a one-domain case as in Figure 4.11.

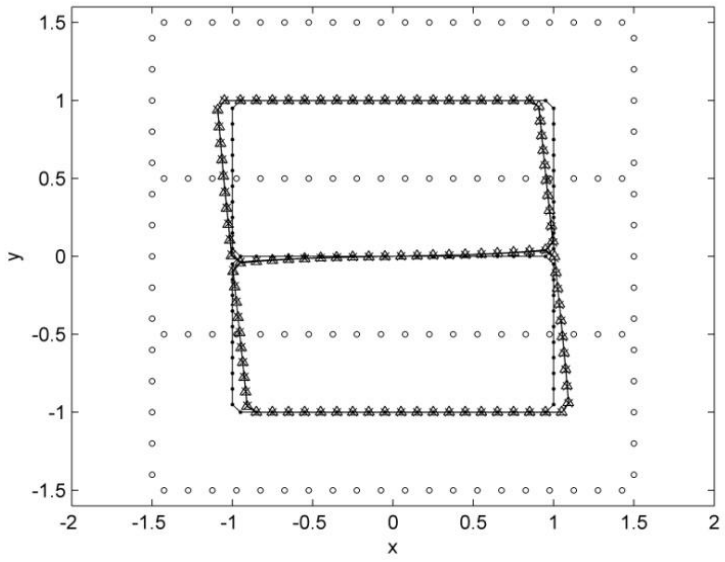

Figure 4.13**:** Case 4.2.2. The deformation, calculated with MFS and NMFS, for a bi-material case with material properties $E^{\mathrm{I}} = E^{\mathrm{II}} = 1\,\mathrm{N/m}^2$, $\nu^{\mathrm{I}} = \nu^{\mathrm{II}} = 0.3$, and $N^{\Gamma} = 80$ and $N^{\Gamma^{\mathrm{I}} \cap \mathrm{II}} = 20$ ($\bullet$: collocation points; $\circ$: source points in MFS; $\times$: MFS solution; $\triangle$: NMFS solution).

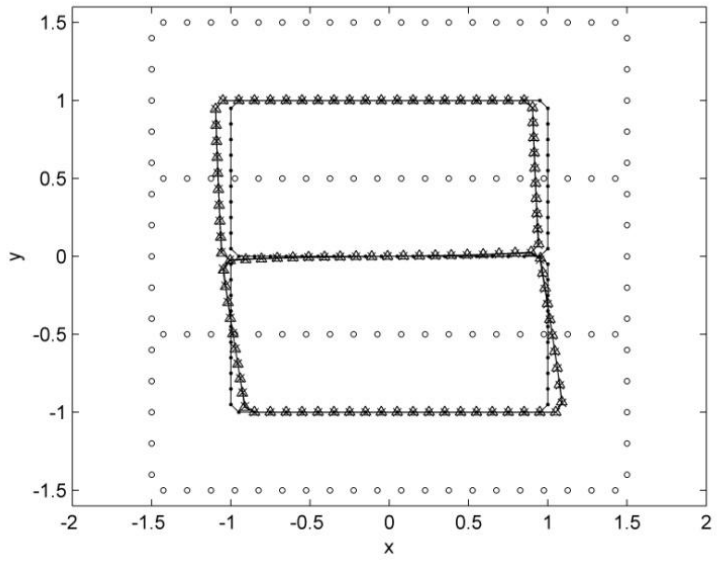

Figure 4.14: Case 4.2.2. The deformation, calculated with MFS and NMFS, for a bi-material case with material properties $E^{\mathrm{I}} = 5\ \mathrm{N/m^2}$, $E^{\mathrm{II}} = 1\ \mathrm{N/m^2}$, $\nu^{\mathrm{I}} = \nu^{\mathrm{II}} = 0.3$ and $N^{\Gamma} = 80$ and $N^{\Gamma^{\mathrm{I}} \cap \mathrm{II}} = 20$ ($\bullet$: collocation points; $\circ$: source points in MFS; $\times$: MFS solution; $\triangle$: NMFS solution) .

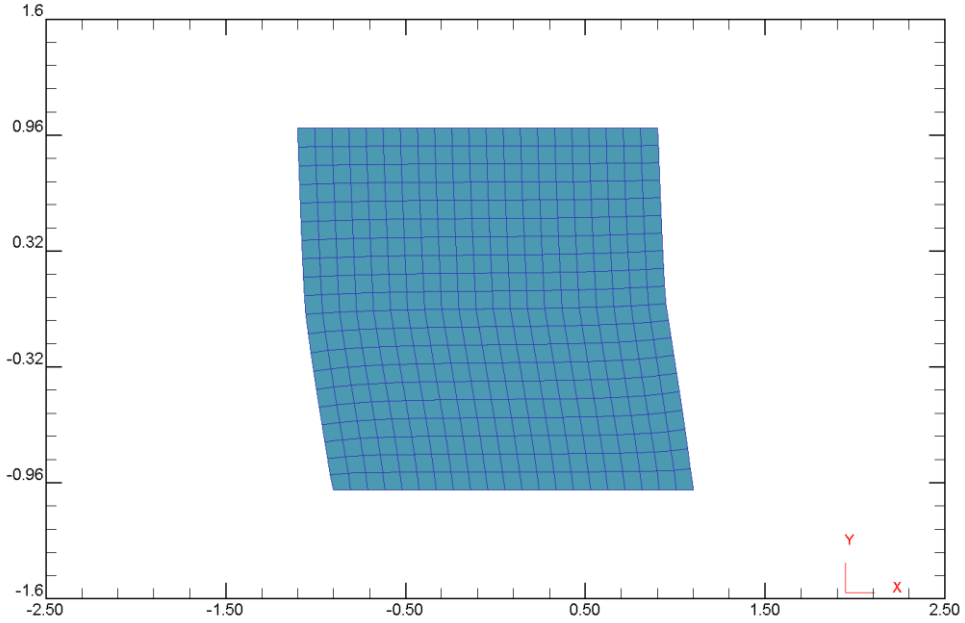

Figure 4.15: Case 4.2.2. The deformation, calculated with FEM by Deform code for a bi-material case as in Figure 4.14.

Table 4.6: Case 4.2.2. The results of MFS and NMFS for example from Figure 4.14.

p_x	p_z	MFS		NMFS	
		$u_x(\times 10^{-2})$	$u_y(\times 10^{-2})$	$u_x(\times 10^{-2})$	$u_y(\times 10^{-2})$
0	0.9000	-9.7338	0.0000	-9.7120	-0.0018
0	0.7000	-9.0963	0.0000	-9.0231	-0.0054
0	0.5000	-8.3310	0.0000	-8.2141	-0.0099
0	0.3000	-7.4769	0.0000	-7.3302	-0.0161
0	0.1000	-6.5940	0.0000	-6.4374	-0.0243
0	-0.1000	-4.4547	0.0000	-4.2997	-0.0277
0	-0.3000	-1.0468	0.0000	-0.8980	-0.0231
0	-0.5000	2.3213	0.0000	2.4442	-0.0170
0	-0.7000	5.5617	0.0000	5.6458	-0.0103
0	-0.9000	8.5810	0.0000	8.6164	-0.0036

4.5 Discussion

Example 4.1 shows good agreement of both NMFS and MFS solutions with the analytical solution. Example 4.2 shows good agreement between the solution of both NMFS and MFS for a single domain region and a solution recalculated with the two regions in ideal mechanical contact and with the same material properties (compare Figure 4.8 with Figure 4.9, and Figure 4.11 with Figure 4.13). The maximum absolute difference in displacements between values in Figure 4.8 and Figure 4.9 at the outer boundary are $\triangle u_x = 0.0011\,\mathrm{m}$ $\triangle u_y = 0.0009\,\mathrm{m}$, and between Figure 4.11 and Figure 4.13 $\triangle u_x = 0.0004\,\mathrm{m}$. $\triangle u_y = 0.0014\,\mathrm{m}$, respectively. At the same time, the result of FEM for a single domain region is shown for comparing with the NMFS (see Figure 4.12). The Cases 4.2.1 and 4.2.2 demonstrate the expected behaviour of the solution when a bi-material with different elasticity parameters is deformed (see Figure 4.10 and Figure 4.14 for MFS and NMFS, Figure 4.15 for FEM).

4.6 Conclusions

A new NMFS (termed also BDSM by Liu (2010)), is extended in this chapter to solve the two-dimensional linear elasticity problems. In this approach, the singular values of fundamental solution are integrated over small circular discs, so that the coefficients of the system of equations can be evaluated analytically in case of displacement boundary conditions, leading to extremely simple computer implementation of this method. In case of traction boundary conditions, two more systems of equations with the same size as the original MFS problem have to be solved to determine the respective desingularized derivatives. The NMFS essentially gives the same results as the classical MFS. It has the advantage that the artificial boundary is not present, however on the expense of solving three times the systems of algebraic equations in comparison with only one solution in MFS. The results obtained using MFS and NMFS are compared to each other. Sensitivity analyses of

the influence of density of points are done and representative numerical examples for singe and bi-materials have been performed. The NMFS method presented in this chapter is very general and it can be adapted or extended to handle many related problems, such as three dimensional elasticity, anisotropic elasticity, and multi-body problems which all represent directions of next chapters. The advantage of not having to generate the artificial boundary is particularly welcome in these types of problems. The developed method most probably represents a simplest known way how to numerically cope with these type of problems.

5. Non-singular Method of Fundamental Solutions for Anisotropic Problems

5.1 Introduction

The purpose of this chapter is to expand the NMFS to the two-dimensional anisotropic linear elasticity problems. The singularities are dealth with in the same way as for isotropic problems. The fundamental solution for anisotropic problems is much more complex than the one for isotropic problems. The desingularisation can not be calculated in a closed form and a numerical evaluation is performed. In case of the Dirichlet boundary conditions, the values of distributed sources are calculated directly and analytically. In case of Neumann boundary conditions, the respective desingularized values of the derivatives of the fundamental solution in the coordinate directions are calculated indirectly.

Two examples are used to demonstrate the feasibility and accuracy of the newly developed method. In the first example, the NMFS solutions are compared with MFS solutions and analytical solutions for a spectra of anisotropic plane strain elasticity problems with entirely Dirichlet boundary conditions and mixed boundary conditions. In the second example, the NMFS is used for bi-material problems and compared with MFS under entirely Dirichlet boundary conditions and mixed boundary conditions. The NMFS turns out to give similar results as the MFS in all spectra of performed tests.

5.2 Solution Procedure

The governing equations of the anisotropic elastic problems are given by Eqs. (3.5) (3.6). The fundamental solution in Eq. (3.21) is used to solve the governing equations. The desingularization (transformation of $U_{\varsigma\xi}(\mathbf{p},\mathbf{s})$ into $\tilde{U}_{\varsigma\xi}(\mathbf{p},\mathbf{s})$) is performed in the following way

$$\tilde{U}_{\varsigma\xi}(\mathbf{p},\mathbf{s}) = \begin{cases} U_{\varsigma\xi}(\mathbf{p},\mathbf{s}); & r > R, \\ \dfrac{1}{\pi R^2} \displaystyle\int_{A(\mathbf{s},R)} U_{\varsigma\xi}(\mathbf{p},\mathbf{s})\, dA; & r \le R, \end{cases} \tag{5.1}$$

where $A(\mathbf{s},R)$ represents a disk with radius R, centered around $\mathbf{s}$. The integral over area A can be calculated by a simple integration formula

$$\int_{A(\mathbf{s},R)} U_{\varsigma\xi}(\mathbf{p},\mathbf{s})\,dA \approx \sum_{k=1}^{K} U_{\varsigma\xi}(\mathbf{p},\mathbf{q}_k)A_k;\; A_k = \frac{R^2(\theta_k-\theta_{k-1})}{2}, \theta_0 = 0, \tag{5.2}$$

with

$$\begin{aligned} U_{\varsigma\xi}(\mathbf{p},\mathbf{q}_k) &= -\frac{1}{\pi}\mathrm{Re}\sum_{m=1}^{3}\gamma_{\varsigma\xi}^{m}\log\left((p_x-q_{kx})+\rho_m(p_y-q_{ky})\right) \\ &= -\frac{1}{\pi}\mathrm{Re}\sum_{m=1}^{3}\gamma_{\varsigma\xi}^{m}\log\left(R\cos\theta_k+\rho_m R\sin\theta_k\right), \end{aligned} \tag{5.3}$$

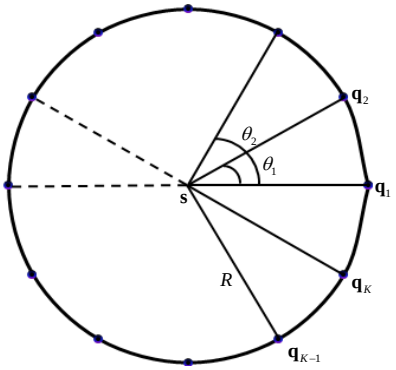

Figure 5.1: Scheme of a simple numerical integration over disk.

For all the collocation points $\mathbf{p}$, we pick the same R and θ_k. Then all of $\tilde{U}_{\varsigma\xi}(\mathbf{p},\mathbf{s})$ $(r \le R)$ will be the same. We only need to calculate the integral (5.2) once. The velue of $\tilde{U}_{\varsigma\xi}(\mathbf{p},\mathbf{s})$ in general depends on the number of integration points. However, in the present case, the value is not sensitive to the number of integration points. However, for possibility other cases, this need to be checked.

Discretisation for single material is the same as described in the Chapter 4.3 and solution procedure for a bi-material is the same as described in Chapter 3.5.

5.3 Numerical Examples

5.3.1 Example 5.1: Single Domain Problem

We consider an anisotropic material (cubic material defined in Chapter 2.4.2.7) in a square $\Omega = (-1\,\text{m}, 1\,\text{m}) \times (-1\,\text{m}, 1\,\text{m})$, subject to Dirichlet boundary conditions, corresponding to the exact solution of the problem, for which

$$u_x = p_x, u_y = p_y. \tag{5.4}$$

We take $c_{11} = 16.84\ \text{N/m}^2$, $c_{12} = 12.14\ \text{N/m}^2$, $c_{66} = 7.54\ \text{N/m}^2$ which is appropriate for crystal copper. Here indicators 1, 2, 6 denote *xx*, *yy*, *xy* as in Eqs. (2.47) and (2.51). The principal directions of crystal coincides with the axes of the Cartesian coordinate system. This convention will be used all over this dissertation for anisotropic materials. The example was already studied in [Berger and Karageorghis (2001)] for plane strain problems using MFS. The distance of the fictitious boundary from the true boundary for the MFS is set $R_M = 5d$. The radius of the disk for the distributed area source covering each node is set to $R = d/5$. The simple reference solution constants used in calculation of the diagonal coefficients are defined as $c_x = c_y = 4\ \text{m}$.

The relationship between the numerically calculated $\tilde{U}_{\varsigma\xi}$ and K is shown in Figure 5.2 (see Eq. (5.2)). We are taking $K = 100$, in all numerical integrations over the disk. We split the Example 5.1 into two different cases. A selection of $N^{\Omega} = 20$ field points inside the domain along the line $p_y = 0\ \text{m}$ with $-0.95\ \text{m} \le p_x \le 0.95\ \text{m}$ is taken for computing the RMS error. The number of boundary nodes used is from 200 to 2000.

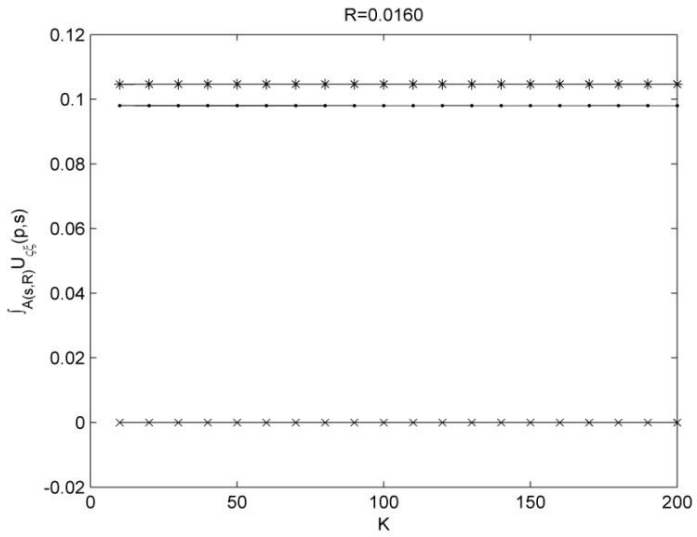

Figure 5.2: Example 5.1. The relationship between the number of the numerical integration nodes K and $\tilde{U}_{\varsigma\xi}$ ($\bullet$: $\tilde{U}_{xx}$, $\times$: $\tilde{U}_{xy}$ and $\tilde{U}_{yx}$, $*$: $\tilde{U}_{yy}$).

Case 5.1.1: Dirichlet Boundary Conditions

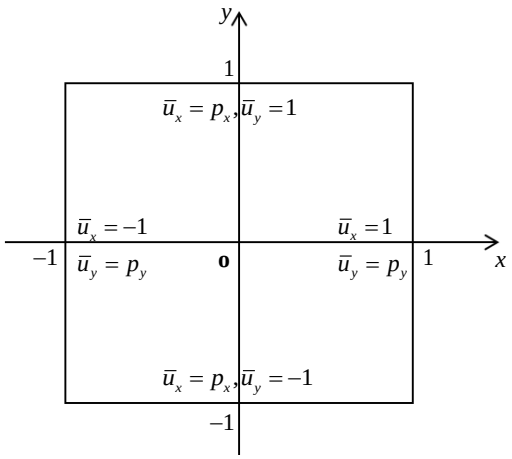

Figure 5.3: Case 5.1.1. Scheme of the geometry and Dirichlet boundary conditions.

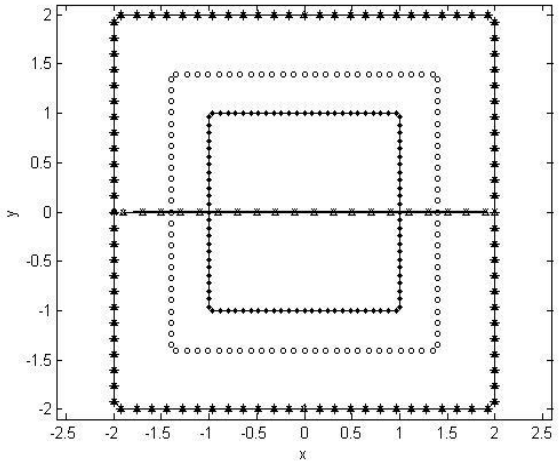

Figure 5.4: Case 5.1.1. The analytical solution and the numerical solution of MFS and NMFS with $N^{\Gamma} = 100$ ($\bullet$: collocation points; $\circ$: source points in MFS; $+$: analytical solution; $\times$: MFS solution; $\triangle$: NMFS solution).

We consider the solution of the governing equations in this square subject to the boundary conditions $\bar{u}_x = p_x$, $\bar{u}_y = p_y$ on all the boundary points (see Figure 5.3). A plot of the deformation, obtained with the analytical solution and the numerical solutions with MFS and NMFS is shown in Figure 5.4, and the result of the domain points is shown in Table 5.1 for the case with $N^{\Gamma} = 100$ nodes. Figure 5.5 shows RMS errors of the results obtained using the NMFS. The errors are already less than 10^{-4} with $N^{\Gamma} = 200$ and the solution converges to the analytical solution with the increasing number of the nodes. A comparison of the NMFS results with the MFS results is given in Table 5.2. Here, it should be noted, that the MFS solution error is rather small, however the convergence is not uniform. This fact is due to the choice

of the artificial boundary position, that was for all node arrangements $R_M = 5d$, and thus most probably not varying optimally.

Table 5.1: Case 5.1.1. The analytical solution and the numerical solutions with MFS and NMFS.

p_x	p_y	Analytical solution		MFS		NMFS	
		u_x	u_y	u_x	u_y	u_x	u_y
-0.95	0.0	-0.9500	0.0000	-0.9500	0.0000	-0.9447	0.0000
-0.85	0.0	-0.8500	0.0000	-0.8500	0.0000	-0.8497	0.0000
-0.75	0.0	-0.7500	0.0000	-0.7500	0.0000	-0.7499	0.0000
-0.65	0.0	-0.6500	0.0000	-0.6500	0.0000	-0.6500	0.0000
-0.55	0.0	-0.5500	0.0000	-0.5500	0.0000	-0.5501	0.0000
-0.45	0.0	-0.4500	0.0000	-0.4500	0.0000	-0.4501	0.0000
-0.35	0.0	-0.3500	0.0000	-0.3500	0.0000	-0.3501	0.0000
-0.25	0.0	-0.2500	0.0000	-0.2500	0.0000	-0.2501	0.0000
-0.15	0.0	-0.1500	0.0000	-0.1500	0.0000	-0.1501	0.0000
-0.05	0.0	-0.0500	0.0000	-0.0500	0.0000	-0.0500	0.0000
0.05	0.0	0.0500	0.0000	0.0500	0.0000	0.0500	0.0000
0.15	0.0	0.1500	0.0000	0.1500	0.0000	0.1501	0.0000
0.25	0.0	0.2500	0.0000	0.2500	0.0000	0.2501	0.0000
0.35	0.0	0.3500	0.0000	0.3500	0.0000	0.3501	0.0000
0.45	0.0	0.4500	0.0000	0.4500	0.0000	0.4501	0.0000
0.55	0.0	0.5500	0.0000	0.5500	0.0000	0.5501	0.0000
0.65	0.0	0.6500	0.0000	0.6500	0.0000	0.6500	0.0000
0.75	0.0	0.7500	0.0000	0.7500	0.0000	0.7499	0.0000
0.85	0.0	0.8500	0.0000	0.8500	0.0000	0.8497	0.0000
0.95	0.0	0.9500	0.0000	0.9500	0.0000	0.9447	0.0000

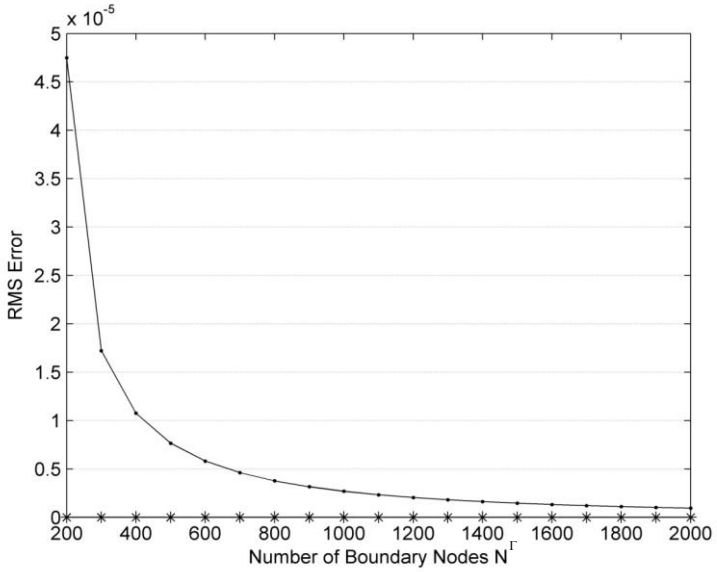

Figure 5.5: Case 5.1.1. The relationship between the RMS errors and the number of boundary nodes, calculated by NMFS ($\bullet : e_x$; $* : e_y$).

Table 5.2: Case 5.1.1. RMS errors of MFS and NMFS solutions with $R_M = 5d$, $R = d/5$.

Number of boundary nodes (N^Γ)	MFS		NMFS	
	$e_x(\times 10^{-5})$	$e_y(\times 10^{-5})$	$e_x(\times 10^{-5})$	$e_y(\times 10^{-5})$
200	0.0001	0.0001	4.7486	0.0000
300	0.0001	0.0000	1.7222	0.0000
400	0.0000	0.0000	1.0754	0.0000
500	0.0000	0.0001	0.7657	0.0000
600	0.0000	0.0000	0.5815	0.0000
700	0.0002	0.0001	0.4610	0.0000
800	0.0000	0.0000	0.3770	0.0000
900	0.0002	0.0002	0.3158	0.0000
1000	0.0002	0.0000	0.2695	0.0000
1100	0.0060	0.0091	0.2335	0.0000
1200	0.0001	0.0002	0.2049	0.0000
1300	0.0000	0.0002	0.1816	0.0000
1400	0.0000	0.0009	0.1625	0.0000
1500	0.0009	0.0005	0.1465	0.0000
1600	0.0000	0.0005	0.1329	0.0000
1700	0.0000	0.0002	0.1214	0.0000
1800	0.0001	0.0002	0.1114	0.0000
1900	0.0029	0.0128	0.1027	0.0000
2000	0.0007	0.0009	0.0951	0.0000

Case 5.1.2: Mixed Boundary Conditions

We consider the solution of the governing equations (3.5) (3.6) in the previously defined square, subject to the boundary conditions $\bar{t}_y = 0\ \mathrm{N/m^2}$ on the points of the side $p_x = 1\,\mathrm{m}$, and $\bar{t}_x = 0\ \mathrm{N/m^2}$ on the side $p_y = 1\,\mathrm{m}$, and $\bar{u}_x = p_x$, $\bar{u}_y = p_y$, on the other boundary points (see Figure 5.6). A plot of the deformation, obtained with the analytical solution and the numerical solutions with MFS and NMFS, is shown in Figure 5.7 for the case with $N^\Gamma = 100$ nodes.

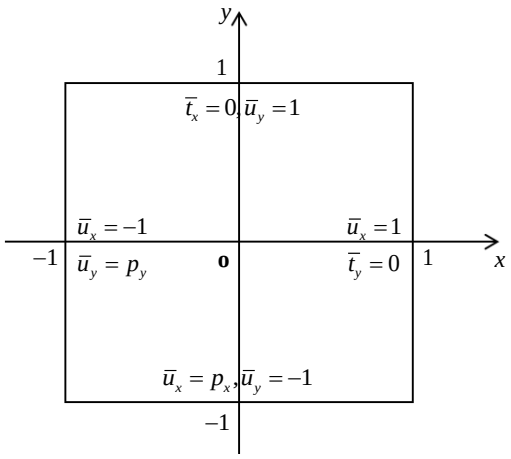

Figure 5.6: Case 5.1.2. Scheme of a square subject to mixed boundary conditions.

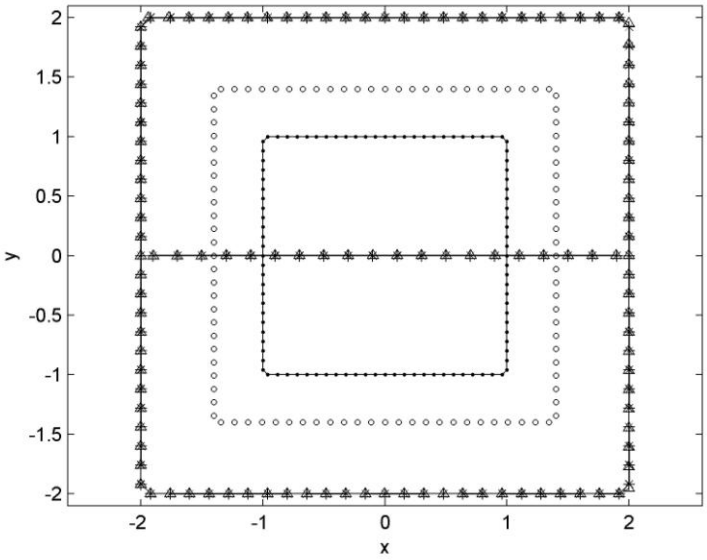

Figure 5.7: Case 5.1.2. The analytical solution and the numerical solution of MFS and NMFS with $N^{\Gamma} = 100$ ($\bullet$: collocation points; $\circ$: source points in MFS; $+$: analytical solution; $\times$: MFS solution; $\triangle$: NMFS solution).

The same selection of the reference points is used as in the previous example, to calculate the RMS error of the solution. The solution is presented in Figure 5.8.

Table 5.3: Case 5.1.2. The analytical and the numerical solution with MFS and NMFS.

p_x	p_y	Analytical solution		MFS		NMFS	
		u_x	u_y	u_x	u_y	u_x	u_x
-0.95	0.0	-0.9500	0.0000	-0.9500	0.0000	-0.9447	-0.0000
-0.85	0.0	-0.8500	0.0000	-0.8500	0.0000	-0.8496	-0.0000
-0.75	0.0	-0.7500	0.0000	-0.7500	0.0000	-0.7497	-0.0000
-0.65	0.0	-0.6500	0.0000	-0.6500	0.0000	-0.6497	0.0000
-0.55	0.0	-0.5500	0.0000	-0.5500	0.0000	-0.5497	0.0001
-0.45	0.0	-0.4500	0.0000	-0.4500	0.0000	-0.4497	0.0002
-0.35	0.0	-0.3500	0.0000	-0.3500	0.0000	-0.3496	0.0002
-0.25	0.0	-0.2500	0.0000	-0.2500	0.0000	-0.2495	0.0003
-0.15	0.0	-0.1500	0.0000	-0.1500	0.0000	-0.1493	0.0004
-0.05	0.0	-0.0500	0.0000	-0.0500	0.0000	-0.0491	0.0004
0.05	0.0	0.0500	0.0000	0.0500	0.0000	0.0512	0.0005
0.15	0.0	0.1500	0.0000	0.1500	0.0000	0.1515	0.0005
0.25	0.0	0.2500	0.0000	0.2500	0.0000	0.2517	0.0005
0.35	0.0	0.3500	0.0000	0.3500	0.0000	0.3519	0.0004
0.45	0.0	0.4500	0.0000	0.4500	0.0000	0.4519	0.0004
0.55	0.0	0.5500	0.0000	0.5500	0.0000	0.5518	0.0003
0.65	0.0	0.6500	0.0000	0.6500	0.0000	0.6516	0.0003
0.75	0.0	0.7500	0.0000	0.7500	0.0000	0.7512	0.0002
0.85	0.0	0.8500	0.0000	0.8500	0.0000	0.8506	0.0002
0.95	0.0	0.9500	0.0000	0.9500	0.0000	0.9451	0.0002

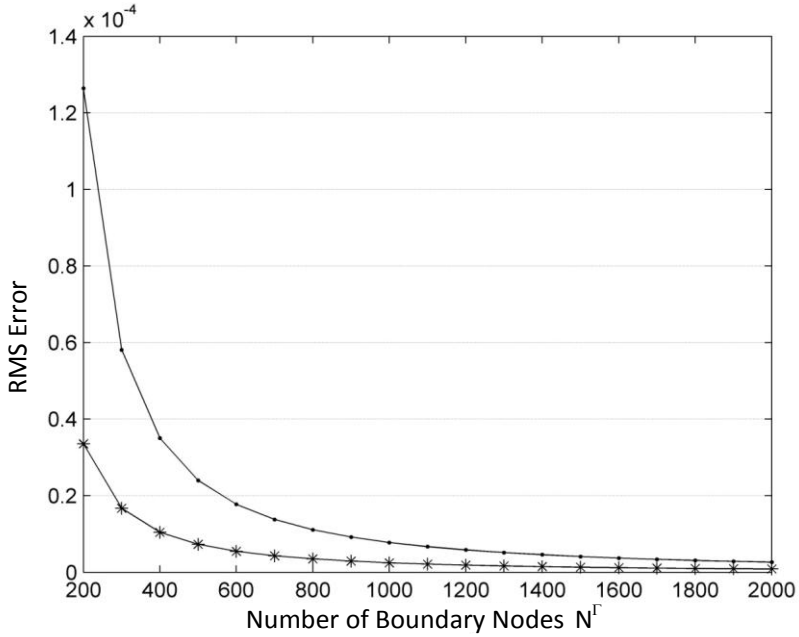

Figure 5.8: Case 5.1.2. The relationship between the RMS errors and the number of boundary nodes, calculated by NMFS ($\bullet: e_x; *: e_y$).

Figure 5.8 shows RMS errors of the results obtained using the NMFS. The errors are already less than 10^{-3} with $N^{\Gamma} = 200$ and the solution converges to the analytical solution with the increasing number of the nodes. A comparison of the NMFS results with the MFS results is shown in Table 5.4.

Table 5.4: Case 5.1.2. RMS errors of MFS and NMFS solutions.

Number of boundary nodes (N^{Γ})	MFS		NMFS	
	$e_x(\times 10^{-4})$	$e_y(\times 10^{-4})$	$e_x(\times 10^{-4})$	$e_y(\times 10^{-4})$
200	0.0002	0.0001	1.2641	0.3357
300	0.0000	0.0000	0.5809	0.1673
400	0.0001	0.0001	0.3504	0.1046
500	0.0003	0.0008	0.2400	0.0732
600	0.0006	0.0016	0.1774	0.0550
700	0.0015	0.0048	0.1379	0.0432
800	0.0001	0.0002	0.1111	0.0351
900	0.0054	0.0161	0.0920	0.0292
1000	0.0036	0.0024	0.0778	0.0249
1100	0.0007	0.0005	0.0670	0.0215
1200	0.0028	0.0018	0.0584	0.0188
1300	0.0253	0.0498	0.0515	0.0166
1400	0.0005	0.0020	0.0459	0.0148
1500	0.0030	0.0020	0.0412	0.0133
1600	0.0011	0.0035	0.0373	0.0121
1700	0.0002	0.0006	0.0339	0.0110
1800	0.0005	0.0003	0.0311	0.0101
1900	0.0017	0.0022	0.0286	0.0093
2000	0.0004	0.0003	0.0264	0.0086

5.3.2 Example 5.2: Bi-material Problem

We split Example 5.2 into three different cases. These cases were studied in [Berger and Karageorghis (2001)] for plane strain problems. We consider the problem of two anisotropic materials in a square $\Omega = (-1\,\text{m}, 1\,\text{m}) \times (-1\,\text{m}, 1\,\text{m})$. The materials are taken to have cubic anisotropy, with $c_{11}^{\text{I}} = 16.84\ \text{N/m}^2$, $c_{12}^{\text{II}} = 12.14\ \text{N/m}^2$ $c_{66}^{\text{I}} = 7.54\ \text{N/m}^2$ and $c_{11}^{\text{II}} = 24.65\ \text{N/m}^2$, $c_{12}^{\text{II}} = 14.73\ \text{N/m}^2$, $c_{66}^{\text{II}} = 12.47\ \text{N/m}^2$. The distance of the fictitious boundary from the true boundary for the MFS is set $R_M^{\text{I}} = R_M^{\text{II}} = 5d$. The radius of the square disk for the distributed area source covering each node is set to $R^{\text{I}} = R^{\text{II}} = d/5$. The simple solution constants, used in calculation of the diagonal coefficients, are defined as $c_x = c_y = 4\,\text{m}$.

Case 5.2.1: Dirichlet Boundary Conditions

We consider the solution of the governing equations in the previously defined square, subject to the boundary conditions $\bar{u}_x^{\mathrm{I}} = \bar{u}_x^{\mathrm{II}} = p_x$, $\bar{u}_y^{\mathrm{I}} = \bar{u}_y^{\mathrm{II}} = p_y$ on all the boundary points (see Figure 5.9). A plot of the deformation, obtained with the analytical solution and the numerical solutions with MFS and NMFS is shown in Figure 5.10 for the case with $N^{\Gamma} = 80$, $N^{\Gamma^{\mathrm{I}\cap\mathrm{II}}} = 20$ nodes.

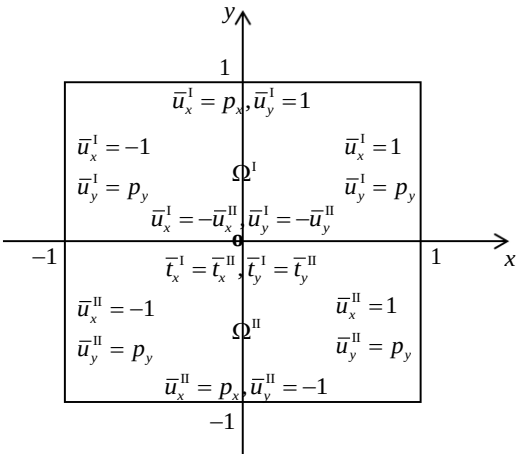

Figure 5.9: Case 5.2.1. Scheme of the square subject to Dirichlet boundary conditions.

$N^{\Omega} = 100$ points are selected inside the domain along the line $p_y = 0\,\mathrm{m}$ with $-0.95\,\mathrm{m} \le p_y \le 0.95\,\mathrm{m}$ to compare the MFS solution with the NMFS solution (see Table 5.5).

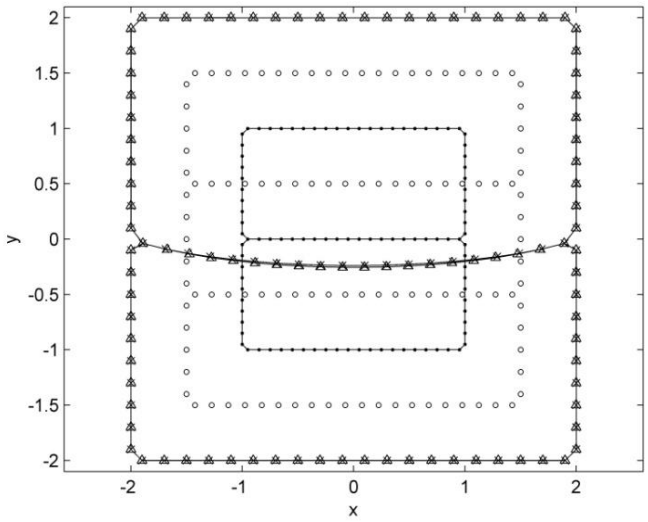

Figure 5.10: Case 5.2.1.The analytical solution and the numerical solution of MFS and NMFS with $N^{\Gamma} = 80$, $N^{\Gamma^{\mathrm{I}\cap\mathrm{II}}} = 20$ ($\bullet$: collocation points; $\circ$: source points in MFS; $\times$: MFS solution; $\triangle$: NMFS solution).

Table 5.5: Case 5.2.1. The analytical solution and the numerical solutions with MFS and NMFS.

p_x	p_y	MFS		NMFS	
		$u_x(\times 10^{-4})$	u_y	$u_x(\times 10^{-4})$	u_y
0.0	-0.95	0.0000	-0.9585	-0.0841	-0.9620
0.0	-0.85	0.0000	-0.8776	-0.1808	-0.8779
0.0	-0.75	0.0000	-0.7992	-0.2859	-0.7987
0.0	-0.65	0.0000	-0.7227	-0.3849	-0.7215
0.0	-0.55	0.0000	-0.6476	-0.4705	-0.6461
0.0	-0.45	0.0000	-0.5735	-0.5366	-0.5718
0.0	-0.35	0.0000	-0.4998	-0.5795	-0.4983
0.0	-0.25	0.0000	-0.4260	-0.5982	-0.4250
0.0	-0.15	0.0000	-0.3518	-0.5939	-0.3515
0.0	-0.05	0.0000	-0.2770	-0.5765	-0.2768
0.0	0.05	0.0000	-0.1763	-0.5347	-0.1828
0.0	0.15	0.0000	-0.0500	-0.5019	-0.0521
0.0	0.25	0.0000	0.0766	-0.4859	0.0739
0.0	0.35	0.0000	0.2034	-0.4741	0.2005
0.0	0.45	0.0000	0.3300	-0.4598	0.3272
0.0	0.55	0.0000	0.4559	-0.4337	0.4533
0.0	0.65	0.0000	0.5806	-0.3858	0.5785
0.0	0.75	0.0000	0.7036	-0.3096	0.7019
0.0	0.85	0.0000	0.8242	-0.2058	0.8228
0.0	0.95	0.0000	0.9422	-0.0905	0.9484

Case 5.2.2: Mixed Boundary Conditions – Stress in *y* direction

Next, we consider a tension problem in the same region. We prescribe the tractions $\bar{t}_x^{\mathrm{I}} = \bar{t}_y^{\mathrm{I}} = 0\ \mathrm{N/m^2}$ and $\bar{t}_x^{\mathrm{II}} = \bar{t}_y^{\mathrm{II}} = 0\ \mathrm{N/m^2}$ on the two vertical sides $p_x = 1\,\mathrm{m}$ and $p_x = -1\,\mathrm{m}$, $\bar{t}_x^{\mathrm{I}} = 0\ \mathrm{N/m^2}$ and $\bar{t}_y^{\mathrm{I}} = 1\ \mathrm{N/m^2}$ on the side $p_y = 1\,\mathrm{m}$, $\bar{u}_x^{\mathrm{II}} = \bar{u}_y^{\mathrm{II}} = 0\,\mathrm{m}$ on the other boundary points (see Figure 5.11). A plot of the deformation, obtained with the analytical solution and the numerical solutions with MFS and NMFS, is shown in Figure 5.12 for the case with $N^{\Gamma} = 80$, $N^{\Gamma^{\mathrm{I}\cap\mathrm{II}}} = 20$ nodes.

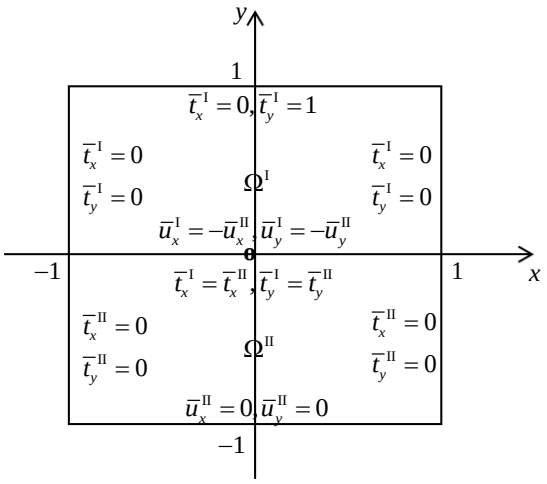

Figure 5.11: Case 5.2.2. Scheme of a square subject to mixed boundary conditions**.**

$N^{\Omega}=20$ points are selected inside the domain along the line $p_y=1\,\mathrm{m}$ with $-0.95\,\mathrm{m}\le p_x\le 0.95\,\mathrm{m}$ to compare with the MFS solution. The solution at these points are given in Figure 5.6.

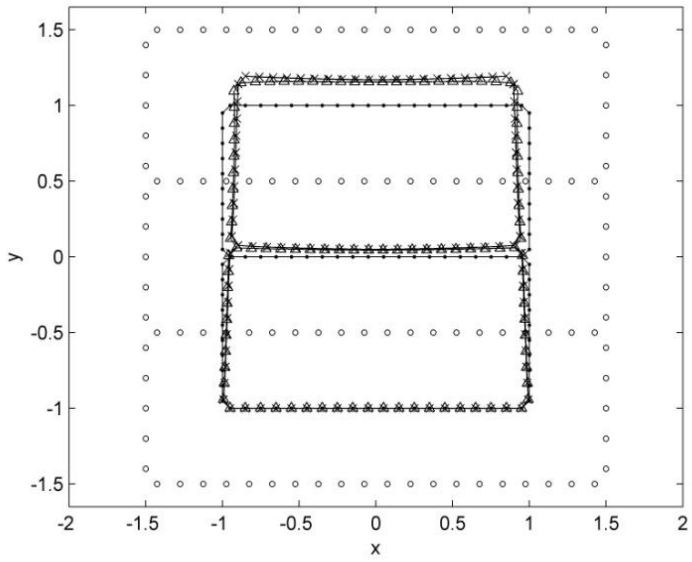

Figure 5.12: Case5. 2.2. The analytical solution and the numerical solution of MFS and NMFS with $N^{\Gamma}=80$, $N^{\Gamma_{\mathrm{I}}\cap\Gamma_{\mathrm{II}}}=20$ ($\bullet$: collocation points; $\circ$: source points in MFS; $\times$: MFS solution; $\triangle$: NMFS solution).

Table 5.6: Case 5.2.2. The analytical and the numerical solution with MFS and NMFS.

p_x	p_y	MFS		NMFS	
		u_x	u_y	u_x	u_y
-0.95	1.0	-0.1012	0.1937	-0.0714	0.1499
-0.85	1.0	-0.0902	0.1885	-0.0662	0.1553
-0.75	1.0	-0.0801	0.1850	-0.0605	0.1581
-0.65	1.0	-0.0701	0.1818	-0.0540	0.1590
-0.55	1.0	-0.0600	0.1789	-0.0469	0.1590
-0.45	1.0	-0.0495	0.1764	-0.0392	0.1584
-0.35	1.0	-0.0389	0.1743	-0.0311	0.1577
-0.25	1.0	-0.0280	0.1726	-0.0226	0.1569
-0.15	1.0	-0.0169	0.1714	-0.0140	0.1563
-0.05	1.0	-0.0056	0.1708	-0.0051	0.1560
0.05	1.0	0.0056	0.1708	0.0038	0.1559
0.15	1.0	0.0169	0.1714	0.0126	0.1562
0.25	1.0	0.0280	0.1726	0.0213	0.1567
0.35	1.0	0.0389	0.1743	0.0299	0.1574
0.45	1.0	0.0495	0.1764	0.0380	0.1581
0.55	1.0	0.0600	0.1789	0.0458	0.1586
0.65	1.0	0.0701	0.1818	0.0531	0.1587
0.75	1.0	0.0801	0.1850	0.0597	0.1577
0.85	1.0	0.0902	0.1885	0.0657	0.1549
0.95	1.0	0.1012	0.1937	0.0715	0.1494

Case 5.2.3: Mixed Boundary Conditions – Stress in *x* direction

For the final case, we consider the same anisotropic material system described above but with more complicated, mixed boundary conditions. Namely, on the rectangular domain described above, we take $\bar{u}_x^{\mathrm{I}} = \bar{u}_y^{\mathrm{I}} = 0\,\mathrm{m}$ along $p_y = 1\,\mathrm{m}$ and $p_x = -1\,\mathrm{m}$, $\bar{u}_x^{\mathrm{II}} = \bar{u}_y^{\mathrm{II}} = 0\,\mathrm{m}$ along $p_y = -1\,\mathrm{m}$ and $p_x = -1\,\mathrm{m}$, and along the edge $p_x = 1\,\mathrm{m}$, we take the mixed boundary conditions $\bar{t}_x^{\mathrm{I}} = \bar{t}_x^{\mathrm{II}} = 1\,\mathrm{N/m^2}$ and $\bar{u}_y^{\mathrm{I}} = \bar{u}_y^{\mathrm{II}} = 0\,\mathrm{m}$ (see Figure 5.13). A plot of the deformation, obtained with the analytical solution and the numerical solution with MFS and NMFS is shown in Figure 5.14 for the case with $N^{\Gamma} = 80$, $N^{\Gamma^{\mathrm{I}} \cap \mathrm{II}} = 20$ nodes. The solution along $p_x = 1\,\mathrm{m}$ is shown in Table 5.7.

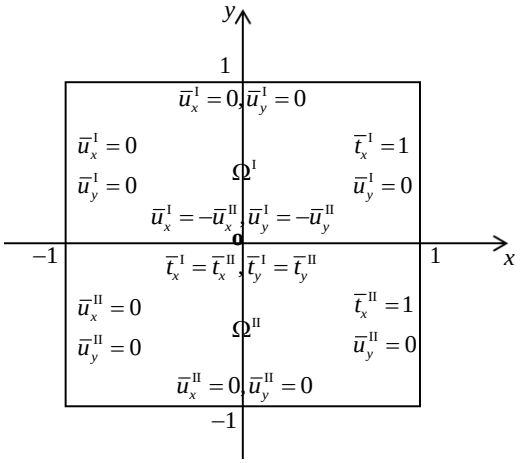

Figure 5.13: Case 5.2.3. Scheme of geometry and mixed boundary conditions.

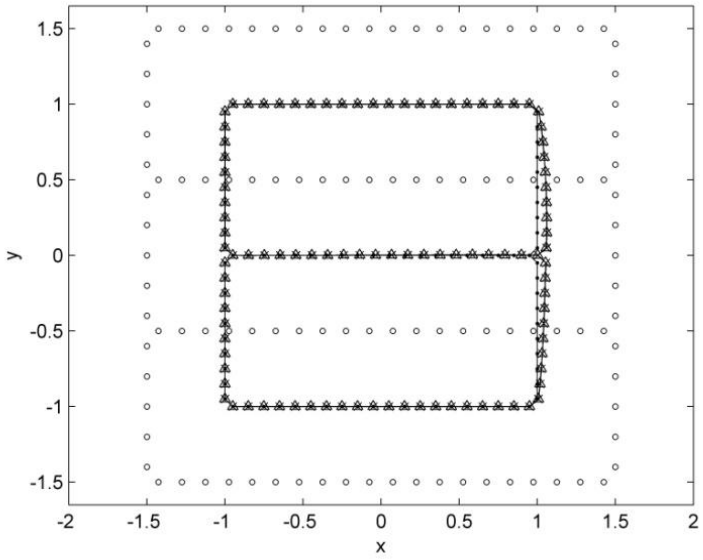

Figure 5.14: Case 5.2.3: The analytical solution and the numerical solution of MFS and NMFS with $N^{\Gamma}=80$, $N^{\Gamma^{\mathrm{I}}\cap\mathrm{II}}=20$ ($\bullet$: collocation points; $\circ$: source points in MFS; $\times$: MFS solution; $\triangle$: NMFS solution).

Table 5.7: Case 5.2.3. The numerical solutions with MFS and NMFS.

p_x	p_y	MFS		NMFS	
		$u_x(\times 10^{-2})$	$u_y(\times 10^{-2})$	$u_x(\times 10^{-2})$	$u_y(\times 10^{-2})$
1.0	-0.95	0.7049	0.0000	0.5520	0.0000
1.0	-0.85	1.6853	0.0000	1.5743	0.0000
1.0	-0.75	2.4329	0.0000	2.3528	0.0000
1.0	-0.65	3.0792	0.0000	2.9956	0.0000
1.0	-0.55	3.6183	0.0000	3.5391	0.0000
1.0	-0.45	4.0914	0.0000	4.0019	0.0000
1.0	-0.35	4.4906	0.0000	4.3967	0.0000
1.0	-0.25	4.8488	0.0000	4.7353	0.0000
1.0	-0.15	5.1557	0.0000	5.0333	0.0000
1.0	-0.05	5.4988	0.0000	5.3181	0.0000
1.0	0.05	5.9330	0.0000	5.5174	0.0000
1.0	0.15	6.1175	0.0000	5.8453	0.0000
1.0	0.25	6.1016	0.0000	5.8914	0.0000
1.0	0.35	5.9262	0.0000	5.7469	0.0000
1.0	0.45	5.5883	0.0000	5.4292	0.0000
1.0	0.55	5.0819	0.0000	4.9395	0.0000
1.0	0.65	4.4101	0.0000	4.2699	0.0000
1.0	0.75	3.5354	0.0000	3.4008	0.0000
1.0	0.85	2.4617	0.0000	2.2826	0.0000
1.0	0.95	1.0173	0.0000	0.7162	0.0000

The example 5.2 shows good agreement between the solutions of MFS and NMFS for a bi-material. One can observe that in Figure 5.10, Figure 5.12 and Figure 5.14, the NMFS solution almost coincides with the MFS solution.

5.4 Discussion

Example 5.1 shows good agreement of both NMFS and MFS solutions with the analytical solution. Example 5.2 shows good agreement between MFS and NMFS solution for a bi-material. The maximum absolute difference in displacements between the values of MFS and NMFS in Table 5.5 on the line $p_x = 0\,\mathrm{m}$ are $\triangle u_x = 0.0000\,\mathrm{m}, \quad \Delta u_y = 0.0066\,\mathrm{m}$. The maximum absolute difference in displacements between the values of MFS and NMFS in Table 5.6 on the line $p_y = 1\,\mathrm{m}$ are $\triangle u_x = 0.0298\,\mathrm{m}, \ \Delta u_y = 0.0433\,\mathrm{m}$. The maximum absolute difference in displacements between values of MFS and NMFS, given in Table 5.7 on the outer boundary of $p_x = 1\,\mathrm{m}$ are $\triangle u_x = 0.0029\,\mathrm{m}, \ \triangle u_y = 0.0000\,\mathrm{m}$.

5.5 Conclusions

The NMFS for isotropic problems is extended to solve the 2D linear anisotropic elasticity problems in this chapter. The fundamental solutions for anisotropic problems are more complex than for isotropic ones. We can not obtain the exact expression of desingularized fundamental solution It is found by numerical methods. The selection of reference field has to be carefully chosen and not all reference solutions are appropriate in NMFS. So we will improve the NMFS, called Improved NMFS (INMFS), for isotropic and anisotropic problems in next chapter. Then the NMFS or INMFS will be used in the future for calculation of multi-grain deformation [Mura (1987)] problems in metals, with realistic grain shapes, obtained from the microscope images. It represents an alternative to the recent development direction of T-Trefftz Voronoi cell finite elements [Dong and Atluri (2011a); Dong and Atluri (2011b); Dong and Atluri (2013)] for macro- & micromechanics of inhomogenous media with inclusions and cracks. The problems with arbitrarily shaped inhomogeneities in the form of elastic inclusions, rigid inclusions and voids, as discussed in [Dong and Atluri, (2012)] will be numerically implemented.

6. Improved Non-singular Method of Fundamental Solutions

6.1 Introduction

The purpose of this chapter is improvement of the NMFS [Liu and Šarler (2013)] for two-dimensional isotropic and anisotropic linear elasticity problems. Because of the limitations of NMFS, that does not perform well for inclusions and voids problems and because of the computational effort needed for solving the three systems of algebraic equations, the INMFS is developed. This method is based on the idea of [Kim (2013)] for potential problems. In steady state potential problems, the balance of the derivatives of the potential field values at the boundary should be zero. However, in the present solid mechanics problems, the balance of the tractions on the boundary should be zero. This idea, together with the assumption of the constant value of the traction near the boundary node allowed for a simple calculation of the diagonal elements of the matrix of fundamental tractions for the Neumann boundary conditions. From this consideration, the values of the fundamental tractions in singular points are obtained. This novel INMFS represents an effective upgrade of NMFS for problems with inclusions and voids. INMFS method reduces the computation time of NMFS method since the system of equations has to be solved only once instead of three times.

Five examples are used to demonstrate the feasibility and accuracy of the INMFS. The first and the fourth examples are used to show the feasibility for single domain problems of isotropic and anisotropic cases. The second example is about the isotropic pressurized cylinder problem to show the advantages as compared with the MFS and the NMFS. In these three examples, the INMFS solutions are compared to the MFS solution, the NMFS solutions and analytical solutions. In the third and the fifth examples, isotropic and anisotropic elastic/rigid inclusions and void problems are solved by the INMFS. They show good agreement of INMFS solutions with MFS solutions.

6.2 Solution Procedure

The governing equations of the isotropic elasticity problems are given in Eq. (3.3) (3.4) and for anisotropic elasticity problems in Eqs. (3.5) (3.6). Kelvin's fundamental solution Eqs. (3.9) is used in solution of the isotropic governing equations, and the fundamental solution in Eq. (3.21) is used in solving anisotropic governing equations.

The desingularization is performed as in Chapter 4.2 for isotropic problems and in Chapter 5.2 for anisotropic problems.

The diagonal terms $\tilde{T}_{\varsigma\xi}(\mathbf{p}_m,\mathbf{p}_m)$, $\varsigma,\xi=x,y, m=1,...,N^\Gamma$ in Eqs. (4.15) (4.16) are in case of NMFS determined indirectly for collocation points on Γ^T. Invoking the fact that the boundary integration of the forces on the body should vanish in mechanical equilibrium, we can improve the NMFS by solving the following system

$$\int_\Gamma t_x(\mathbf{p})d\Gamma=\sum_{n=1}^{N^\Gamma}\int_\Gamma \tilde{T}_{xx}(\mathbf{p}_m,\mathbf{p}_n)d\Gamma\alpha_n+\sum_{n=1}^{N^\Gamma}\int_\Gamma \tilde{T}_{xy}(\mathbf{p}_m,\mathbf{p}_n)d\Gamma\beta_n=0 \tag{6.1}$$

$$\int_\Gamma t_y(\mathbf{p})d\Gamma=\sum_{n=1}^{N^\Gamma}\int_\Gamma \tilde{T}_{yx}(\mathbf{p}_m,\mathbf{p}_n)d\Gamma\alpha_n+\sum_{n=1}^{N^\Gamma}\int_\Gamma \tilde{T}_{yy}(\mathbf{p}_m,\mathbf{p}_n)d\Gamma\beta_n=0. \tag{6.2}$$

Eqs. (6.1)(6.2) should be satisfied since these represent the equilibrium equations. The traction conditions are always satisfied if we write

$$\int_\Gamma \tilde{T}_{xx}(\mathbf{p}_m,\mathbf{p}_n)d\Gamma=\int_\Gamma \tilde{T}_{xy}(\mathbf{p}_m,\mathbf{p}_n)d\Gamma=0, \tag{6.3}$$

$$\int_\Gamma \tilde{T}_{yx}(\mathbf{p}_m,\mathbf{p}_n)d\Gamma=\int_\Gamma \tilde{T}_{yy}(\mathbf{p}_m,\mathbf{p}_n)d\Gamma=0, \tag{6.4}$$

and $\tilde{T}_{\varsigma\xi}(\mathbf{p}_m,\mathbf{p}_m)$ can be evaluated as

$$\tilde{T}_{xx}(\mathbf{p}_n,\mathbf{p}_n)=-\frac{1}{l_n}\sum_{m=1,m\neq n}^{N^\Gamma}\tilde{T}_{xx}(\mathbf{p}_m,\mathbf{p}_n)l_m, \tag{6.5}$$

$$\tilde{T}_{xy}(\mathbf{p}_n,\mathbf{p}_n)=-\frac{1}{l_n}\sum_{m=1,m\neq n}^{N^\Gamma}\tilde{T}_{xy}(\mathbf{p}_m,\mathbf{p}_n)l_m, \tag{6.6}$$

$$\tilde{T}_{yx}(\mathbf{p}_n,\mathbf{p}_n)=-\frac{1}{l_n}\sum_{m=1,m\neq n}^{N^\Gamma}\tilde{T}_{yx}(\mathbf{p}_m,\mathbf{p}_n)l_m, \tag{6.7}$$

$$\tilde{T}_{yy}(\mathbf{p}_n,\mathbf{p}_n)=-\frac{1}{l_n}\sum_{m=1,m\neq n}^{N^\Gamma}\tilde{T}_{yy}(\mathbf{p}_m,\mathbf{p}_n)l_m. \tag{6.8}$$

Solution procedure for a bi-material is the same as described in Chapter 3.5.

6.3 Numerical Examples

6.3.1 Example 6.1: Single Isotropic Material

Example 6.1 is the same as Case 4.1.1 in Example 4.1 (see Figure 4.2). A plot of the RMS errors of boundary points, obtained with the numerical solutions with NMFS and INMFS is shown in Figure 6.1, and the values are given in Table 6.1. The

number of boundary nodes used is from 100 to 1924. The radius of the circular disk for the distributed area source covering each node is set to $R = d/5$.

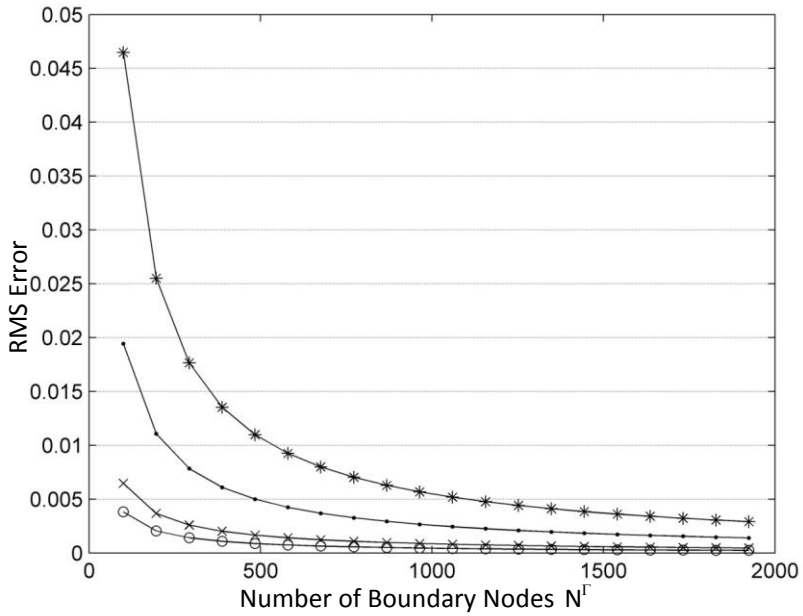

Figure 6.1: Example 6.1. The relationship between the RMS errors of boundary points and the number of boundary nodes, calculated by NMFS and INMFS (NMFS: e_x : ◦, e_y : × . INMFS: e_x : •, e_y : ∗).

Figure 6.1 shows RMS errors of boundary points obtained using the NMFS and INMFS. The solution converges to the analytical solution with the increasing number of the nodes. In this case, both the results of u_x and u_y obtaied with INMFS are not better than the NMFS results for boundary points. But the results of INMFS for u_y is better than NMFS for points on the line $-0.95\,\mathrm{m} \le p_x = p_y \le 0.95\,\mathrm{m}$ (see Figure 6.2 and Table 6.2). On the other hand, the NMFS can't solve the external problems. And the INMFS can solve these problems very well.

Table 6.1: Example 6.1. RMS errors of MFS, NMFS and INMFS solutions for boundary points with $R_M = 5d$, $R = d/5$.

Number of boundary nodes (N^{Γ})	MFS		NMFS		INMFS	
	$e_x(\times 10^{-2})$	$e_y(\times 10^{-2})$	$e_x(\times 10^{-2})$	$e_y(\times 10^{-2})$	$e_x(\times 10^{-2})$	$e_y(\times 10^{-2})$
100	0.0001	0.0001	0.3812	0.6467	1.9429	4.6479
196	0.0000	0.0000	0.2044	0.3672	1.1073	2.5512
292	0.0000	0.0000	0.1408	0.2595	0.7833	1.7660
388	0.0067	0.0073	0.1078	0.2017	0.6090	1.3531
484	0.0086	0.0055	0.0875	0.1654	0.4995	1.0979
580	0.0001	0.0001	0.0737	0.1405	0.4242	0.9243
676	0.0000	0.0000	0.0638	0.1222	0.3690	0.7986
772	0.0005	0.0002	0.0562	0.1082	0.3268	0.7032
868	0.0007	0.0003	0.0503	0.0972	0.2935	0.6283
964	0.0181	0.0139	0.0455	0.0882	0.2664	0.5679
1060	0.0849	0.0556	0.0416	0.0808	0.2440	0.5183
1156	0.0002	0.0004	0.0383	0.0746	0.2252	0.4766
1252	0.0004	0.0005	0.0355	0.0693	0.2091	0.4412
1348	0.1234	0.0840	0.0331	0.0647	0.1952	0.4108
1444	0.0003	0.0003	0.0310	0.0606	0.1831	0.3843
1540	0.0003	0.0004	0.0292	0.0571	0.1724	0.3610
1636	0.0001	0.0002	0.0275	0.0540	0.1629	0.3404
1732	0.0000	0.0001	0.0261	0.0512	0.1545	0.3221
1828	0.0001	0.0001	0.0248	0.0486	0.1469	0.3056
1924	0.3393	0.2868	0.0236	0.0464	0.1400	0.2908

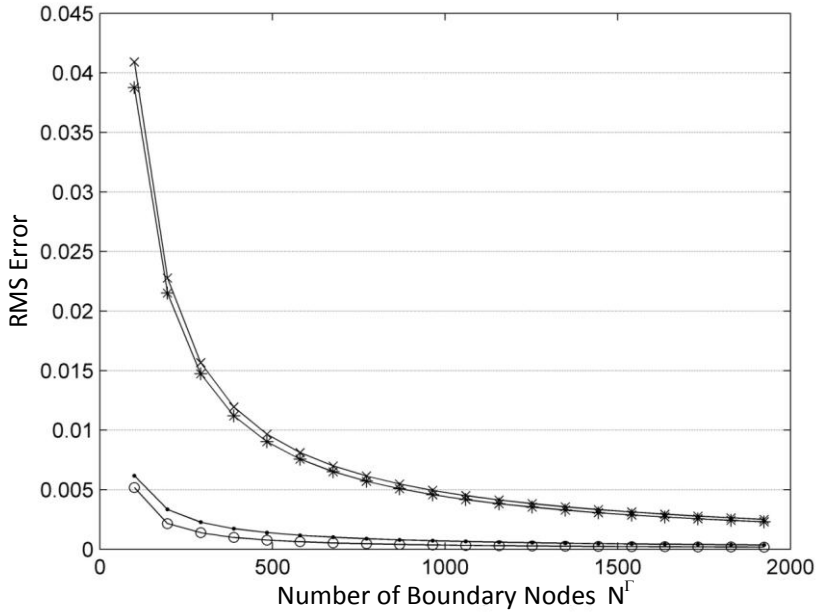

Figure 6.2: Example 6.1. The relationship between the RMS errors in domain points $-0.95\,\mathrm{m} \le p_x = p_y \le 0.95\,\mathrm{m}$ and the number of boundary nodes, calculated by NMFS and INMFS. $N^{\Omega} = 20$ (NMFS: e_x : $\circ$, e_y : $\times$. INMFS: e_x : $\bullet$, e_y : $*$).

Table 6.2: Example 6.1. RMS errors of MFS, NMFS and INMFS solutions for domain points with $R_M = 5d$, $R = d/5$.

Number of boundary nodes (N^{Γ})	MFS		NMFS		INMFS	
	$e_x(\times 10^{-2})$	$e_y(\times 10^{-2})$	$e_x(\times 10^{-2})$	$e_y(\times 10^{-2})$	$e_x(\times 10^{-2})$	$e_y(\times 10^{-2})$
100	0.0001	0.0001	0.5183	4.0917	0.6170	3.8754
196	0.0000	0.0000	0.2148	2.2766	0.3346	2.1505
292	0.0033	0.0019	0.1395	1.5666	0.2276	1.4734
388	0.0007	0.0003	0.0999	1.1949	0.1734	1.1197
484	0.0129	0.0034	0.0775	0.9662	0.1402	0.9027
580	0.0048	0.0070	0.0633	0.8113	0.1177	0.7561
676	0.0006	0.0004	0.0535	0.6993	0.1014	0.6504
772	0.0034	0.0032	0.0463	0.6146	0.0891	0.5706
868	0.0034	0.0013	0.0409	0.5482	0.0794	0.5082
964	0.0420	0.0139	0.0366	0.4949	0.0717	0.4581
1060	0.0160	0.0163	0.0331	0.4510	0.0653	0.4170
1156	0.0346	0.0182	0.0303	0.4143	0.0599	0.3827
1252	0.1029	0.0855	0.0279	0.3831	0.0554	0.3536
1348	0.0651	0.0556	0.0259	0.3563	0.0515	0.3286
1444	0.0184	0.0040	0.0241	0.3331	0.0481	0.3069
1540	0.0164	0.0115	0.0226	0.3126	0.0451	0.2878
1636	0.0049	0.0047	0.0213	0.2946	0.0425	0.2710
1732	0.3685	0.0693	0.0201	0.2785	0.0402	0.2561
1828	0.0092	0.0028	0.0190	0.2641	0.0381	0.2427
1924	0.0192	0.0296	0.0181	0.2511	0.0362	0.2307

6.3.2 Example 6.2: Isotropic Pressurized Cylinder Problem

In this example, consider the hollow cylinder shown in Figure 6.3. The inner radius is denoted as $r_i = 4$ mm and outer radius $r_o = 12$ mm. The cylinder is subjected to an internal pressure $F = 100$ Mpa. The analytical solutions for the problems are given as (in Cartesian coordinate system, see [Aliabadi (2002)] and Figure 6.3).

$$u_x = \frac{(1-\nu)Fr}{E\left[\left(\frac{r_o}{r_i}\right)^2 - 1\right]}\left[\left(\frac{r_o}{r}\right)^2 + (1-2\nu)\right]\cos\theta, \tag{6.9}$$

$$u_y = \frac{(1-\nu)Fr}{E\left[\left(\frac{r_o}{r_i}\right)^2 - 1\right]}\left[\left(\frac{r_o}{r}\right)^2 + (1-2\nu)\right]\sin\theta, \tag{6.10}$$

where $r = \sqrt{p_x^2 + p_y^2}$, $\cos\theta = p_x / r$. Elastic media is defined by $E = 730000$ Mpa , $v = 0.32$.

We consider a solution of the Navier's equations in this cylinder subject to the boundary conditions $\bar{t}_x = 0$ N/m^2 and $\bar{u}_y = 0$ mm when $\theta = 0$ and π on the side of $r = r_o$; $\bar{u}_x = 0$ mm and $\bar{t}_y = 0$ N/m^2 when $\theta = \pi / 2$ and $3\pi / 2$ on the side of $r = r_o$ (because the solution of the PDE is on our case also solution plus a constant); $\bar{t}_x = 0$ N/m^2 and $\bar{t}_y = 0$ N/m^2 on the other points of the side $r = r_o$; $\bar{t}_x = F\cos\theta$ N/m^2 and $\bar{t}_y = F\sin\theta$ N/m^2 on the side of $r = r_i$.

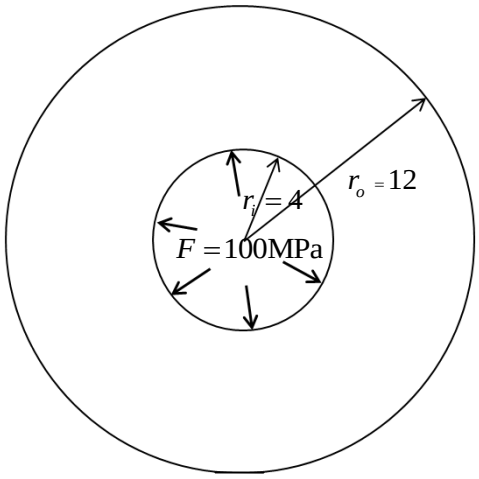

Figure 6.3: Example 6.2. A pressurized cylinder.

A plot of the deformation, obtained with the analytical solution and the numerical solutions with MFS, NMFS and INMFS is shown in Figure 6.4 for the case with 32 nodes. The distance of the fictitious boundary from the true boundary for the MFS is set $R_M = 5d$. The radius of the circular disk for the distributed area source covering each node is set to $R = d / 5$.

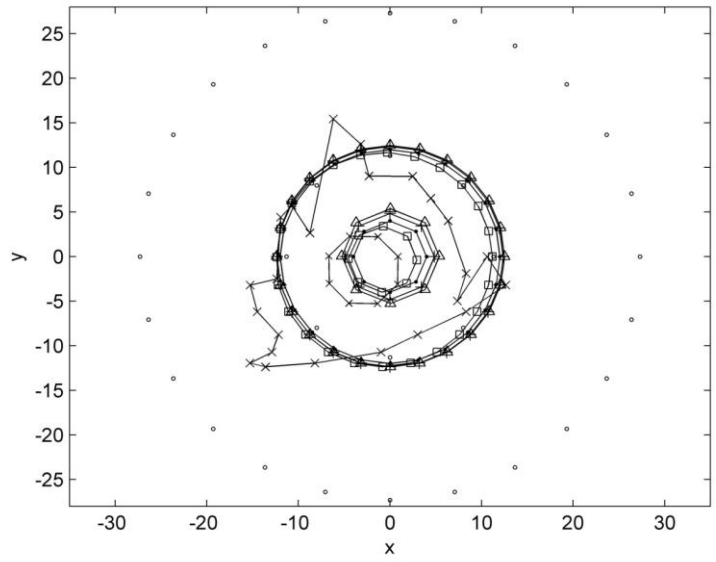

Figure 6.4: Example 6.2. The analytical solution and the numerical solution of MFS, NMFS and INMFS with $N^{\Gamma} = 32$ ($\bullet$: collocation points; $\circ$: source points in MFS; $+$: analytical solution; $\times$: MFS solution; $\square$: NMFS solution; $\triangle$: INMFS solution).

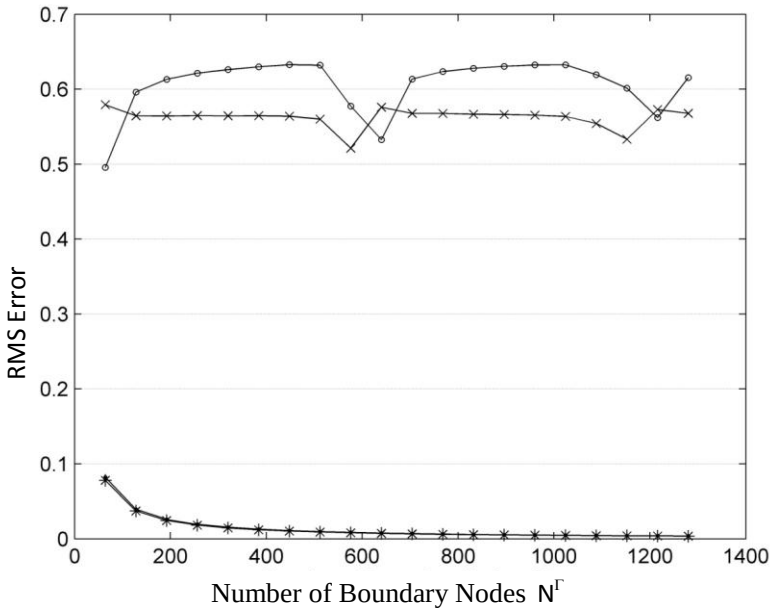

Figure 6.5: Example 6.2. The relationship between the RMS errors and the number of boundary nodes for boundary points, calculated by NMFS and INMFS (NMFS: e_x: $\circ$, e_y: $\times$. INMFS: e_x: $\bullet$, e_y: $*$).

From Figure 6.4, we can see that the result of MFS is unacceptable. This is because the hole inside is too small to accommodate the source points. The location of the

source points for MFS in the domain would lead to wrong results. On the other side, the result of INMFS are much better than the NMFS.

A plot of the RMS errors of boundary points, obtained with the numerical solutions with NMFS and INMFS is shown in Figure 6.5 and the values are given in Table 6.3. The number of boundary nodes used is from 64 to 1280 . The radius of the circular disk for the distributed area source covering each node is set to $R = d / 5$.

Table 6.3: Example 6.2. The RMS errors of Boundary points.

Number of boundary nodes e (N^{Γ})	MFS		NMFS		INMFS	
	e_x	e_y	e_x	e_y	e_x	e_y
64	0.4310	0.3651	0.4955	0.5793	0.0823	0.0780
128	0.0000	0.0000	0.5961	0.5644	0.0394	0.0372
192	0.0000	0.0000	0.6132	0.5644	0.0260	0.0245
256	0.0000	0.0000	0.6213	0.5648	0.0194	0.0182
320	0.0000	0.0000	0.6261	0.5645	0.0154	0.0145
384	0.0000	0.0000	0.6299	0.5646	0.0128	0.0121
448	0.0000	0.0000	0.6327	0.5640	0.0110	0.0103
512	0.0000	0.0000	0.6321	0.5600	0.0096	0.0090
576	0.0000	0.0000	0.5775	0.5213	0.0085	0.0080
640	0.0000	0.0000	0.5326	0.5760	0.0077	0.0072
704	0.0000	0.0000	0.6135	0.5677	0.0070	0.0066
768	0.0000	0.0000	0.6234	0.5676	0.0064	0.0060
832	0.0000	0.0000	0.6279	0.5666	0.0059	0.0055
896	0.0000	0.0000	0.6306	0.5662	0.0055	0.0051
960	0.0000	0.0000	0.6324	0.5654	0.0051	0.0048
1024	0.0000	0.0000	0.6325	0.5635	0.0048	0.0045
1088	0.0000	0.0000	0.6193	0.5542	0.0045	0.0042
1152	0.0000	0.0000	0.6014	0.5333	0.0042	0.0040
1216	0.0000	0.0000	0.5621	0.5728	0.0040	0.0038
1280	0.0000	0.0000	0.6155	0.5677	0.0038	0.0036

From Figure 6.5 we see, that the solution of INMFS converges to the analytical solution with the increasing number of the nodes and it is much better than the solution of NMFS.

6.3.3 Example 6.3: Isotropic Elastic/Rigid Inclusions and Void Problems

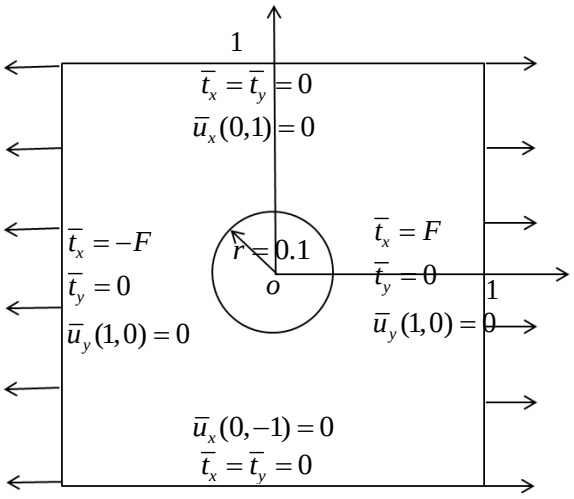

Figure 6.6: Example 6.3. A square plate with a circlar hole (or elastic/rigid inclusion) under tension, isotropic material.

We consider a square with the side length $a = 2\,\text{m}$ in Example 6.3. We distinguish five cases. In the first one, the square domain is a homogenous materal. In other cases, there is a circular domain with radius $r = 0.1\,\text{m}$ inserted in the square. In all of these cases, we consider the solution of the Navier's equations in this square subject to the boundary conditions $\bar{u}_x = 0\,\text{m}$ on the points $(0\,\text{m}, 1\,\text{m})$ and $(0\,\text{m}, -1\,\text{m})$; $\bar{u}_y = 0\,\text{m}$ on the points $(1\,\text{m}, 0\,\text{m})$ and $(-1\,\text{m}, 0\,\text{m})$; $\bar{t}_x = F$, $\bar{t}_y = 0\,\text{N/m}^2$ on the east sides of the square with $p_x = 1\,\text{m}$; $\bar{t}_x = -F$, $\bar{t}_y = 0\,\text{N/m}^2$ on the west sides of the square with $p_x = -1\,\text{m}$; $\bar{t}_x = 0\,\text{N/m}^2$, $\bar{t}_y = 0\,\text{N/m}^2$ on the other points of north and south sides of the square with $p_y = -1\,\text{m}$ and $p_y = 1\,\text{m}$. The following parameters have been used $R = d/5$, $R^{\text{II}} = d^{\text{II}}/5$. The distance of the fictitious boundary from the true boundary in case of MFS is $R_M = 5d$, $R_M^{\text{II}} = 5d^{\text{II}}$. $F = 0.5\,\text{Pa}$ (see Figure 6.6).

Case 6.3.1: Single Domain Problem

In Case 6.3.1, the square domain is a homogenous materal with properties $E = 1\,\text{N/m}^2$, $\nu = 0.25$. A plot of the deformation is shown in Figure 6.7.

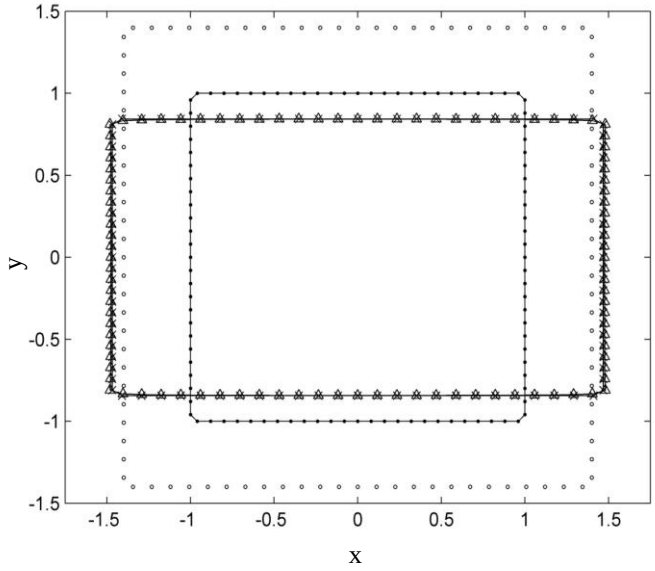

Figure 6.7: Case 6.3.1. The deformation, calculated with MFS and INMFS with $E = 1\,\mathrm{N/m^2}$, $\nu = 0.25$, $N^{\Gamma} = 100$ ($\bullet$: collocation points; $\circ$: source points in MFS; $\times$: MFS solution; $\triangle$: INMFS solution).

From Figure 6.7, we see that INMFS results almost coincide with the MFS results in case with no inclusions. We also see that the method can capture the elastic inclusion problem with the same property as the elastic square matrix.

Case 6.3.2: Void Problem

In Case 6.3.2, the circular domain is empty. The square domain has the same properties as in Case 6.3.1. A plot of the deformation is shown in Figure 6.8.

In Figure 6.8, $N^{\Gamma} = 540$ was used for MFS and $N^{\Gamma} = 108$ was used for INMFS. It is because there is not enough space inside for source points for MFS when $N^{\Gamma} = 108$ and the result is not clear in the picture for INMFS when $N^{\Gamma} = 540$. It can be observed from Figure 6.8, that MFS solution and INMFS solution almost coincide. The maximum absolute difference in displacements between MFS solution and INMFS solution at the boundary are $\triangle u_x = 0.0125\,\mathrm{m}$, $\triangle u_y = 0.0101\,\mathrm{m}$, when $N^{\Gamma} = 540$. The results of domain points are given in Table 6.4.

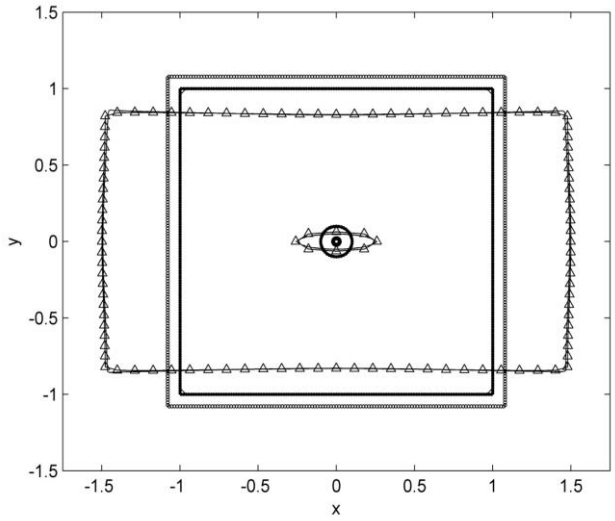

Figure 6.8: Case 6.3.2. The deformation, calculated with MFS and INMFS, for void problem with $E = 1\,\mathrm{N/m^2}$, $\nu = 0.25$, $N^{\Gamma} = 108$ ($\bullet$: collocation points; $\circ$: source points in MFS; $-$: MFS solution; $\triangle$: INMFS solution).

Table 6.4: Case 6.3.2. The deformation for domain point in Figure 6.9.

p_x	p_y	MFS		INMFS		$\triangle u_x$	$\triangle u_y$
		u_x	u_y	u_x	u_y		
0.00	0.50	-0.0003	-0.0969	-0.0000	-0.0954	0.0003	0.0015
0.25	0.50	0.1206	-0.0894	0.1211	-0.0883	0.0005	0.0012
0.50	0.50	0.2432	-0.0808	0.2438	-0.0801	0.0006	0.0007
0.50	0.25	0.2559	-0.0379	0.2562	-0.0374	0.0002	0.0005
0.50	0.00	0.2661	-0.0004	0.2661	-0.0000	0.0000	0.0004

In this case, the boundary conditions are symmetrical about the x and y axises. So u_x should be 0 at point $(0\,\mathrm{m}, 0.5\,\mathrm{m})$ on the axises of symmetry of y and and u_y should equal 0 at point $(0.5\,\mathrm{m}, 0\,\mathrm{m})$ on the axises of symmetry of x. From Table 6.4, we see the results with INMFS are better than with the MFS for this case.

Case 6.3.3: Elastic Inclusion Problem with the Same Inclusion and Matrix Properties

In Case 6.3.3, the circular domain is elastic material with properties $E^{\mathrm{II}} = 1\,\mathrm{N/m^2}$, $\nu^{\mathrm{II}} = 0.25$. The square domain is the same as in the Case 6.3.1. A plot of the deformation is shown in Figure 6.9. $N^{\Gamma} = 500$ for MFS and $N^{\Gamma} = 100$ for INMFS are used for Figure 6.9, Figure 6.10 and Figure 6.11.

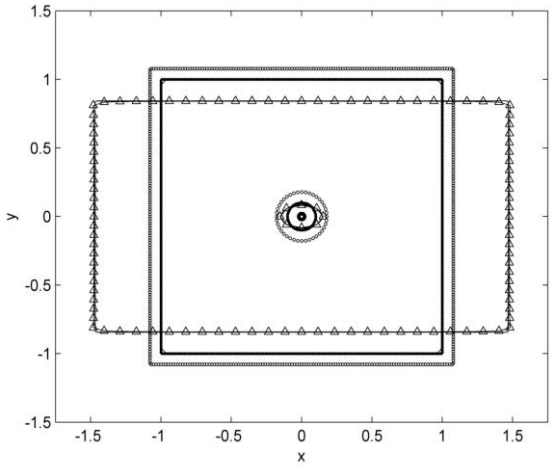

Figure 6.9: Case 6.3.3. The deformation, calculated with MFS and INMFS, for the elastic inclusion problem with $E = E^{\mathrm{II}} = 1\,\mathrm{N/m^2}$, $\nu = \nu^{\mathrm{II}} = 0.25$ ($\bullet$: collocation points; $\circ$: source points in MFS; $-$: MFS solution; $\triangle$: INMFS solution).

In Figure 6.9, the two materials have the same property. The INMFS result is used to compare with the MFS and almost the same as the MFS result. On the other hand, the INMFS result is also used to compare with itself for the single material in the Figure 6.7. The maximum absolute difference in displacements between Figure 6.7 and Figure 6.9 calculated by INMFS at the boundary are $\triangle u_x = 0.0013\mathrm{m}$ and $\triangle u_y = 0.0005\,\mathrm{m}$ under the case $N^{\Gamma} = 100$.

Case 6.3.4: Elastic Inclusion Problem with Different Inclusion and Matrix Properties

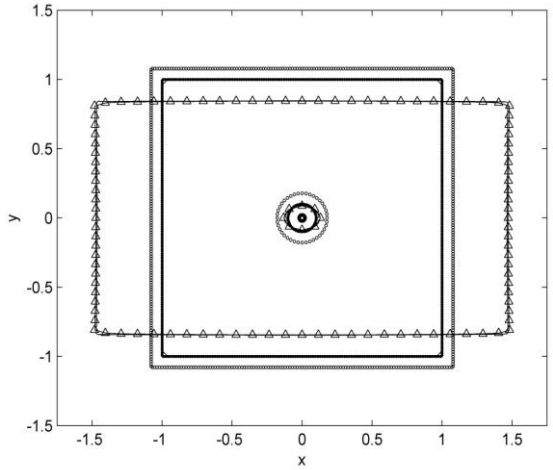

Figure 6.10: Case 6.3.4. The deformation, calculated with MFS and INMFS, for elastic inclusion problem with $E = 1\,\mathrm{N/m^2}$, $\nu = 0.25$ and $E^{\mathrm{II}} = 2\,\mathrm{N/m^2}$, $\nu^{\mathrm{II}} = 0.3$ ($\bullet$: collocation points; $\circ$: source points in MFS; $-$: MFS solution; $\triangle$: INMFS solution).

In Case 6.3.4, the circular domain is elastic material with properties $E^{\mathrm{II}} = 2\ \mathrm{N/m}^2$, $\nu^{\mathrm{II}} = 0.3$. The square domain is the same as in Case 6.3.1. A plot of the deformation is shown in Figure 6.10.

Case 6.3.5: Rigid Inclusion Problem

In Case 6.3.5, the circular inclusion is a rigid material and the square domain is the same as in Case 6.3.1. A plot of the deformation is shown in Figure 6.11.

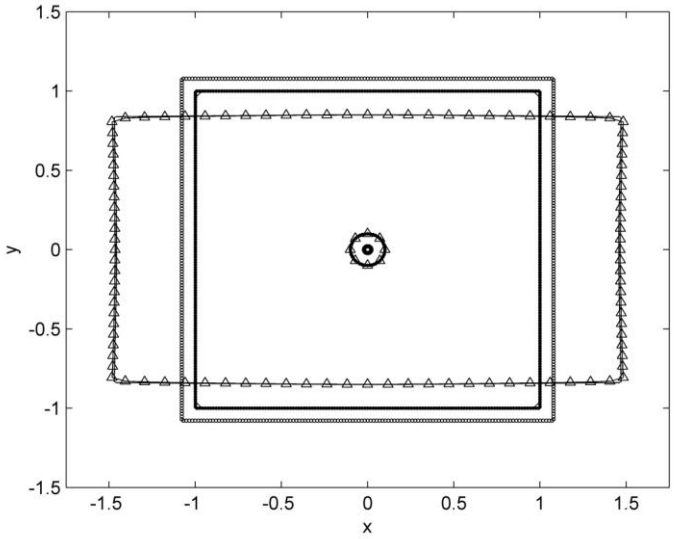

Figure 6.11: Case 6.3.5. The deformation, calculated with MFS and INMFS, for rigid inclusion problem with $E = 1\ \mathrm{N/m}^2$, $\nu = 0.25$ ($\bullet$: collocation points; $\circ$: source points in MFS; $-$: MFS solution; $\triangle$: INMFS solution).

In Figure 6.10 and Figure 6.11, the harder elastic and the rigid inclusion problems are presented. The INMFS was used to compare with the MFS. And the results are almost the same. But more boundary nodes was used for MFS than for INMFS.

6.3.4 Example 6.4: Single Anisotropic Material

In Example 6.4, we use the same example as Example 5.1 (see Figure 5.3 and Figure 5.6). A selection of $N^{\Omega} = 20$ field points inside the domain along the line $p_y = 0\ \mathrm{m}$ with $-0.95\ \mathrm{m} \le p_x \le 0.95\ \mathrm{m}$ is taken for computing the RMS error. The number of boundary nodes used is from 200 to 2000.

Case 6.4.1: Dirichlet Boundary Conditions

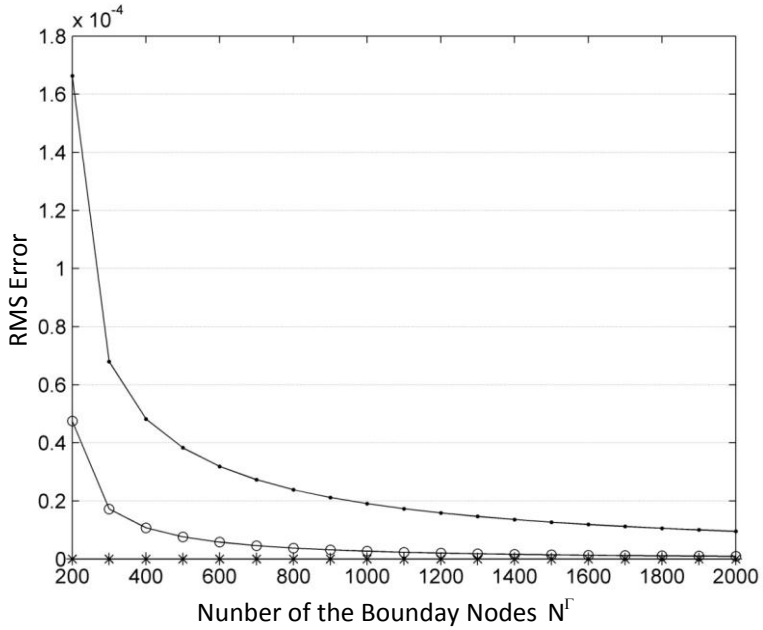

Figure 6.12: Case 6.4.1. The relationship between the RMS errors of domain points $p_y = 0\,\mathrm{m}$ and $-0.95\,\mathrm{m} \le p_x \le 0.95\,\mathrm{m}$ and the number of boundary nodes, calculated by NMFS and INMFS. $N^{\Omega} = 20$ (NMFS: e_x : $\circ$, e_y : $\times$. INMFS: e_x : $\bullet$, e_y : $*$).

Table 6.5: Case 6.4.1. RMS errors of MFS, NMFS and INMFS solutions with $R_M = 5d$, $R = d/5$.

Number of boundary nodes (N^{Γ})	MFS		NMFS		INMFS	
	$e_x(\times 10^{-4})$	$e_y(\times 10^{-4})$	$e_x(\times 10^{-4})$	$e_y(\times 10^{-4})$	$e_x(\times 10^{-4})$	$e_y(\times 10^{-4})$
200	0.0000	0.0000	0.4749	0.0000	1.6637	0.0000
300	0.0001	0.0001	0.1722	0.0000	0.6793	0.0000
400	0.0000	0.0000	0.1075	0.0000	0.4821	0.0000
500	0.0004	0.0012	0.0766	0.0000	0.3831	0.0000
600	0.0000	0.0000	0.0582	0.0000	0.3186	0.0000
700	0.0005	0.0006	0.0461	0.0000	0.2728	0.0000
800	0.0000	0.0000	0.0377	0.0000	0.2385	0.0000
900	0.0001	0.0004	0.0316	0.0000	0.2119	0.0000
1000	0.0000	0.0001	0.0269	0.0000	0.1906	0.0000
1100	0.0014	0.0003	0.0233	0.0000	0.1732	0.0000
1200	0.0001	0.0004	0.0205	0.0000	0.1588	0.0000
1300	0.0003	0.0005	0.0182	0.0000	0.1465	0.0000
1400	0.0025	0.0004	0.0162	0.0000	0.1360	0.0000
1500	0.0003	0.0001	0.0146	0.0000	0.1269	0.0000
1600	0.0000	0.0001	0.0133	0.0000	0.1190	0.0000
1700	0.0011	0.0009	0.0121	0.0000	0.1120	0.0000
1800	0.0002	0.0001	0.0111	0.0000	0.1057	0.0000
1900	0.0006	0.0001	0.0103	0.0000	0.1001	0.0000
2000	0.0007	0.0005	0.0095	0.0000	0.0951	0.0000

Case 6.4.2: Mixed Boundary Conditions

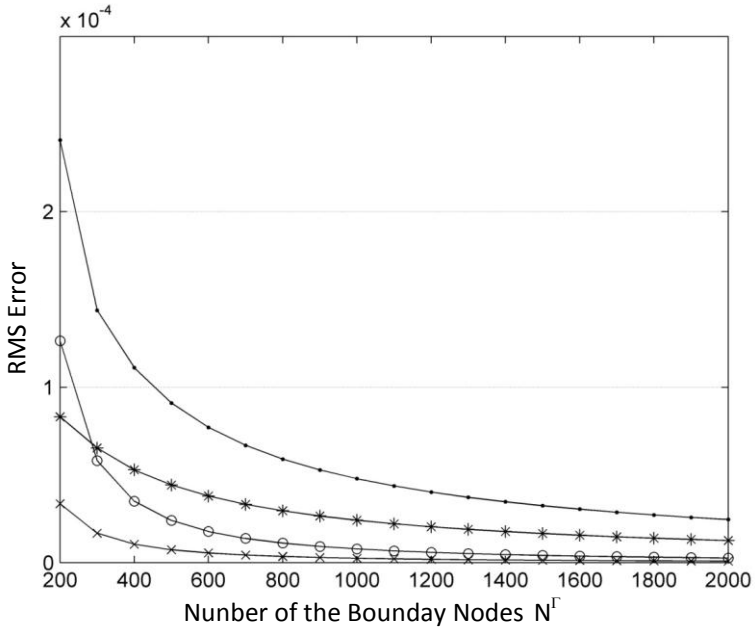

Figure 6.13: Case 6.4.2. The relationship between the RMS errors of domain points $p_y = 0\,\mathrm{m}$ and $-0.95\,\mathrm{m} \le p_x \le 0.95\,\mathrm{m}$ and the number of boundary nodes, calculated by NMFS and INMFS. $N^{\Omega} = 20$ (NMFS: e_x : $\circ$, e_y : $\times$. INMFS: e_x : $\bullet$, e_y : $*$).

Table 6.6: Case 6.4.2. RMS errors of MFS, NMFS and INMFS solutions with $R_M = 5d$, $R = d/5$.

Number of boundary nodes (N^{Γ})	MFS		NMFS		INMFS	
	$e_x(\times 10^{-4})$	$e_y(\times 10^{-4})$	$e_x(\times 10^{-4})$	$e_y(\times 10^{-4})$	$e_x(\times 10^{-4})$	$e_y(\times 10^{-4})$
200	0.0009	0.0027	1.2641	0.3357	2.4085	0.8312
300	0.0003	0.0002	0.5809	0.1673	1.4388	0.6534
400	0.0022	0.0081	0.3504	0.1046	1.1108	0.5289
500	0.0015	0.0014	0.2400	0.0732	0.9101	0.4424
600	0.0014	0.0042	0.1774	0.0550	0.7710	0.3796
700	0.0015	0.0013	0.1379	0.0432	0.6688	0.3322
800	0.0009	0.0015	0.1111	0.0351	0.5904	0.2952
900	0.0004	0.0009	0.0920	0.0292	0.5285	0.2656
1000	0.0175	0.0438	0.0778	0.0249	0.4784	0.2414
1100	0.0011	0.0007	0.0670	0.0215	0.4369	0.2212
1200	0.0096	0.0192	0.0584	0.0188	0.4020	0.2041
1300	0.0032	0.0126	0.0515	0.0166	0.3723	0.1895
1400	0.0112	0.0105	0.0459	0.0148	0.3467	0.1768
1500	0.2267	0.3238	0.0412	0.0133	0.3244	0.1657
1600	0.0062	0.0084	0.0373	0.0121	0.3048	0.1559
1700	0.0067	0.0169	0.0339	0.0110	0.2874	0.1473
1800	0.0124	0.0294	0.0311	0.0101	0.2719	0.1395
1900	0.0070	0.0046	0.0286	0.0093	0.2580	0.1325
2000	0.0074	0.0050	0.0264	0.0086	0.2454	0.1262

In both of the above cases, the solution converges to the analytical solution with the increasing number of the nodes. The results of u_x and u_y, computed with INMFS are not more accurate than the ones with NMFS. However the external problems, the void problems and the inclusion problems cannot be solved by NMFS. And the INMFS is suitable for solving these types of problems.

6.3.5 Example 6.5: Anisotropic Elastic/Rigid Inclusions and Void Problems

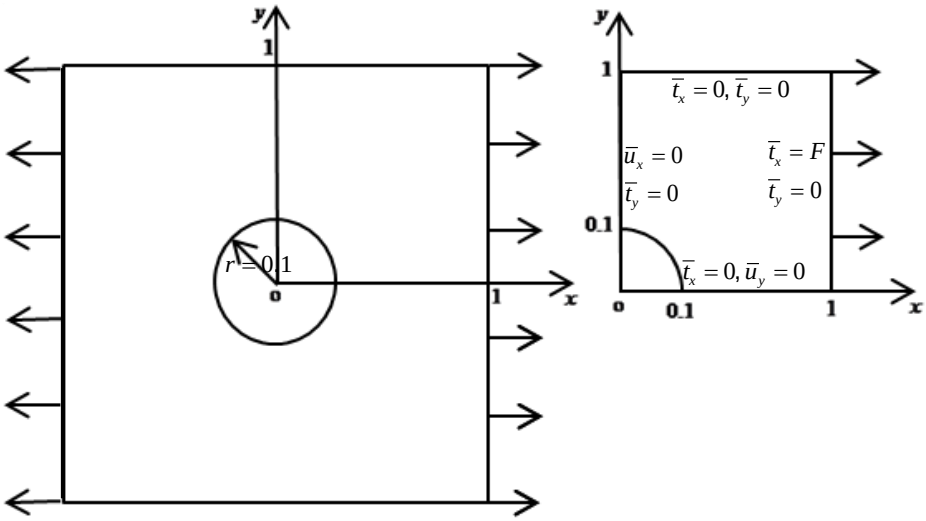

Figure 6.14: Example 6.5. A square plate with a circular hole (or elastic/rigid inclusion) under tension, anisotropic material.

Consider a square with the side length $a = 2\text{m}$ under the symmetrical tensile stresses in Example 6.5. We distinguish five cases. In the first case, the square domain is a homogenous cubic anisotropic materal. In other cases, there is a circular domain with the radius $r = 0.1\,\text{m}$ in the square. The defined problems is symmetry around x as well as y axis. Respectively, a quarter of this domain can be selected for computational purposes, demonstrating the feasibility of INMFS for this type of problems. On the other side, a quarter of this domain is chosen to allow the source points of MFS to be located outside the domain. We consider the boundary conditions $\bar{t}_x = F$, $\bar{t}_y = 0\ \text{N/m}^2$ on the east side of the square with $p_x = 1\,\text{m}$; $\bar{t}_x = 0\ \text{N/m}^2$, $\bar{t}_y = 0\ \text{N/m}^2$ on the north side of the square with $p_y = 1\,\text{m}$; $\bar{u}_x = 0\,\text{m}$, $\bar{t}_y = 0\ \text{N/m}^2$ on the west side of the square with $p_y = 0\,\text{m}$; $\bar{t}_x = 0\ \text{N/m}^2$, $\bar{u}_y = 0\,\text{m}$ on the south side of the square with $p_x = 0\,\text{m}$. The following parameters have been used $R = d/5$, $R^{\text{II}} = d^{\text{II}}/5$. The distance of the fictitious boundary from the true boundary in case of MFS is $R_M = 4d$, $R_M^{\text{II}} = 4d^{\text{II}}$. $F = 0.5\ \text{Pa}$ (see Figure 6.14).

Case 6.5.1: single domain

In Case 6.5.1, the square domain is a homogenous cubic anisotropic materal with properties $c_{11} = 16.84\ \text{N/m}^2$, $c_{12} = 12.14\ \text{N/m}^2$, $c_{66} = 7.54\ \text{N/m}^2$. A plot of the deformation is shown in Figure 6.15.

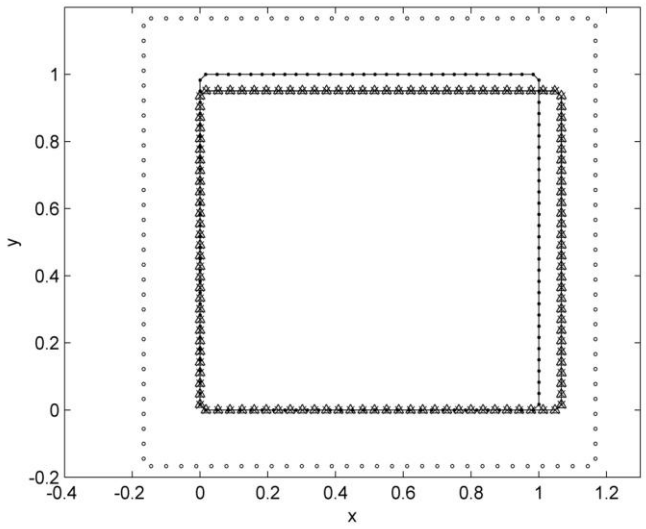

Figure 6.15: Case 6.5.1. The deformation, calculated with MFS and INMFS, $N^{\Gamma} = 120$ ($\bullet$: collocation points; $\circ$: source points in MFS; $\times$: MFS solution; $\triangle$: INMFS solution).

From Figure 6.15, we see that INMFS results almost coincide with the MFS results in case with no inclusions. We see also that the method can capture the elastic inclusion problem with the same property as the elastic square matrix.

Case 6.5.2: Void Problem

In Case 6.5.2, the circular domain is empty. The square domain has the same properties as in Case 6.5.1. A plot of the deformation is shown in Figure 6.16.

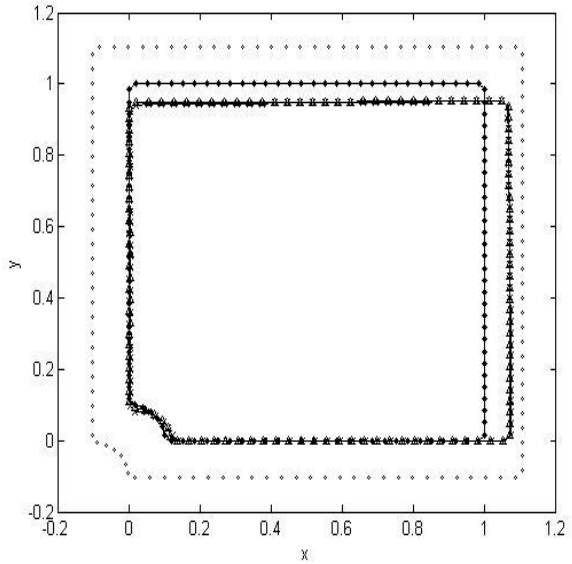

Figure 6.16: Case 6.5.2. The deformation, calculated with MFS and INMFS, for void problem with $N^{\Gamma} = 120$ ($\bullet$: collocation points; $\circ$: source points in MFS; $\times$: MFS solution; $\triangle$: INMFS solution).

It can be observed from Figure 6.16 that the MFS solution and the INMFS solutions almost coincide. And the maximum absolute difference in displacements between MFS solution and INMFS solution at the boundary are $\triangle u_x = 0.0005$,. $\triangle u_y = 0.0133$ The results of domain points are given in Table 6.7.

Table 6.7: Case 6.5.2. The deformation of domain points.

p_x	p_y	MFS		INMFS		$\triangle u_x$	$\triangle u_y$
		u_x	u_y	u_x	u_y		
0.15	0.15	0.0138	-0.0096	0.0129	-0.0070	0.0009	0.0026
0.25	0.25	0.0197	-0.0147	0.0188	-0.0121	0.0009	0.0026
0.35	0.35	0.0262	-0.0199	0.0251	-0.0172	0.0011	0.0027
0.45	0.45	0.0327	-0.0249	0.0315	-0.0222	0.0012	0.0028
0.55	0.55	0.0388	-0.0296	0.0380	-0.0270	0.0009	0.0025
0.65	0.65	0.0446	-0.0339	0.0443	-0.0318	0.0003	0.0021
0.75	0.75	0.0501	-0.0380	0.0506	-0.0364	0.0005	0.0016
0.85	0.85	0.0553	-0.0421	0.0567	-0.0409	0.0015	0.0013
0.95	0.95	0.0602	-0.0467	0.0628	-0.0452	0.0026	0.0014

Case 6.5.3: Elastic Inclusion Problem with the Same Inclusion and Matrix Properties

In Case 6.5.3, the circular inclusion domain is elastic material with properties $c_{11}^{\mathrm{II}} = 16.84\ \mathrm{N/m^2}$, $c_{12}^{\mathrm{II}} = 12.14\ \mathrm{N/m^2}$, $c_{66}^{\mathrm{II}} = 7.54\ \mathrm{N/m^2}$. The square domain is the same as in Case 6.5.1. A plot of the deformation is shown in Figure 6.17.

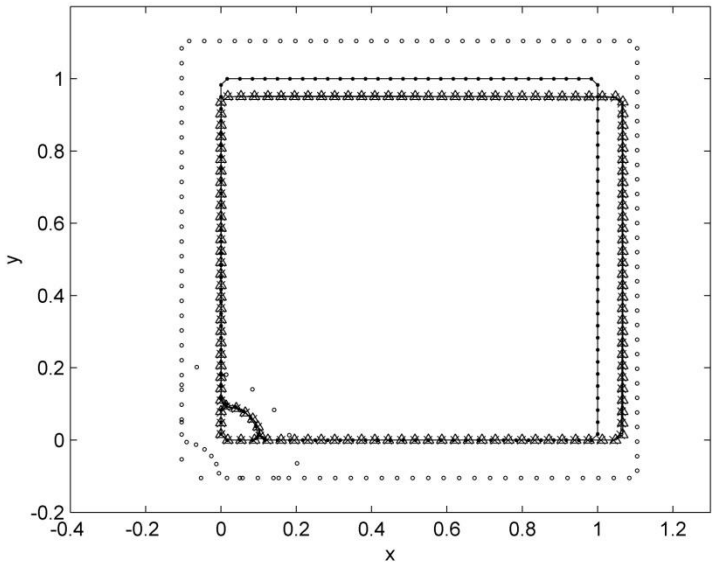

Figure 6.17: Case 6.5.3. The deformation, calculated with MFS and INMFS, for elastic inclusion problem with $c_{11} = c_{11}^{\mathrm{II}} = 16.84\ \mathrm{N/m^2}$, $c_{12} = c_{12}^{\mathrm{II}} = 12.14\ \mathrm{N/m^2}$ and $c_{66} = c_{66}^{\mathrm{II}} = 7.54\ \mathrm{N/m^2}$, $N^{\Gamma} = 120$ ($\bullet$: collocation points; $\circ$: source points in MFS; $\times$: MFS solution; $\triangle$: INMFS solution).

In Figure 6.17, the two materials have the same property. The INMFS result is used to compare with the MFS and the results almost coincide on the boundary. The maximum absolute difference in displacements between MFS solution and INMFS solution at the boundary are $\triangle u_x = 0.0058\,\mathrm{m}$, $\triangle u_y = 0.0033\,\mathrm{m}$. On the other hand, the INMFS result is also used to compare with itself for the single material in Figure 6.15 The maximum absolute difference in displacements between Figure 6.15 and Figure 6.17 calculated by INMFS on the boundary are $\triangle u_x = 0.0014\,\mathrm{m}$, $\triangle u_y = 5.5160\times10^{-4}\,\mathrm{m}$, when $N^{\Gamma} = 120$.

Case 6.5.4: Elastic Inclusion Problems with Different Inclusion and Matrix Properties

In Case 6.5.4, the circular domain is elastic material with properties $c_{11}^{\mathrm{II}} = 24.65\,\mathrm{N/m^2}$, $c_{12}^{\mathrm{II}} = 14.73\,\mathrm{N/m^2}$, $c_{66}^{\mathrm{II}} = 12.47\,\mathrm{N/m^2}$, $\nu^{\mathrm{II}} = 0.3$. The square domain is the same as in Case 6.5.1. A plot of the deformation is shown in Figure 6.18.

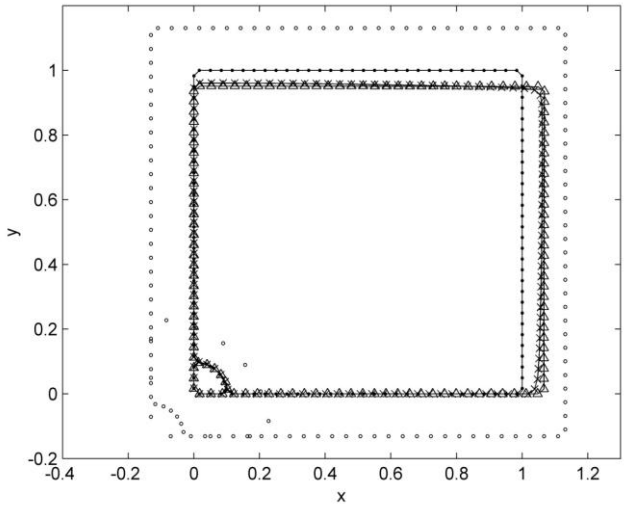

Figure 6.18: Case 6.5.4. The deformation, calculated with MFS and INMFS, for elastic inclusion problem with $c_{11} = 16.84\,\mathrm{N/m^2}$, $c_{12} = 12.14\,\mathrm{N/m^2}$ $c_{66} = 7.54\,\mathrm{N/m^2}$ and $c_{11}^{\mathrm{II}} = 24.65\,\mathrm{N/m^2}$, $c_{12}^{\mathrm{II}} = 14.73\,\mathrm{N/m^2}$, $c_{66}^{\mathrm{II}} = 12.47\,\mathrm{N/m^2}$. $N^{\Gamma} = 120$ ($\bullet$: collocation points; $\circ$: source points in MFS; $\times$: MFS solution; $\triangle$: INMFS solution).

In Figure 6.18, the results of INMFS almost coincide with the MFS results. The maximum absolute difference in displacements between MFS solution and INMFS solution at the boundary are . $\triangle u_x = 0.0047\,\mathrm{m}$, $\triangle u_y = 0.0037\,\mathrm{m}$.

Case 6.5.5: Rigid Inclusion Problems

In Case 6.5.5, the circular domain is a rigid material and the square matrix is the same as in Case 6.5.1. A plot of the deformation is shown in Figure 6.19.

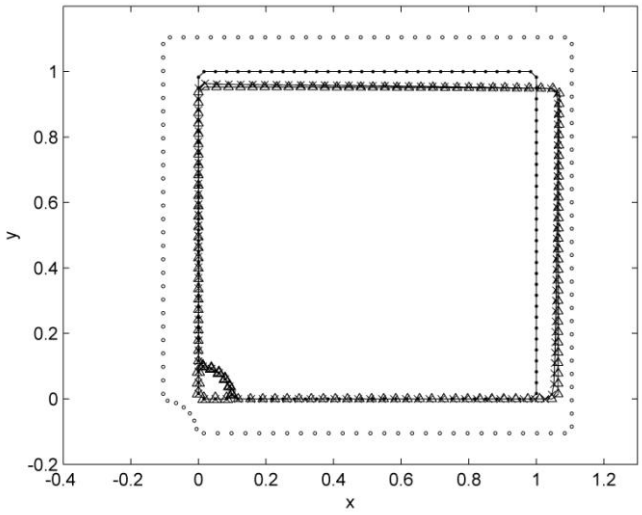

Figure 6.19: Case 6.5.5. The deformation, calculated with MFS and INMFS, for rigid inclusion problems with $N^{\Gamma} = 120$ ($\bullet$: collocation points; $\circ$: source points in MFS; $\times$: MFS solution; $\triangle$: INMFS solution).

In Figure 6.19, the maximum absolute difference in displacements between MFS solution and INMFS solution at the boundary are $\triangle u_x = 0.0202\,\mathrm{m}$, $\triangle u_y = 0.0121\,\mathrm{m}$.

6.4 Discussion

Examples 6.1 and 6.4 show good agreement of INMFS, NMFS and MFS solutions with the analytical solution in a single material problem. Example 6.2 shows feasibility and accuracy of the INMFS solution in isotropic pressurized cylinder problem. Examples 6.3 and 6.5 show the advantages of the INMFS solution for the elastic/rigid inclusions and the void problems.

6.5 Conclusions

The NMFS is improved in this chapter for solving 2D linear isotropic and anisotropic elasticity problems. The singularities are removed in the same way as in the NMFS. The improvement reflects in the calculation of the diagonal elements of the matrix of fundamental tractions for the Neumann boundary conditions by assumption that the sum of all forces on the body should vanish in the mechanical equilibrium. The INMFS essentially gives better results for elastic/rigid inclusions and void problems than NMFS. On the other hand, the INMFS also reduces the computing time. Two novel methods have been represented. Both of these two methods can be used to solve the multi-grain problems as described in the next chapter.

7. Non-singular Method of Fundamental Solutions and Improved Non-singular Method of Fundamental Solutions for Multi-grain Problems

7.1 Introduction

The purpose of this chapter is to demonstrate the application of developed NMFS and INMFS to the multi-grain problems. It is achieved by solving coupled PDEs for each of the grains. The coupling of PDEs is achieved through the boundary conditions on the interfaces of each of the grains. The multi-grain problem can form a part of the macroscopic deformation model.

Five examples are used to demonstrate the feasibility and the accuracy of the NMFS and the INMFS for the multi-grain problems. In the first example, the NMFS is used to solve four and nine grains isotropic problems and the solutions are compared with MFS solution with the normal stress and shear stress boundary conditions, respectively. In the second example, the same case is used for anisotropic problem. In the third and fourth examples, the INMFS is used to solve the nine grains isotropic problems. But the grains have irregular geometries. The last example is more complex. There are nine grains with different properties in the test domain and the properties of one of these nine grains are given in different Cartesian coordinate systems. All the NMFS and INMFS solutions compare well with MFS solution, and turn out to give similar results as the MFS results in all tests. At last, a simulation of deformation of a peace of a realistic microstructure of a spring steel C45 on a 50μm square with 19 grains is given.

7.2 Governing Equations and Solution Procedure

We consider a two-dimensional domain Ω with boundary Γ, divided into M sub-domains $\Omega = \Omega^{\mathrm{I}} \cup \Omega^{\mathrm{II}} \cup \cdots \cup \Omega^{M}$ with boundaries

$\Gamma = (\Gamma^{\mathrm{I}} \cup \Gamma^{\mathrm{II}} \cup \cdots \cup \Gamma^{M}) - \Gamma^{\mathrm{I\text{-}II}} - \cdots - \Gamma^{\mathrm{I}\text{-}M} - \cdots - \Gamma^{(\mathrm{M\text{-}I})\text{-}M}$ as shown in Figure 7.1. Each of the sub-domains is filled with an isotropic or anisotropic, idealy ellastic material with different material properties, in general. The governing equations are formally the same as Eqs. (3.3) (3.4) for isotropic materials and Eqs.(3.5) (3.6) for anisotropic materials with

$$\nu = \begin{cases} \nu^{\mathrm{I}} & \mathbf{p} \in \Omega^{\mathrm{I}}, \\ \nu^{\mathrm{II}} & \mathbf{p} \in \Omega^{\mathrm{II}}, \\ \cdots & \\ \nu^{M} & \mathbf{p} \in \Omega^{M}, \end{cases} \quad u_{\varsigma} = \begin{cases} u_{\varsigma}^{\mathrm{I}} & \mathbf{p} \in \Omega^{\mathrm{I}}, \\ u_{\varsigma}^{\mathrm{II}} & \mathbf{p} \in \Omega^{\mathrm{II}}, \\ \cdots & \\ u_{\varsigma}^{M} & \mathbf{p} \in \Omega^{M}, \end{cases} \quad \varsigma = x, \tag{7.1}$$

and

$$c_{ij} \begin{cases} c_{ij}^{\mathrm{I}} & \mathbf{p} \in \Omega^{\mathrm{I}}, \\ c_{ij}^{\mathrm{II}} & \mathbf{p} \in \Omega^{\mathrm{II}}, \\ \cdots & \\ c_{ij}^{M} & \mathbf{p} \in \Omega^{M}. \end{cases} \tag{7.2}$$

The boundary Γ is divided into two not necessarily connected parts $\Gamma = \Gamma^{D} + \Gamma^{T}$. On the part Γ^{D} the Dirichlet boundary conditions are given, and on the part Γ^{T} the Neumann boundary conditions are given

$$\begin{aligned} &\chi^{\mathrm{I}} u_{\varsigma}^{\mathrm{I}}(\mathbf{p}) + \chi^{\mathrm{II}} u_{\varsigma}^{\mathrm{II}}(\mathbf{p}) + \cdots + \chi^{M} u_{\varsigma}^{M}(\mathbf{p}) = \bar{u}_{\varsigma}(\mathbf{p}), \quad \varsigma = x, y, \mathbf{p} \in \Gamma^{D}, \\ &\chi^{\mathrm{I}} t_{\varsigma}^{\mathrm{I}}(\mathbf{p}) + \chi^{\mathrm{II}} t_{\varsigma}^{\mathrm{II}}(\mathbf{p}) + \cdots + \chi^{M} t_{\varsigma}^{M}(\mathbf{p}) = \bar{t}_{\varsigma}(\mathbf{p}), \quad \varsigma = x, y, \mathbf{p} \in \Gamma^{T}, \end{aligned} \tag{7.3}$$

where

$$\chi^{\mathrm{I}} = \begin{cases} 1 & \mathbf{p} \in \Gamma^{m}, \\ 0 & \mathbf{p} \notin \Gamma^{m}, \end{cases} \tag{7.4}$$

On the interface between different regions, displacement continuity and traction equilibrium conditions have been assumed,

$$\begin{aligned} &u_{\varsigma}^{m}(\mathbf{p}) - u_{\varsigma}^{k}(\mathbf{p}) = 0, \quad \varsigma = x, y, \mathbf{p} \in \Gamma^{m} \cap \Gamma^{k}, \\ &t_{\varsigma}^{m}(\mathbf{p}) + t_{\varsigma}^{k}(\mathbf{p}) = 0, \quad \varsigma = x, y, \mathbf{p} \in \Gamma^{m} \cap \Gamma^{k}, \end{aligned} \quad m, k = \mathrm{I}, \mathrm{II}, \cdots, M. \tag{7.5}$$

Kelvin's fundamental solutions in Eq. (3.9) are used to solve the isotropic governing equations, and the fundamental solution in Eq. (3.21) is for anisotropic governing equations. The parameters are different when they belong to the different grains.

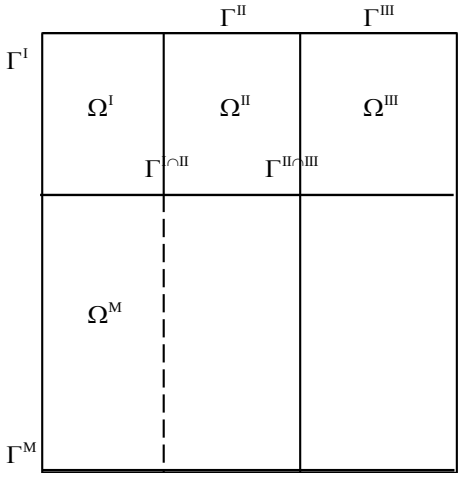

Figure 7.1: A scheme of a multiregional problem. Each of the sub-domains can have different elastic properties, including different type and orientation of anisotropy.

Solution procedure is the same as described in Chapter 4.2 and 4.3 for NMFS and Chapter 6.2 for INMFS.

7.3 Numerical Examples

A square with side $a = 3\,\mathrm{m}$ centered around $p_x = 0\,\mathrm{m}$, $p_y = 0\,\mathrm{m}$ is considered in Chapter 7.3.

7.3.1 Example 7.1: NMFS for Isotropic Multi-grain Problems

We distinguish three cases. In the first one, the homogenous square is occupied by one material, with the material properties $E = 1\,\mathrm{N/m}^2$ $\nu = 0.3$, in the second one, the square is split into four parts with the same material properties as in the first case $E^{\mathrm{I}} = E^{\mathrm{II}} = E^{\mathrm{III}} = E^{\mathrm{IV}} = 1\,\mathrm{N/m}^2$, $\nu^{\mathrm{I}} = \nu^{\mathrm{II}} = \nu^{\mathrm{III}} = \nu^{\mathrm{IV}} = 0.3$; and in the third one, the square is split into nine parts with the same material properties as in the first case $E^{\mathrm{I}} = E^{\mathrm{II}} = \cdots = E^{\mathrm{IX}} = 1\,\mathrm{N/m}^2$, $\nu^{\mathrm{I}} = \nu^{\mathrm{II}} = \cdots = \nu^{\mathrm{IX}} = 0.3$. The distance of the fictitious boundary from the true boundary for the MFS is set to $R_M = 5d$, $R_M^{\mathrm{I}} = 5d^{\mathrm{I}}, \cdots, R_M^{\mathrm{IX}} = 5d^{\mathrm{IX}}$. The following parameters have been used $R = d/5$, $R^{\mathrm{I}} = d^{\mathrm{I}}/5, \cdots, R^{\mathrm{IX}} = d^{\mathrm{IX}}/5$, $c_x = c_y = c_x^{\mathrm{I}} = c_y^{\mathrm{I}} = \cdots = c_x^{\mathrm{IX}} = c_y^{\mathrm{IX}} = 4\,\mathrm{m}$.

Case 7.1.1: Normal Stress Problem

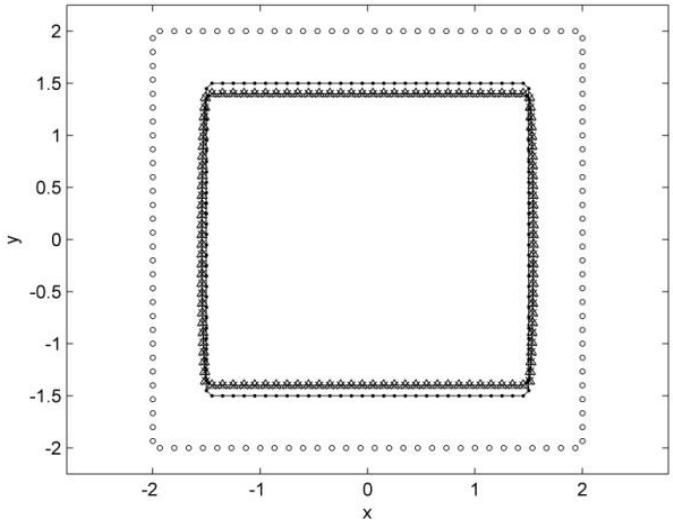

Figure 7.2: Case 7.1.1. The deformation calculated with MFS and NMFS, for a one-domain case with $E=1\,\mathrm{N/m^2}$, $\nu=0.3$ and $N^{\Gamma}=120$ ($\bullet$: collocation points, $\circ$: source points, $\times$: MFS solution, $\triangle$: NMFS solution).

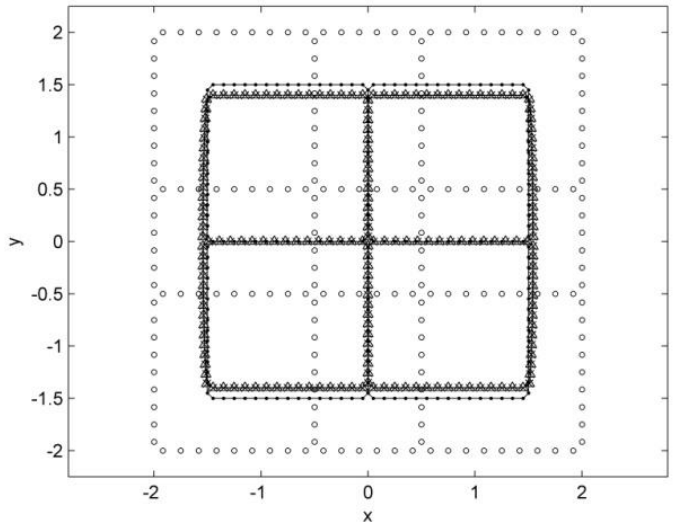

Figure 7.3: Case 7.1.1. The deformation calculated with MFS and NMFS, for a nine-domain case $E^{\mathrm{I}}=E^{\mathrm{II}}=E^{\mathrm{III}}=E^{\mathrm{IV}}=1\,\mathrm{N/m^2}$, $\nu^{\mathrm{I}}=\nu^{\mathrm{II}}=\cdots=\nu^{\mathrm{IX}}=0.3$ and $N^{\Gamma}=120$ ($\bullet$: collocation points, $\circ$: source points, $\times$: MFS solution, $\triangle$: NMFS solution). The position of the source points in MFS is around squares of the square physical sub-domains

We consider the solution of the Navier's equations in this square subject to the following boundary conditions: $\bar{u}_x = 0\,\text{m}$, $\bar{u}_y = -0.1\,\text{m}$ on the north side boundary with $p_y = 1.5\,\text{m}$; $\bar{u}_x = 0\,\text{m}$, $\bar{u}_y = 0.1\,\text{m}$ on the south side boundary with $p_y = -1.5\,\text{m}$, $\bar{t}_x = 0\ \text{N/m}^2$, $\bar{t}_y = 0\ \text{N/m}^2$ on the east side boundary with $p_x = 1.5\,\text{m}$ and on west side boundary with $p_x = -1.5\,\text{m}$. A plot of the deformation, calculated with the defined three cases is shown in Figure 7.2, Figure 7.3 and Figure 7.4, respectively.

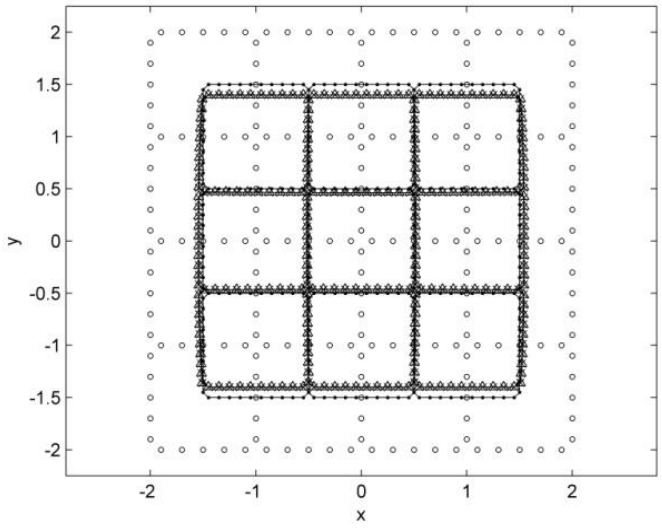

Figure 7.4: Case 7.1.1. The deformation calculated with MFS and NMFS, for a nine-domain case $E^{\text{I}} = E^{\text{II}} = \cdots = E^{\text{IX}} = 1\ \text{N/m}^2$, $\nu^{\text{I}} = \nu^{\text{II}} = \cdots = \nu^{\text{IX}} = 0.3$ and $N^{\Gamma} = 120$ ($\bullet$: collocation points, $\circ$: source points, $\times$: MFS solution, $\triangle$: NMFS solution). The position of the source points in MFS is around squares of the square physical sub-domains.

A good agreement between the solution for a one domain region and the solution with the four and nine regions in ideal mechanical contact and with the same material properties can be observed in Figure 7.2, Figure 7.3 and Figure 7.4. The maximum absolute difference in displacements of NMFS between values in Figure 7.2 and Figure 7.3 at the outer boundary are $\triangle u_x = 9.5197\times10^{-4}$ m, $\triangle u_y = 6.1311\times10^{-4}$ m, and between Figure 7.2 and Figure 7.4 $\triangle u_x = 0.0017\,\text{m}$, $\triangle u_y = 0.0012\,\text{m}$ $\triangle u_y = 0.0012\text{m}$, respectively.

Case 7.1.2: Shear Stress Problem

We consider the solution of the Navier's equations in this square subject to the following boundary conditions: $\bar{u}_x = -0.1\,\text{m}$, $\bar{u}_y = 0\,\text{m}$ on the north side boundary with $p_y = 1.5\,\text{m}$; $\bar{u}_x = 0.1\,\text{m}$, $\bar{u}_y = 0\,\text{m}$ on the south side boundary with $p_y = -1.5\,\text{m}$, the others are the same with Case 7.1.1. A plot of the deformation, calculated with the defined three cases is shown in Figure 7.5, Figure 7.6 and Figure 7.7, respectively.

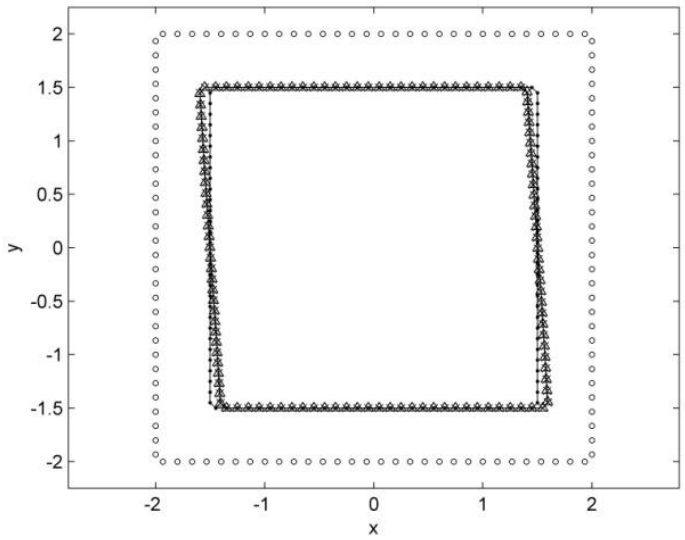

Figure 7.5: Case 7.1.2. The deformation calculated with MFS and NMFS, for a one-domain case with $E = 1\,\mathrm{N/m^2}$, and $N^{\Gamma} = 120$ ($\bullet$: collocation points, $\circ$: source points, $\times$: MFS solution, $\triangle$: NMFS solution).

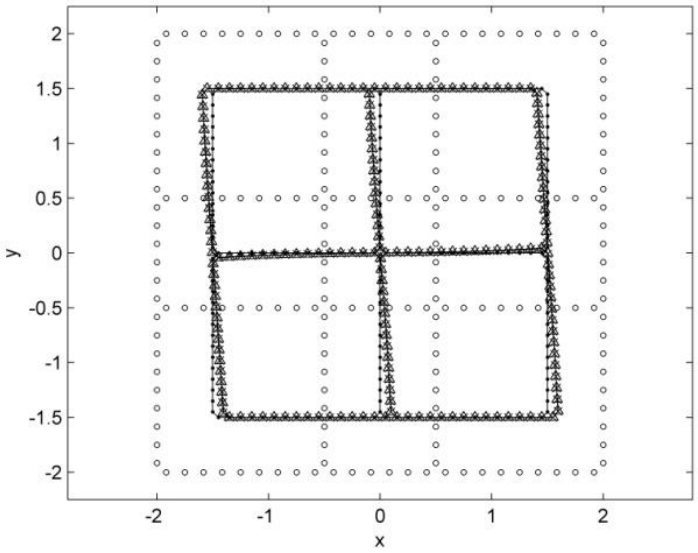

Figure 7.6: Case 7.1.2. The deformation calculated with MFS and NMFS, for a four-domain case $E^{\mathrm{I}} = E^{\mathrm{II}} = E^{\mathrm{III}} = E^{\mathrm{IV}} = 1\,\mathrm{N/m^2}$, $\nu^{\mathrm{I}} = \nu^{\mathrm{II}} = \nu^{\mathrm{III}} = \nu^{\mathrm{IV}} = 0.3$, and $N^{\Gamma} = 120$ ($\bullet$: collocation points, $\circ$: source points, $\times$: MFS solution, $\triangle$: NMFS solution). The position of the source points in MFS is around squares of the square physical sub-domains.

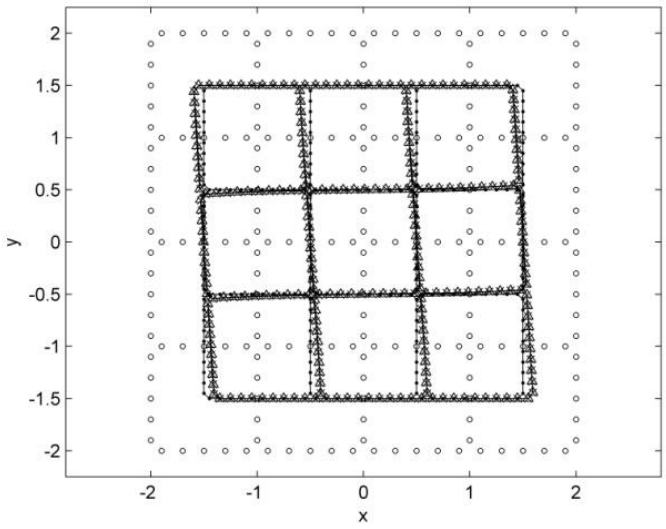

Figure 7.7: Case 7.1.2. The deformation calculated with MFS and NMFS for a nine-domain case $E^{\mathrm{I}} = E^{\mathrm{II}} = \cdots = E^{\mathrm{IX}} = 1\ \mathrm{N/m^2}$, $\nu^{\mathrm{I}} = \nu^{\mathrm{II}} = \cdots = \nu^{\mathrm{IX}} = 0.3$ and $N^{\Gamma} = 120$ ($\bullet$: collocation points, $\circ$: source points, $\times$: MFS solution, $\triangle$: NMFS solution). The position of the source points in MFS is around squares of the square physical sub-domains.

A good agreement between solution for a one domain region and solutions with four and nine subregions in ideal mechanical contact and with the same material properties is observed in Figure 7.5, Figure 7.6 and Figure 7.7. The maximum absolute difference in displacements of NMFS between values in Figure 7.5 and Figure 7.6 at the outer boundary are $\triangle u_x = 0.0016\ \mathrm{m}$, $\triangle u_y = 0.0011\ \mathrm{m}$,and between Figure 7.5 and Figure 7.7 $\triangle u_x = 0.0031\ \mathrm{m}$, $\triangle u_y = 0.0014\ \mathrm{m}$,respectively.

7.3.2 Example 7.2: NMFS for Anisotropic Multi-grain Problems

We define three cases. In the first one, the homogenous square is occupied by one material, with the material properties $c_{11} = 16.84\ \mathrm{N/m^2}$, $c_{12} = 12.14\ \mathrm{N/m^2}$, $c_{66} = 7.54\ \mathrm{N/m^2}$, in the second one, the square is split into four parts with the same material properties as in the first case $c_{11}^{\mathrm{I}} = c_{11}^{\mathrm{II}} = c_{11}^{\mathrm{III}} = c_{11}^{\mathrm{IV}} = 16.84\ \mathrm{N/m^2}$, $c_{12}^{\mathrm{I}} = c_{12}^{\mathrm{II}} = c_{12}^{\mathrm{III}} = c_{12}^{\mathrm{IV}} = 12.14\ \mathrm{N/m^2}$, $c_{66}^{\mathrm{I}} = c_{66}^{\mathrm{II}} = c_{66}^{\mathrm{III}} = c_{66}^{\mathrm{IV}} = 7.54\ \mathrm{N/m^2}$, and in the third one, the square is split into nine parts with the same material properties as in the first case $c_{11}^{\mathrm{I}} = c_{11}^{\mathrm{II}} = \cdots = c_{11}^{\mathrm{IX}} = 16.84\ \mathrm{N/m^2}$, $c_{12}^{\mathrm{I}} = c_{12}^{\mathrm{II}} = \cdots = c_{12}^{\mathrm{IX}} = 12.14\ \mathrm{N/m^2}$, $c_{66}^{\mathrm{I}} = c_{66}^{\mathrm{II}} = \cdots = c_{66}^{\mathrm{IX}} = 7.54\ \mathrm{N/m^2}$. The distance of the fictitious boundary from the true boundary for the MFS is set to $R_M = 5d, R_M^{\mathrm{I}} = 5d^{\mathrm{I}}, \cdots, R_M^{\mathrm{IX}} = 5d^{\mathrm{IX}}$. The following parameters have been used $R = d/5, R^{\mathrm{I}} = d^{\mathrm{I}}/10, \cdots, R^{\mathrm{IX}} = d^{\mathrm{IX}}/10$. $c_x = c_y = c_x^{\mathrm{I}} = c_y^{\mathrm{I}} = \cdots = c_x^{\mathrm{IX}} = c_y^{\mathrm{IX}} = 4\ \mathrm{m}$.

Case 7.2.1: Normal Stress Problem

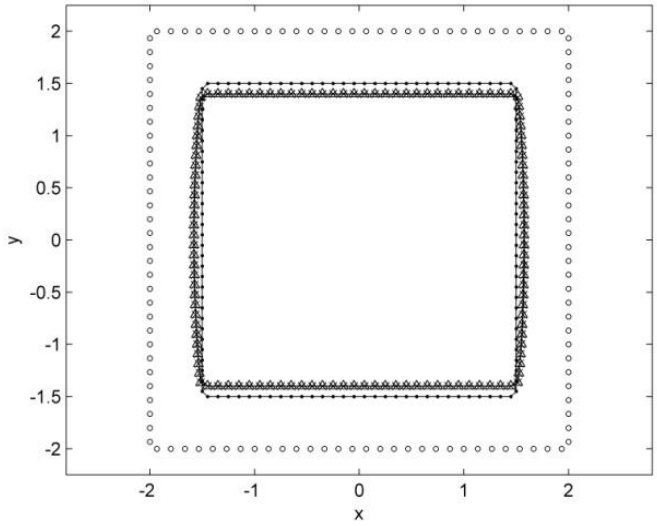

Figure 7.8: Case 7.2.1. The deformation calculated with MFS and NMFS, for a one-domain case with $c_{11} = 16.84\ \text{N/m}^2$, $c_{12} = 12.14\ \text{N/m}^2$, $c_{66} = 7.54\ \text{N/m}^2$ and $N^{\Gamma} = 120$ ($\bullet$: collocation points, $\circ$: source points, $\times$: MFS solution, $\triangle$: NMFS solution).

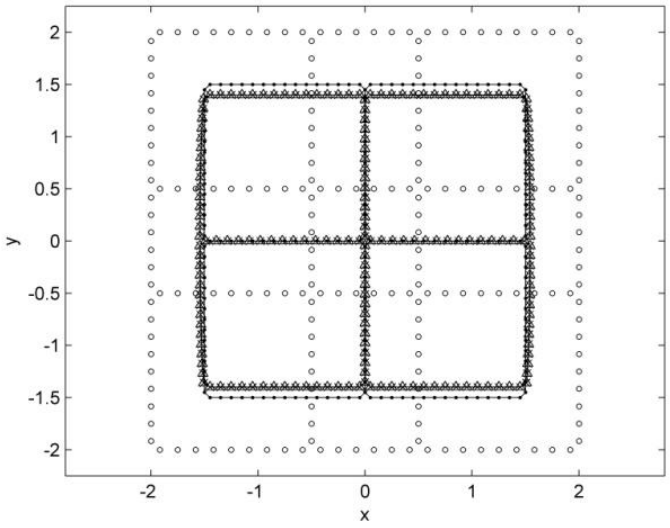

Figure 7.9: Case 7.2.1. The deformation calculated with MFS and NMFS, for a four-domain case $c_{11}^{\text{I}} = c_{11}^{\text{II}} = c_{11}^{\text{III}} = c_{11}^{\text{IV}} = 16.84\ \text{N/m}^2$, $c_{12}^{\text{I}} = c_{12}^{\text{II}} = c_{12}^{\text{III}} = c_{12}^{\text{IV}} = 12.14\ \text{N/m}^2$, $c_{66}^{\text{I}} = c_{66}^{\text{II}} = c_{66}^{\text{III}} = c_{66}^{\text{IV}} = 7.54\ \text{N/m}^2$ and $N^{\Gamma} = 120$ ($\bullet$: collocation points, $\circ$: source points, $\times$: MFS solution, $\triangle$: NMFS solution). The position of the source points in MFS is around squares of the square physical sub-domains.

We consider the same boundary conditions as in Case 7.1.1. A plot of the deformation, calculated with the defined three cases is shown in Figure 7.8, Figure 7.9 and Figure 7.10, respectively.

A good agreement between solution for a one domain region and solutions with four and nine subregions in ideal mechanical contact and with the same material properties is observed in Figure 7.8, Figure 7.9 and Figure 7.10. The maximum absolute difference in displacements of NMFS between values in Figure 7.8 and Figure 7.9 at the outer boundary are $\triangle u_x = 0.0044\,\text{m},\ \triangle u_y = 0.0052\,\text{m}$, and between Figure 7.8 and Figure 7.10 $\triangle u_x = 0.0062\,\text{m},\ \triangle u_y = 0.0054\,\text{m}$, respectively.

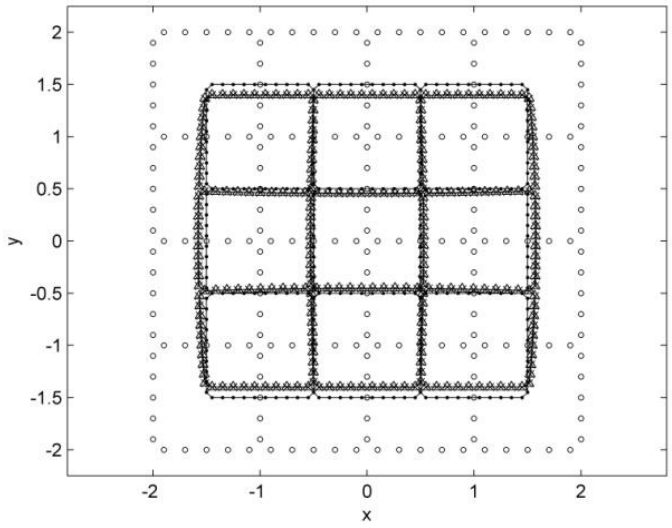

Figure 7.10: Case 7.2.1. The deformation calculated with MFS and NMFS for a nine-domain case $c_{11}^{\text{I}} = c_{11}^{\text{II}} = \cdots = c_{11}^{\text{IX}} = 16.84\ \text{N/m}^2$, $c_{12}^{\text{I}} = c_{12}^{\text{II}} = \cdots = c_{12}^{\text{IX}} = 12.14\ \text{N/m}^2$, $c_{66}^{\text{I}} = c_{66}^{\text{II}} = \cdots = c_{66}^{\text{IX}} = 7.54\ \text{N/m}^2$ and $N^{\Gamma} = 120$ ($\bullet$: collocation points, $\circ$: source points, $\times$: MFS solution, $\triangle$: NMFS solution). The position of the source points in MFS is around squares of the square physical sub-domains.

Case 7.2.2: Shear Stress Problem

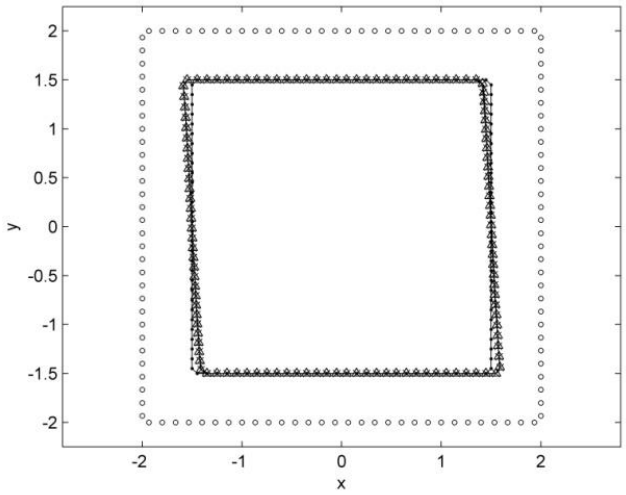

Figure 7.11: Case 7.2.2. The deformation calculated with MFS and NMFS for a one-domain case with $c_{11} = 16.84\ \text{N/m}^2$, $c_{12} = 12.14\ \text{N/m}^2$, $c_{66} = 7.54\ \text{N/m}^2$ and $N^{\Gamma} = 120$ ($\bullet$: collocation points, $\circ$: source points, $\times$: MFS solution, $\triangle$: NMFS solution).

We consider the same boundary conditions as in case 7.1.2. A plot of the deformation, calculated with the defined three cases is shown in Figure 7.11, Figure 7.12 and Figure 7.13, respectively.

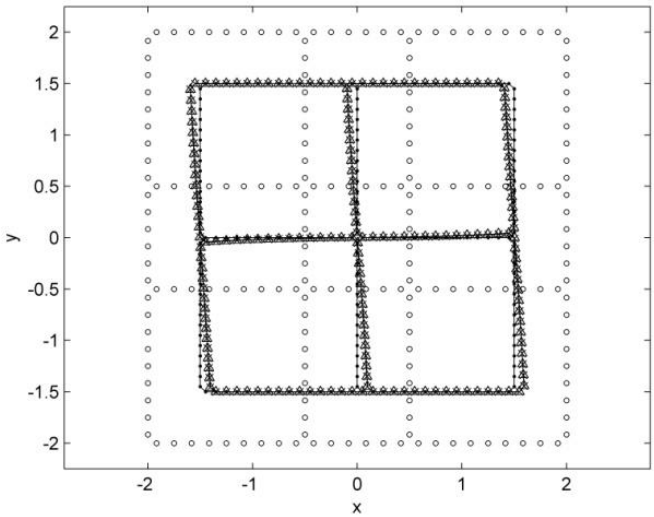

Figure 7.12: Case 7.2.2. The deformation calculated with MFS and NMFS, for a four-domain case $c_{11}^{\text{I}} = c_{11}^{\text{II}} = c_{11}^{\text{III}} = c_{11}^{\text{IV}} = 16.84\ \text{N/m}^2$, $c_{12}^{\text{I}} = c_{12}^{\text{II}} = c_{12}^{\text{III}} = c_{12}^{\text{IV}} = 12.14\ \text{N/m}^2$, $c_{66}^{\text{I}} = c_{66}^{\text{II}} = c_{66}^{\text{III}} = c_{66}^{\text{IV}} = 7.54\ \text{N/m}^2$ and $N^{\Gamma} = 120$ ($\bullet$: collocation points, $\circ$: source points, $\times$: MFS solution, $\triangle$: NMFS solution). The position of the source points in MFS is around squares of the square physical sub-domains.

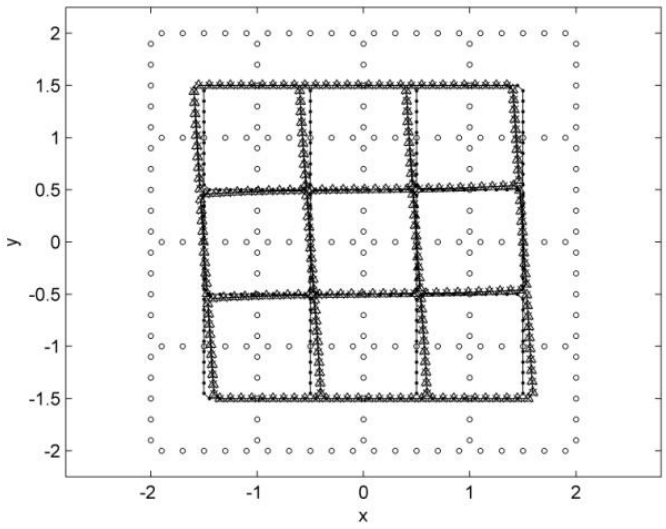

Figure 7.13: Case 7.2.2. The deformation calculated with MFS and NMFS, for a nine-domain case $c_{11}^{\mathrm{I}} = c_{11}^{\mathrm{II}} = \cdots = c_{11}^{\mathrm{IX}} = 16.84\ \mathrm{N/m^2}$, $c_{12}^{\mathrm{I}} = c_{12}^{\mathrm{II}} = \cdots = c_{12}^{\mathrm{IX}} = 12.14\ \mathrm{N/m^2}$, $c_{66}^{\mathrm{I}} = c_{66}^{\mathrm{II}} = \cdots = c_{66}^{\mathrm{IX}} = 7.54\ \mathrm{N/m^2}$ and $N^{\Gamma} = 120$ ($\bullet$: collocation points, $\circ$: source points, $\times$: MFS solution, $\triangle$: NMFS solution). The position of the source points in MFS is around squares of the square physical sub-domains.

A good agreement between solution for a one domain region and solutions with four and nine subregions in ideal mechanical contact and with the same material properties is observed in Figure 7.11, Figure 7.12 and Figure 7.13. The maximum absolute difference in displacements of NMFS values in Figure 7.11 and Figure 7.12 at the outer boundary are $\triangle u_x = 0.0079\ \mathrm{m}$, $\triangle u_y = 0.0346\ \mathrm{m}$, and between Figure 7.11 and Figure 7.13 $\triangle u_x = 0.0082\ \mathrm{m}$, $\triangle u_y = 0.0055\ \mathrm{m}$, respectively

7.3.3 Example 7.3: INMFS for Isotropic Multi-grain Problems

We define two cases. In the first one, the homogenous square is occupied by one material, with the material properties. $E = 1\ \mathrm{N/m^2}$ $\nu = 0.3$, in the second one, the square is split into nine irregular geometry parts with the same material properties as in the first case $E^{\mathrm{I}} = E^{\mathrm{II}} = \cdots = E^{\mathrm{IX}} = 1\ \mathrm{N/m^2}$, $\nu^{\mathrm{I}} = \nu^{\mathrm{II}} = \cdots = \nu^{\mathrm{IX}} = 0.3$. The following parameters have been used $R = d/5$, $R^{\mathrm{I}} = d^{\mathrm{I}}/5, \cdots, R^{\mathrm{IX}} = d^{\mathrm{IX}}/5$.

Case 7.3.1: Normal Stress Problem

We consider the same boundary conditions as in case 7.1.1. A plot of the deformation, calculated with the defined two cases is shown in Figure 7.14 and Figure 7.15, respectively.

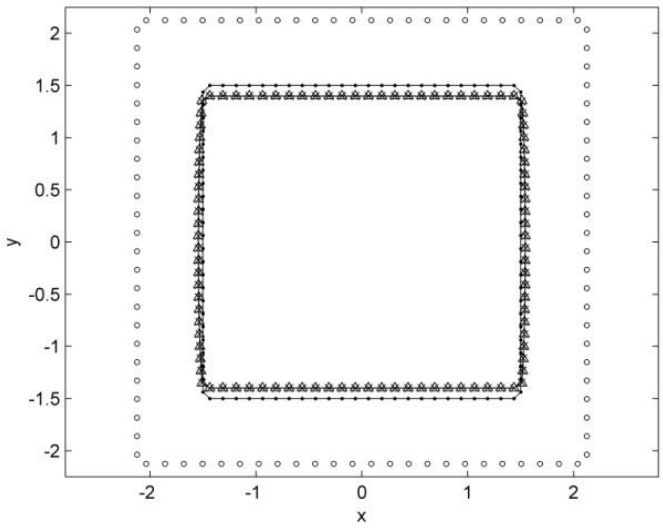

Figure 7.14: Case 7.3.1. The deformation calculated with MFS and INMFS, for a one-domain case with $E = 1\,\mathrm{N/m^2}$, $\nu = 0.3$ and $N^{\Gamma} = 96$ ($\bullet$: collocation points, $\circ$: source points, $\times$: MFS solution, $\triangle$: INMFS solution).

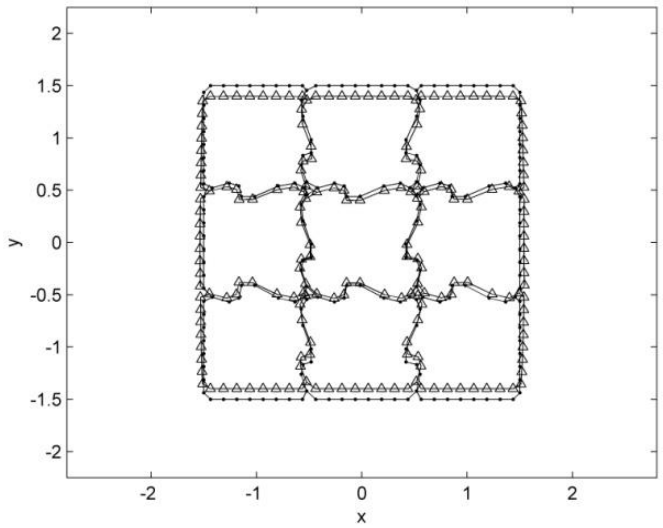

Figure 7.15: Case 7.3.1. The deformation calculated with INMFS, for a nine sub-domain case $E^{\mathrm{I}} = E^{\mathrm{II}} = \cdots = E^{\mathrm{IX}} = 1\,\mathrm{N/m^2}$, $\nu^{\mathrm{I}} = \nu^{\mathrm{II}} = \cdots = \nu^{\mathrm{IX}} = 0.3$, and $N^{\Gamma} = 96$ ($\bullet$: collocation points, $\triangle$: NMFS solution).

A good agreement between solution for a one domain region and solutions with nine irregular geometry subregions in ideal mechanical contact and with the same material properties is observed in Figure 7.14 and Figure 7.15. The maximum absolute difference in displacements of INMFS between values in Figure 7.14 and Figure 7.15 at the outer boundary are $\triangle u_x = 0.0097$ m, $\triangle u_y = 0.0087$ m .

Case 7.3.2: Shear Stress Problem

We consider the same boundary conditions as in case 7.1.2. A plot of the deformation, calculated with the defined two cases is shown in Figure 7.16 and Figure 7.17, respectively.

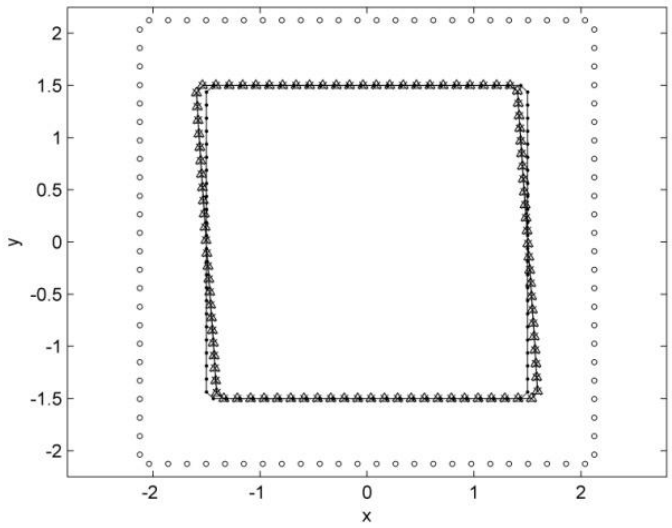

Figure 7.16: Case 7.3.2. The deformation calculated with MFS and INMFS, for a one-domain case with $E = 1\,\mathrm{N/m^2}$, $\nu = 0.3$ and $N^{\Gamma} = 96$ ($\bullet$: collocation points, $\circ$: source points, $\times$: MFS solution, $\triangle$: NMFS solution).

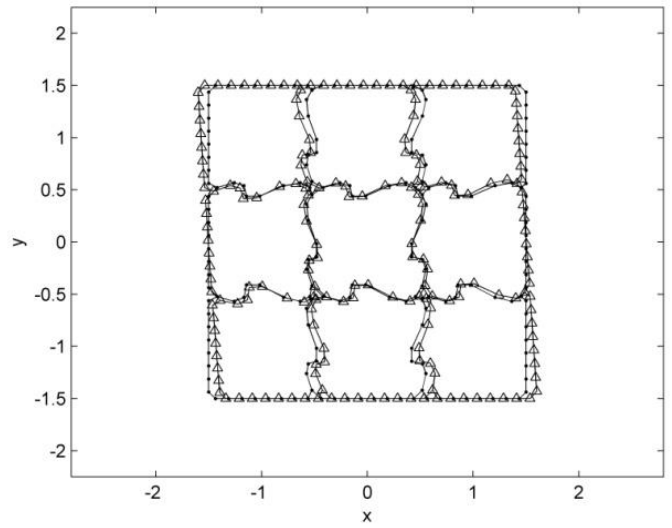

Figure 7.17: Case 7.3.2. The deformation calculated with INMFS, for a nine sub-domain case $E^{\mathrm{I}} = E^{\mathrm{II}} = \cdots = E^{\mathrm{IX}} = 1\,\mathrm{N/m^2}$, $\nu^{\mathrm{I}} = \nu^{\mathrm{II}} = \cdots = \nu^{\mathrm{IX}} = 0.3$, and $N^{\Gamma} = 96$ ($\bullet$: collocation points, $\triangle$: NMFS solution).

A good agreement between solution for a one domain region and solutions with nine irregular geometry subregions in ideal mechanical contact and with the same material properties is observed in Figure 7.16 and Figure 7.17. The maximum absolute difference in displacements of INMFS between values in Figure 7.16 and Figure 7.17 at the outer boundary are $\triangle u_x = 0.0099\,\text{m}$, $\triangle u_y = 0.0038\,\text{m}$.

7.3.4 Example 7.4: INMFS for Anisotropic Multi-grain Problems

We define two cases. In the first one, the homogenous square is occupied by one material, with the material properties $c_{11} = 16.84\,\text{N/m}^2$, $c_{12} = 12.14\,\text{N/m}^2$, $c_{44} = 7.54\,\text{N/m}^2$, in the second one, the square is split into nine irregular geometry parts with the same material properties as in the first case $c_{11}^{\text{I}} = c_{11}^{\text{II}} = \cdots = c_{11}^{\text{IX}} = 16.84\,\text{N/m}^2$, $c_{12}^{\text{I}} = c_{12}^{\text{II}} = \cdots = c_{12}^{\text{IX}} = 12.14\,\text{N/m}^2$, $c_{66}^{\text{I}} = c_{66}^{\text{II}} = \cdots = c_{66}^{\text{IX}} = 7.54\,\text{N/m}^2$. The distance of the fictitious boundary from the true boundary for the MFS is set to $R_M = d/5, R_M^{\text{I}} = 5d^{\text{I}}, \cdots, R_M^{\text{IM}} = 5d^{\text{IX}}$. The following parameters have been used $R = d/5, R^{\text{I}} = d^{\text{I}}/5, \cdots, R^{\text{IX}} = d^{\text{IX}}/5.$ $c_x = c_y = c_x^{\text{I}} = c_y^{\text{I}} = \cdots = c_x^{\text{IX}} = c_y^{\text{IX}} = 4$.

Case 7.4.1: Normal Stress Problem

We consider the same boundary conditions as in case 7.1.1. A plot of the deformation, calculated with the defined two cases is shown in Figure 7.18 and Figure 7.19, respectively.

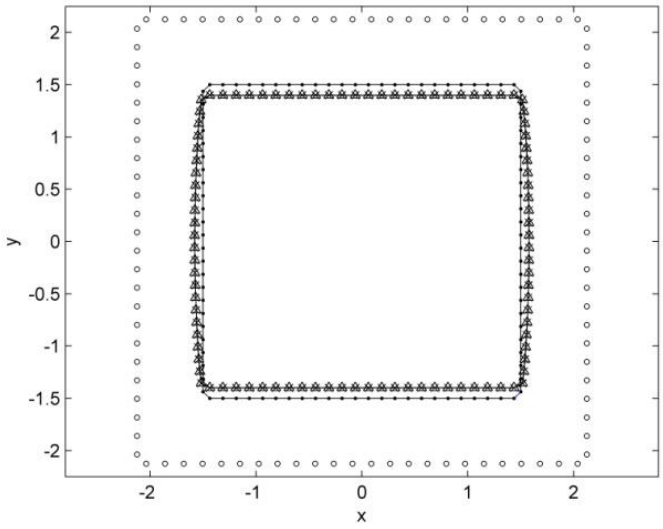

Figure 7.18: Case 7.4.1. The deformation calculated with MFS and INMFS, for a one-domain case with $c_{11} = 16.84\,\text{N/m}^2$, $c_{12} = 12.14\,\text{N/m}^2$, $c_{66} = 7.54\,\text{N/m}^2$, and $N^{\Gamma} = 96$ ($\bullet$: collocation points, $\circ$: source points, $\times$: MFS solution, $\triangle$: NMFS solution).

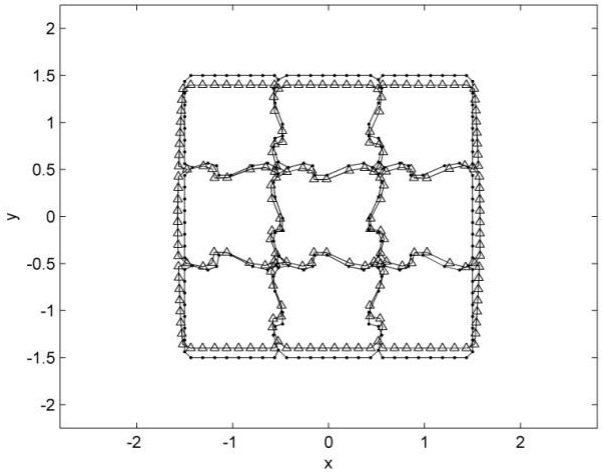

Figure 7.19: Case 7.4.1. The deformation calculated with INMFS, for a nine sub-domain case $c_{11}^{\mathrm{I}} = c_{11}^{\mathrm{II}} = \cdots = c_{11}^{\mathrm{IX}} = 16.84\ \mathrm{N/m^2}$, $c_{12}^{\mathrm{I}} = c_{12}^{\mathrm{II}} = \cdots = c_{12}^{\mathrm{IX}} = 12.14\ \mathrm{N/m^2}$, $c_{66}^{\mathrm{I}} = c_{66}^{\mathrm{II}} = \cdots = c_{66}^{\mathrm{IX}} = 7.54\ \mathrm{N/m^2}$, and $N^{\Gamma} = 96$ ($\bullet$: collocation points, $\triangle$: NMFS solution).

A good agreement between solution for a one domain region and solutions with nine irregular geometry subregions in ideal mechanical contact and with the same material properties is observed in Figure 7.18 and Figure 7.19. The maximum absolute difference in displacements of INMFS between values in Figure 7.18 and Figure 7.19 at the outer boundary are $\triangle u_x = 0.0100\ \mathrm{m}$, $\triangle u_y = 0.0067\ \mathrm{m}$.

Case 7.4.2: Shear Stress Problem

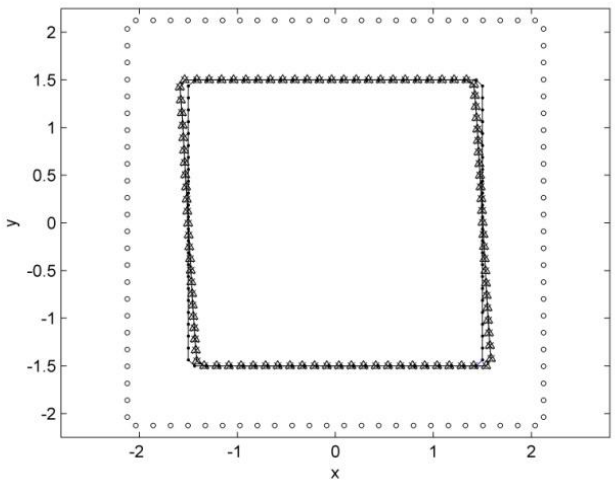

Figure 7.20: Case 7.4.2. The deformation calculated with MFS and INMFS, for a one-domain case with $c_{11} = 16.84\ \mathrm{N/m^2}$, $c_{12} = 12.14\ \mathrm{N/m^2}$, $c_{44} = 7.54\ \mathrm{N/m^2}$, and $N^{\Gamma} = 96$ ($\bullet$: collocation points, $\circ$: source points, $\times$: MFS solution, $\triangle$: NMFS solution).

We consider the same boundary conditions as in case 7.1.2. A plot of the deformation, calculated with the defined two cases, is shown in Figure 7.20 and Figure 7.21, respectively.

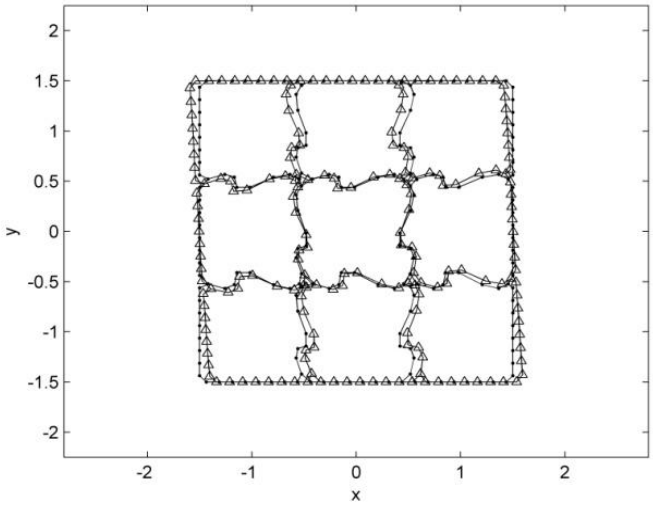

Figure 7.21: Case 7.4.2. The deformation calculated with INMFS, for a nine sub-domain case $c_{11}^{\mathrm{I}} = c_{11}^{\mathrm{II}} = \cdots = c_{11}^{\mathrm{IX}} = 16.84\ \mathrm{N/m^2}$, $c_{12}^{\mathrm{I}} = c_{12}^{\mathrm{II}} = \cdots = c_{12}^{\mathrm{IX}} = 12.14\ \mathrm{N/m^2}$, $c_{44}^{\mathrm{I}} = c_{44}^{\mathrm{II}} = \cdots = c_{44}^{\mathrm{IX}} = 7.54\ \mathrm{N/m^2}$ and $N^{\Gamma} = 96$ ($\bullet$: collocation points, $\triangle$: NMFS solution).

A good agreement between the solution for a one domain region and solutions with nine irregular geometry subregions in ideal mechanical contact and with the same material properties is observed in Figure 7.20 and Figure 7.21. The maximum absolute difference in displacements of INMFS between values in Figure 7.20 and Figure 7.21 at the outer boundary are $\triangle u_x = 0.0102\ \mathrm{m}$, $\triangle u_y = 0.0102\ \mathrm{m}$.

7.3.5 Example 7.5: NMFS and INMFS for Anisotropic Multi-grain Problems with Different Properties

In this example, we use the same domains as in example 7.3.2 and distinguish four cases, in which the middle part is orthotropic body with different properties. The other parts are cubic materials with (Aluminum) $E_{xx} = E_{yy} = E_{zz} = 69\ \mathrm{Gpa}$, $G_{xy} = G_{yz} = G_{xz} = 24\ \mathrm{Gpa}$, $v_{xy} = v_{yx} = v_{xz} = v_{zx} = v_{yz} = v_{zy} = 0.334$. We considered the solution of the system (3.5) (3.6) in this square subject to the following boundary conditions $\bar{u}_x = 0\ \mathrm{m}$, $\bar{u}_y = -0.5\ \mathrm{m}$ on the north side boundary with $p_y = 1.5\ \mathrm{m}$; $\bar{u}_x = 0\ \mathrm{m}$, $\bar{u}_y = 0.5\ \mathrm{m}$ on the south side boundary with $p_y = -1.5\mathrm{m}$ and $\bar{t}_x = 0\mathrm{N/m^2}$, $\bar{t}_y = 0\mathrm{N/m^2}$ on the east side boundary with $p_x = 1.5\mathrm{m}$ and west side boundary with $p_x = -1.5\mathrm{m}$.

Case 7.5.1: Central Sub-domain with the Same Properties in x and y directions

In Case 7.5.1, the properties for the middle part are $E_{xx} = E_{yy} = E_{zz} = 200\,\text{Gpa}$, $G_{xy} = G_{yz} = G_{xz} = 73\,\text{Gpa}$ (steel) and $v_{xy} = v_{yx} = v_{xz} = v_{zx} = v_{yz} = v_{zy} = 0.3$. A plot of the deformation is shown in Figure 7.22.

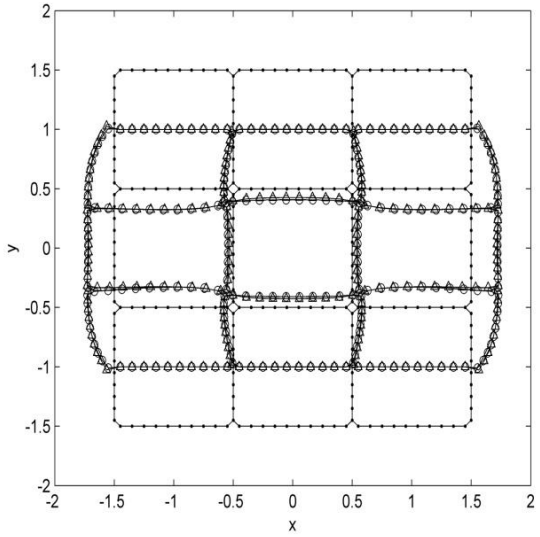

Figure 7.22: Case 7.5.1. The deformation calculated with NMFS and INMFS with the same material properties in sub-domains (• : collocation points, ○ : NMFS solution, △ : INMFS solution)

Case 7.5.2: Central Sub-domain with Different Properties in x and y directions

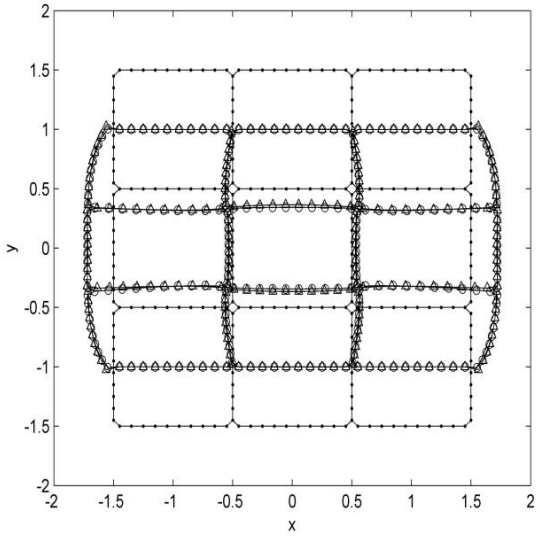

Figure 7.23: Case 7.5.2. The deformation calculated with NMFS and INMFS with the harder material in the center (• : collocation points, ○ : NMFS solution, △ : INMFS solution).

In Case 7.5.2, $E_{xx} = 200\ \text{Gpa} \times 1.5 = 300\ \text{Gpa}$, $E_{yy} = 200\ \text{Gpa} \times 0.5 = 100\ \text{Gpa}$, $E_{zz} = 200\ \text{Gpa}$, $G_{xy} = G_{yz} = G_{xz} = 73\ \text{Gpa}$, $v_{xy} = v_{xz} = 0.45$, $v_{yx} = v_{yz} = 0.15$, $v_{zx} = v_{zz} = 0.3$. A plot of the deformation is shown in Figure 7.23.

Case 7.5.3: Central Sub-domain with Different Properties in x and y directions Due to Rotation of the Axes

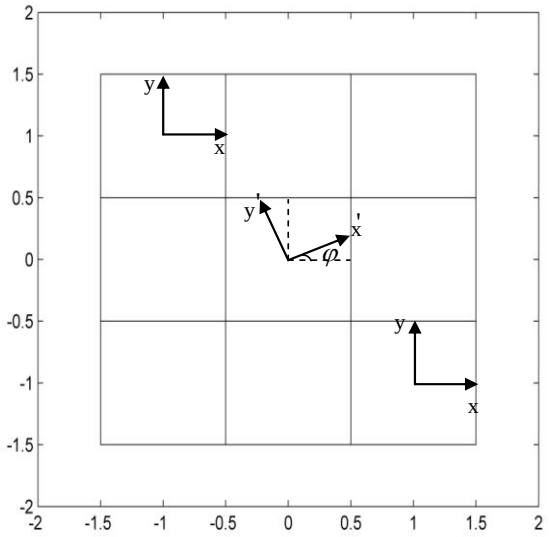

Figure 7.24: Case 7.5.3. Scheme of the sub-domains with different material properties and different orientations of anisotropy.

Case 7.5.3 has the same properties with the second one, but the axis of central body is x' and y', respectively (see Figure 7.24). Then $E'_{xx} = 300\ \text{Gpa}$, $E'_{yy} = 100\ \text{Gpa}$, $E'_{zz} = 200\ \text{Gpa}$, $G'_{xy} = G'_{yz} = G'_{xz} = 73\ \text{Gpa}$, $v'_{xy} = v'_{xz} = 0.45$, $v'_{yx} = v'_{yz} = 0.15$, $v'_{zx} = v'_{zy} = 0.3$. We use the Catesian coordinate system x, y as main coordinate system, and all the data were changed into the Catesian coordinate system x, y by rotating for $\varphi = 0, \frac{\pi}{6}, \frac{\pi}{3}, \frac{\pi}{2}$ in the calculation procedure.

In Figure 7.25, the shape of the central part changed less than the same part in Figure 7.22. And we get the consistent result by using NMFS and INMFS. In Figure 7.25, the central body has harder properties in x direction than in y direction. So when the rotation from $\varphi = 0$ to $\varphi = -\frac{\pi}{2}$ is performed, the y direction became harder and harder, and the displacement would be smaller and smaller.

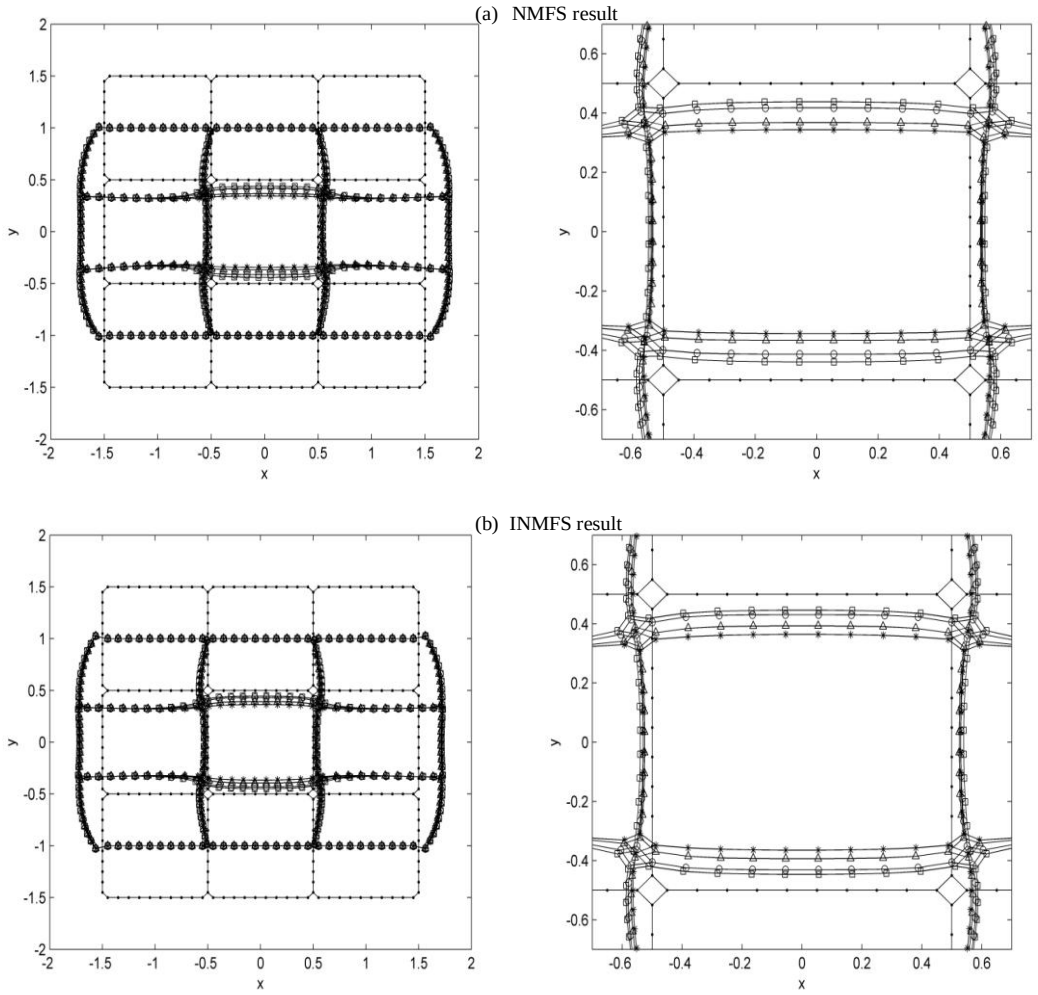

Figure 7.25: Case 7.5.3. The deformation calculated with (a) NMFS and (b) INMFS with the hard material in the center and different φ ($\bullet$: collocation points, $*$: $\varphi = 0$, $\triangle$: $\varphi = \frac{\pi}{6}$, $\circ$: $\varphi = \frac{\pi}{3}$, $\square$: $\varphi = \frac{\pi}{2}$).

Case 7.5.4: Central Sub-domain with a Hole and the Different Properties on x and y directions

Case 7.5.4 has the same properties as the second one, but there is a hole in the middle with radius $r = 0.3\,\mathrm{m}$.

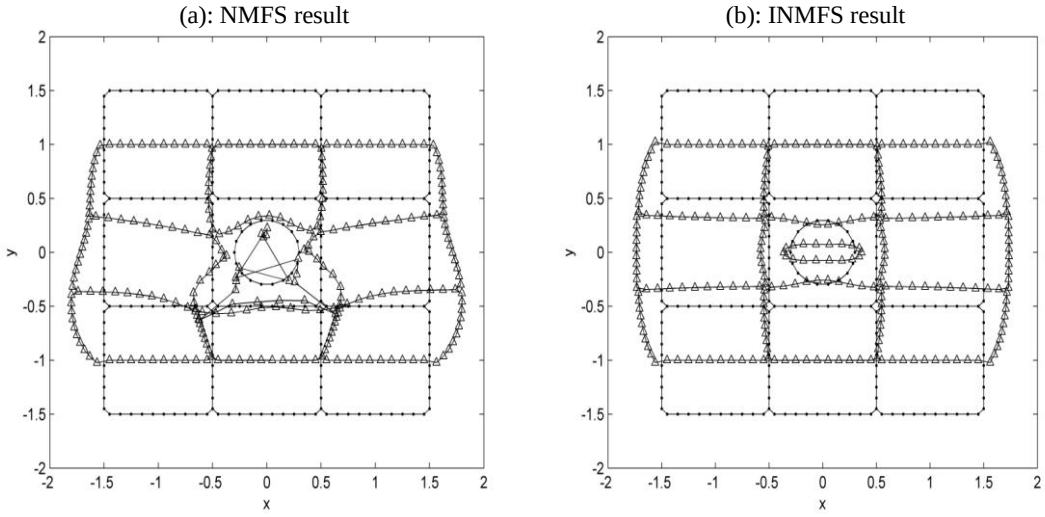

Figure 7.26: Case 7.5.4. The deformation calculated with NMFS and INMFS with a hole in the center of a hard body (• : collocation points, △ : NMFS and INMFS solutions).

It is shown on Figure 7.26, that the NMFS doesn't work in this case. But the INMFS can solve this problem very well. This is the advantage of INMFS compared with NMFS.

7.4 Simulation of Deformation of a Section of a Realistic Microstructure

The original material of a spring steel C45 is given in Figure 7.27. In this part we only use a 50 μm square of Figure 7.27 (see Figure 7.28).

Figure 7.27: The original material.

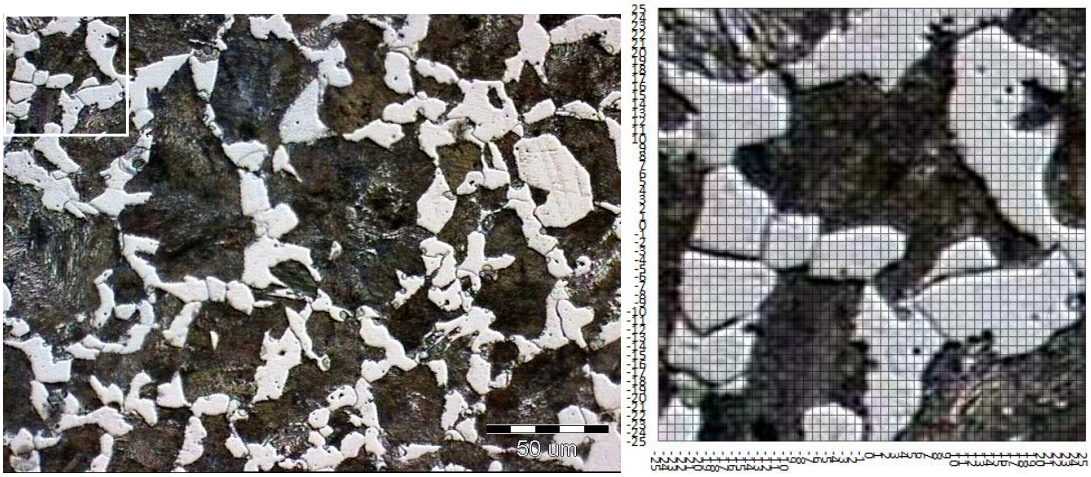

Figure 7.28: A square 50 μm part of the original material.

This square contains 19 grains (see Figure 7.29). The 19 grains are of the same material with the properties of steel C45 at temperature 25 C $E = 210 \times 10^{-3}$ N/μm^2, $v = 0.29$. We distinguish two cases with normal stress and shear stress, respectively. The following parameters have been used $R = d / 5$.

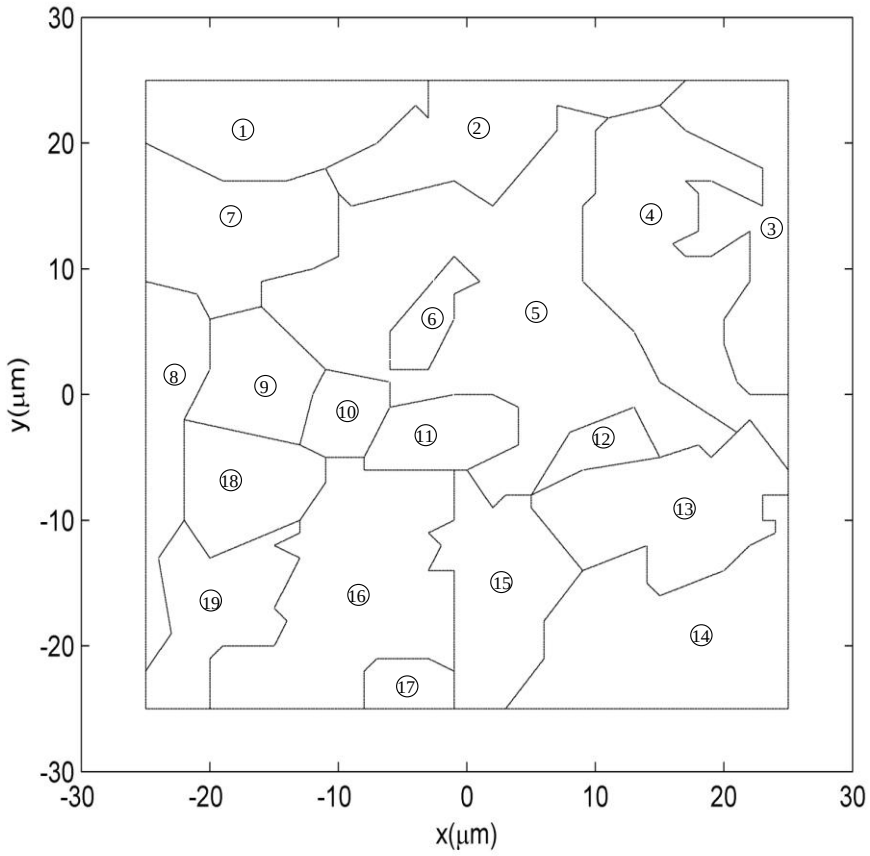

Figure 7.29：The square domain with 19 grains.

Case 7.4.1: Normal Stress

The boundary conditions: $\bar{u}_x = 0\ \mu\text{m}$, $\bar{u}_y = -5\ \mu\text{m}$ are imposed on the north side boundary with $p_y = 25\ \mu\text{m}$; $\bar{u}_x = 0\ \mu\text{m}$, $\bar{u}_y = 5\ \mu\text{m}$ on the south side boundary with $p_y = -25\ \mu\text{m}$; $\bar{t}_x = 0\ \text{N/m}^2$, $\bar{t}_y = 0\ \text{N/m}^2$ on the east side boundary with $p_x = 25\ \mu\text{m}$ and on west side boundary with $p_x = -25\ \mu\text{m}$. A plot of the deformation is shown in Figure 7.30

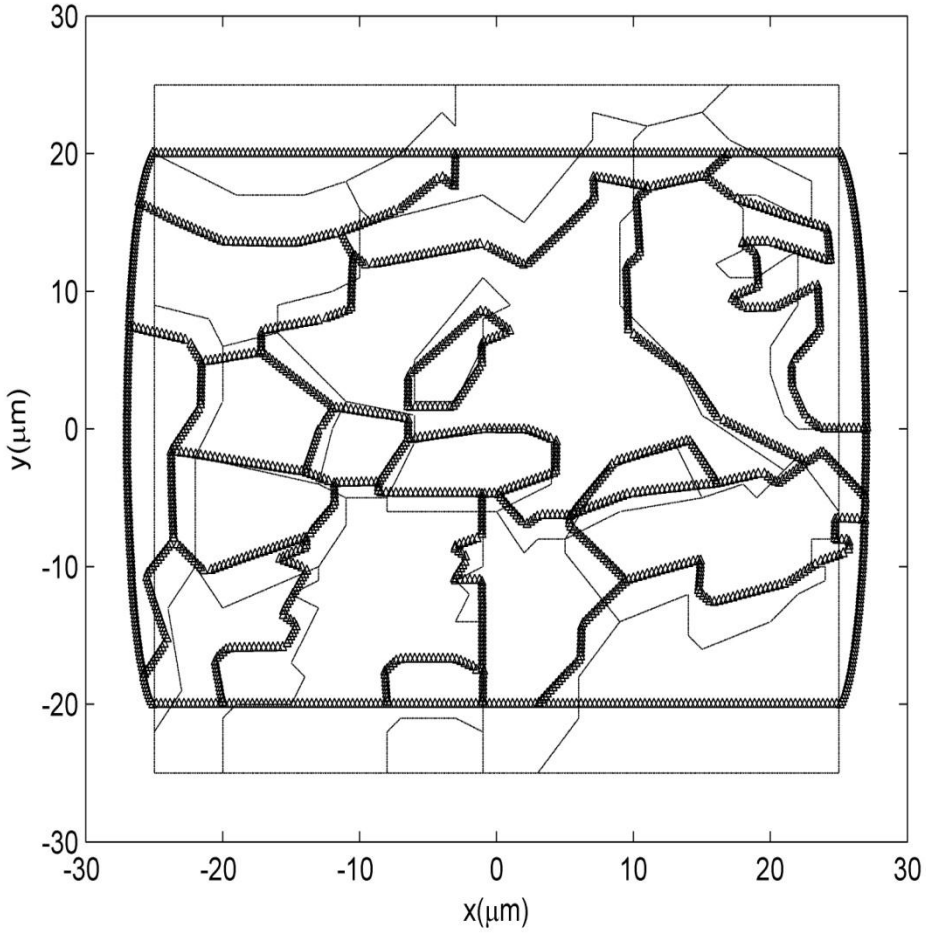

Figure 7.30: Case 7.4.1. Microstructure problem. Normal deformation calculation with INMFS.

Case 7.4.2: Shear Stress

The boundary conditions: $\bar{u}_x = -5\ \mu\text{m}$, $\bar{u}_y = 0\ \mu\text{m}$ are imposed on the north side boundary with $p_y = 25\ \mu\text{m}$; $\bar{u}_x = 5\ \mu\text{m}$, $\bar{u}_y = 0\ \mu\text{m}$ on the south side boundary with $p_y = -25\ \mu\text{m}$; $\bar{t}_x = 0\ \text{N/m}^2$, $\bar{t}_y = 0\ \text{N/m}^2$ on the east side boundary with $p_x = 25\ \mu\text{m}$ and on west side boundary with $p_x = -25\ \mu\text{m}$. A plot of the deformation is shown in Figure 7.31

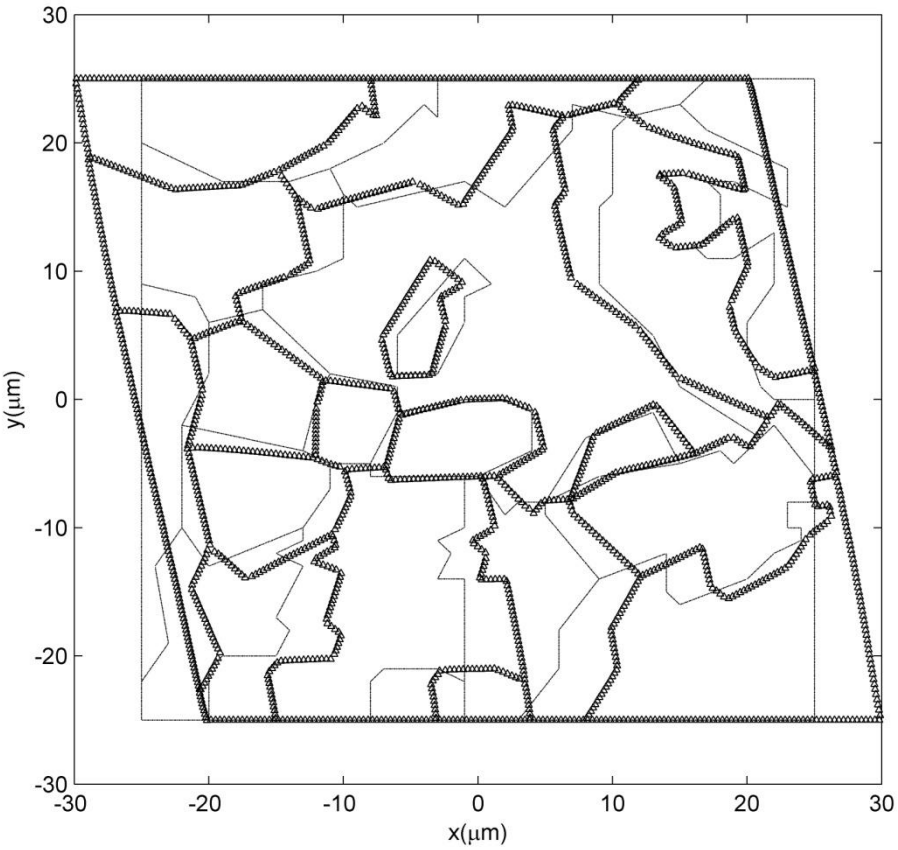

Figure 7.31: Case 7.4.1. Microstructure problem. Shear deformation calculation with INMFS.

7.5 Discussion

Examples 7.1 and 7.2 show good agreement of NMFS solutions with MFS solutions in multi-grain problems. Examples 7.3 and 7.4 show good agreement of INMFS solutions in multi-grain problem with single grain material. Example 7.5 demonstrates the suitability of NMFS and INMFS for the multi-grain problem with different properties and the rotation of the axes of a coordinate system, and especially INMFS, for void problems. And in all of the discussed examples, not more than 120 bounday nodes were used. Because both NMFS and INMFS solutions converge with the increasing number of the nodes, the results would be better in case more boundary nodes would be used. Because of the feasibility and the accuracy of the INMFS, a simulation of deformation of a peace of a realistic microstructure of a spring steel C45 on a 50μm square with 19 grains were given in INMFS.

7.6 Conclusions

The application of the NMFS and INMFS to solve the multi-grain problems is presented in this chapter. The most important is that both of the Dirichlet and Neumann boundary conditions on the interfaces for elastic inclusions and connected multi-grain problems are used in one system (3.41) to make sure that the matrix **A** is square. So that the inverse of the **A** can be calculated. A limitation that one boundary collocation point can belong to only two regions at once is considered in all the calculations. Respectively, the discretisation points have not been placed on the corners where three or more regions meet. All the tests show the feasibility and accuracy of NMFS and INMFS in different cases. One simulation under two different boundary conditions is presented in this chapter. The practical problems are more complex not only becase of the number of the grains but also because of the more complex geometries. The methods applied in this chapter can be used for modelling and simulation of much more complicated practical problems and this is also our work in the future.

8. Conclusions

8.1 Performed Work

The research described in this dissertation has been focused on development of a novel MFS for solving two-dimensional linear elasticity problems. The purpose of the developments is the use of the developed method for numerical modelling and simulation of deformation of microstructure of multi-grain materials such as metals. This approach enables to calculate the deformation of multi-grain materials as a function of the shape and mechanical properties of each of the grains that can be anisotropic and differently oriented. Respectively, the macroscopic mechanical response can be obtained from the defined properties of its microscopic constituent parts. The novelty of the developed approach is in the removal of the fictitious boundary where in MFS the poles of the fundamental solution are placed. The fictitious boundary represents the main drawback of MFS. This drawback makes the application of MFS to multi-grain materials very complicated. With the goal to make the artificial boundary coincide with the physical boundary of the grain are the singular point sources of the fundamental solution replaced by distributed sources over circular discs around the singularity. The magnitude and the shape of the fundamental solution inside the disk is adjusted by the average value of the domain integral of the fundamental solution over the disk and by coinciding of the shape of the related function with the fundamental solution and its first and second derivatives on the border of the disc.

In case of displacement (Dirichlet) boundary conditions, the values of distributed sources are calculated directly and analytically for isotropic problems and numerically for anisotropic problems. In case of traction (Neumann) boundary conditions, the respective desingularized values of the derivatives of the fundamental solution in the coordinate directions, as required in the calculations, are calculated indirectly from the construction of two reference solutions of the linearly varying simple displacement fields in the first variant of the novel method, termed NMFS. However on the expense of solving three times the systems of algebraic equations in comparison with only one solution in MFS. In addition, the related reference fields have to be carefully chosen in order to get the proper solution. In the second variant of the novel method, termed INMFS, the respective desingularized values of the derivatives of the fundamental solution in the poles are calculated from the assumption that the sum of the forces on the body should vanish in mechanical equilibrium. The system of algebraic equations is solved only once as in the MFS and there is no need to employ the two reference solutions as in NMFS. A free parameter – radius of the desingularization disk appears in both non-singular methods. It turns out that a suitable choice for this parameter is around 20% of the distance between the neighbouring nodes on the boundary.

Conclusions

In order to demonstrate the feasibility, accuracy and convergence of the newly developed methods, the NMFS and the INMFS solutions are compared to the MFS solution and analytical solutions for a spectra of plane strain problems. Analysis of the method includes isotropic and anisotropic materials, single and multidomain problems. Special attention is devoted to problems with elastic or rigid inclusions as well as voids. A list of performed calculations is as follows:

In Chapter 4 isotropic elastic material is considered. NMFS method for this type of materials is presented in detail. Two examples are presented to demonstrate the feasibility and the accuracy of NMFS. Example 4.1 tackles a single isotropic elastic domain with mixed boundary conditions and is divided into two cases: Case 4.1.1 represents stretching and Case 4.1.2 bending, respectively. In Example 4.1, the results were compared with the analytical solutions and the results of MFS. The convergence rate is assessed by a root mean square error measure. It can be observed that the solution coverges to the analytical solution with the increasing number of the boundary nodes. Example 4.2 tackles a bi-material with mixed boundary conditions and is divided into two cases: In Case 4.2.1 normal stresses are applied and in Case 4.2.2 shear stresses are applied. The results of Example 4.2 were compared with the result of MFS to prove similar accuracy and convergence.

In Chapter 5 anisotropic elastic material is considered. NMFS method for this type of material is presented in detail. Two examples are presented to demonstrate the feasibility and the accuracy of NMFS. In Example 5.1, stretching example with analytical solution for a single anisotropic elastic domain is discussed. The example is divided into two cases with Dirichlet (Case 5.1.1) and mixed (Case 5.1.2) boundary conditions. The same convergence is observed as for the isotropic material. The Example 5.2 considers a bi-material and is divided into three cases with Drichlet boundary conditions (Case 5.2.1) and mixed boundary conditions (stresses in x-direction (Case 5.2.3) and y-direction (Case 5.2.2). The numerical results of these examples are compared with the result of MFS to prove similar accuracy and convergence as in NMFS.

In Chapter 6 isotropic and anisotropic elastic materials are considered. INMFS method for both types of materials is developed. Five examples are presented to demonstrate the feasibility and the accuracy of INMFS. The Example 6.1. is dealing with isotropic material in single domain and is defined the same as Case 4.1.1. The Example 6.4 is dealing with anisotropic material in single domain and is defined the same as Example 5.1. The results are compared with the analytical solutions and the results of MFS and NMFS. The solution coverges to the analytical solution with the increasing number of the boundary nodes. An isotropic pressurized cylinder problem is used to demonstrate the advantages of the INMFS compared with MFS and NMFS in Example 6.2. The INMFS is used to solve the inclusions and void problems for isotropic and anisotropic materials in Example 6.3 and Example 6.5, respectively.

In Chapter 7 isotropic and anisotropic multi-grain materials are considered. NMFS and INMFS methods for this type of problems were considerd. Five examples are presented to demonstrate the feasibility and the accuracy of NMFS and INMFS. Example 7.1 and Example 7.3 deal with NMFS and INMFS for the isotropic material,

respectively. In Examples 7.2 and 7.4, NMFS and INMFS are assessed for the anisotropic material, respectively. All the grains in these four examples have the same properties. And all of this four examples are divided into two cases with normal stresses and shear stresses. Example 7.5 is divided into five cases. Nine grains are used in all of the five cases and the grain in the center has different properties with the other eight grains. In Case 7.5.1, the property of the central grain is the same in x and y direction. In Case 7.5.2, the property of the central grain is the different in x and y direction. Hirisontal direction has higher Young's modulus than the vertical direction. In Case 7.5.3, the rotation of the axes of a coordinate system of the central grain (with the same properties as in Case 7.5.2) is studied. In the final Case 7.5.5, the central grain with a void has the same property as in Case 7.5.2. Case 7.5.5 shows that INMFS can be use to solve more coplex problems as void problems. Because of the feasibility and the accuracy of the INMFS, a simulation of deformation of a peace of a realistic microstructure of a spring steel C45 on a square 50μm with 19 grains were given in INMFS. In these problems, a proper consideration of the boundary conditions on the interface is very important. We have to use both the displacement and the traction boundary conditions one the interfaces for elastic inclusions and connected multi-grain problems to make sure the respective algebraic equation system is square. In all the calculations, a limitation that one boundary collocation point can belong to only two regions at once is considered. Respectively, the discretisation points have not been placed on the corners where three or more regions meet.

Both, the NMFS and the INMFS methods, turn out to give in engineering sence similar results than the classical MFS method in all spectra of the performed tests. Because INMFS is simpler and more efficient than the NMFS, INMFS is a preferred method for use.

The represented work display a first use of MFS for solid mechanics problems without the fictitious boundary. The developed approach is clearly better than the classical finite element method for this type of problems, since discretisation is performed only on the boundary. The newly generated knowledge will be incorporated in microstructure deformation model, coupled with the macroscopic simulation system for continuous casting, hot rolling and heat treatment of metals.

8.2 Originality

Both versions of the non-singular MFS, developed in this dissertation, were not known before for isotropic and anisotropic elasticity problems. Moreover, because of the complexity of the fundamental solution, particularly for anisotropic problems, only a few publications dealth with related MFS before. The main originality of the method is discretisation of the boundary of the elastic domain only, which enables the method to be straightforwardly used for many bodies in contact. Future application of these methods to realistic industrial micromechanics problems is very important, since the methods reduces the amount of discretisation, needed in the classical mesh based methods. The INMFS will serve as a new powerful tool for simulations devoted to engineering design, fabrication, and analysis of a wide range

of materials including polycrystalline, composite, geotechnical, biological, and electronic materials. Optimum microstructures and their properties can be, by use of modeling and simulation, forecasted rather than found by trial and error. Fracture and fatigue of solids and structures, martensitic transformations, interphases in composites, and dispersion hardening of alloys are examples of the phenomena that are being elucidated and qualified by micromechanics.

8.3 Advantages

The NMFS and the INMFS have many advantages. The most notable are:

- There is no need to put the source points of fundamental solution outside the physical domain. It thus avoids the problems of artificial boundary. The problems, where there is a limited space for source points (like small inclusions) can be dealt with in a straightforward manner. This is for such situations not possible with the classical MFS.

- Collocation points coincide with the source points. Respectively, the generation of the nodes is relatively simple and easy to program. Except in the desingularization procedure, there are no integrations involved in the method.

- There is no need to know the neighbouring or any other point information for integrating (desingularizing) the fundamental solution on a circular disk.

- The method requires no domain discretisation as for example FEM. So it is more easily applicable for microstructure problems with high number and high geometrical complexity of each of the grains.

8.4 Intended Work

The novel INMFS is in the present dissertation used for simulating a deformation of a part of a realistic microstructure on an elastic square domain with 19 grains. It represents first steps in using this method for practical problems. In our future work, the INMFS will be upgraded for solving the 3D microstructures as done in paper [Benedetti and Aliabadi (2013)]. But the meshing was needed in above method and will not be needed by INMFS. Then the INMFS will be applied for the 3D microstructures with thousands of grains (see Figure 8.1).

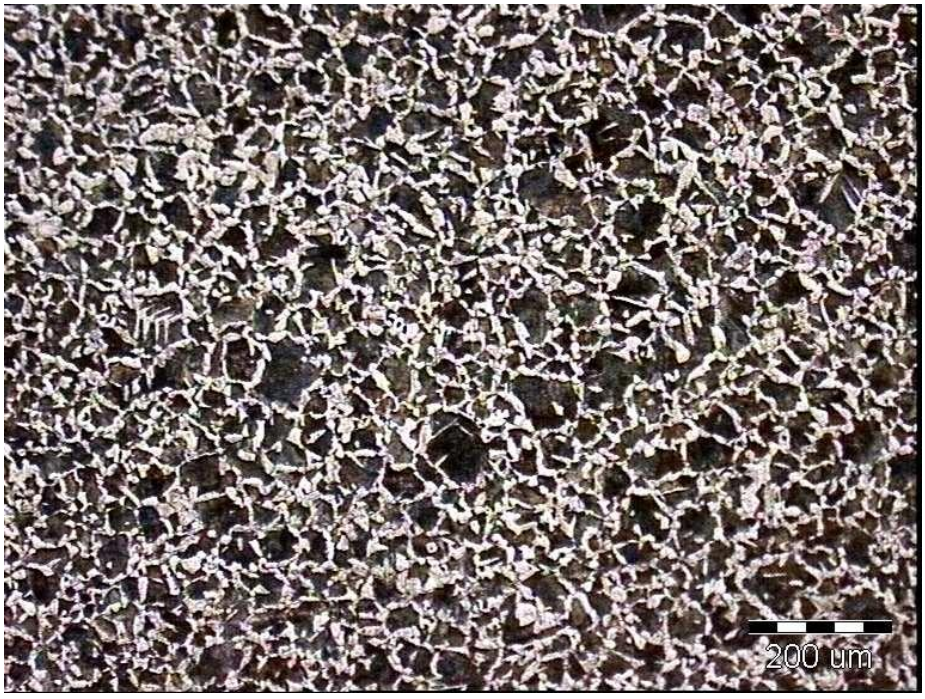

Figure 8.1: An example of microstructure of a material with thousands of grains.

For this purpose, the desingularisation of a 3D fundamental solutions is needed, which would be more complex than the 2D one. Also the discretisation will be more complex.

Since many materials behave not only lineraly elastic, but experience some other, more complex form of rheology, such as plasticity, this will also be taken into account in the future. For this purpose, the works of Kołodzej would serve as a starting point (see [Kołodziej and Gorzelanczyk (2012); Kołodziej, Jankowska and Mierzwiczak (2013)]).

8.5 Publications

A part of the developments in this dissertation have been already published in the following journal papers:

LIU, Qingguo, ŠARLER, Božidar. Non-singular Method of Fundamental Solutions for anisotropic elasticity. /Engineering analysis with boundary elements/, ISSN 0955-7997, 2014, vol. 45, pp. 68-78, doi: 10.1016/j.enganabound.2014.01.020 [COBISS.SI-ID 3222779]

LIU, Qingguo, ŠARLER, Božidar. Non-singular method of fundamental solutions for two-dimensional isotropic elasticity problems. /Computer modeling in engineering & sciences. CMES/, ISSN 1526-1492. 2013, vol. 91, pp. 235-267. [COBISS.SI-ID 2750203]

Conclusions

LIU, Qingguo, ŠARLER, Božidar. Non-singular method of fundamental solutions for the deformation of two-dimensional elastic bodies in contact . /Materials and technologies/, ISSN 1580-2949, 2013, vol. 47, pp. 789-793. . [COBISS.SI-ID 2980091]

and are prepared for publication

LIU, Qingguo, ŠARLER, Božidar. Improved non-singular method of fundamental solutions for two-dimensional isotropic elasticity problems and application for elastic/rigid inclusions or void problems. / Computational Mechanics/.

The following conference presentations appear from the parts of the dissertation:

ŠARLER, Božidar, LIU, Qingguo. Non-sinular MFS for anisotropic elasticity. In: LIU, Gui-Rong (Ed.), LIU, Z. S. (Ed.). /Proceedings of the 5th Asia Pacific Congress on Computational Mechanics (APCOM2013) and 4th International Symposium on Computational Mechanics (ISCM2013), 11th-14th December 2013, Singapore/., 2013, 1 p. [COBISS.SI-ID 3032315]

LIU, Qingguo, ŠARLER, Božidar. Improved non-singular method of fundamental solutions for two-dimensional isotropic elasticity problems. In: 21st International Conference on Materials and Technology, 13-15 November 2013, Portorož, Slovenia. GODEC, Matjaž (Ed.), et al. /Program and book of abstracts/. Ljubljana: Institute of metals and technology, 2013, pp. 122. [COBISS.SI-ID 3067643]

ŠARLER, Božidar, LIU, Qingguo. Non-singular method of fundamental solutions for elasticity problems. In: /ECCOMAS 2012 : Book of Abstracts: Proceedings of the 6th European Congress on Computational Methods in Applied Sciences and Engineering (ECCOMAS 2012), September 10-14, 2012, Vienna, Austria/. Vienna: University of Technology, 2012, pp. 354. [COBISS.SI-ID 2649595]

LIU, Qingguo, ŠARLER, Božidar. A non-singular method of fundamental solutions and its application to two dimensional multi-body elasticity problems. In: 20. Jubilee Conference on Materaisl and technologies, 17.-19. October 2012, Portorož, Slovenia. GODEC, Matjaž (Ed.), et al. /Program and book of abstracts/. Ljubljana: Institute of Metals and Technology, 2012, pp. 92. [COBISS.SI-ID 2632955]

Appendix

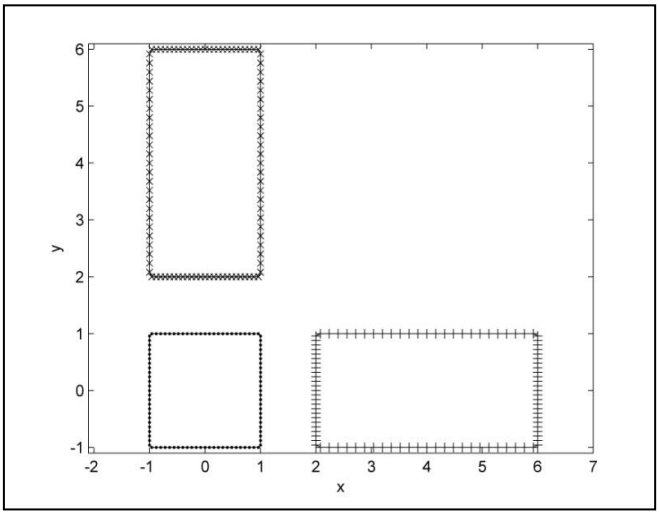

Figure A: Case 4.1.1. The known two reference solutions of the governing equation ($\bullet$: initial layout, $+$: $\bar{u}_x(\mathbf{p}) = p_x + 4\,\text{m}$, $\bar{u}_y(\mathbf{p}) = 0\,\text{m}$, $\times$: $\bar{u}_x(\mathbf{p}) = 0\,\text{m}$, $\bar{u}_y(\mathbf{p}) = p_y + 4\,\text{m}$.), used in calculation of the desingularized values of fundamental solution in traction boundary condition points, that give proper NMFS solution.

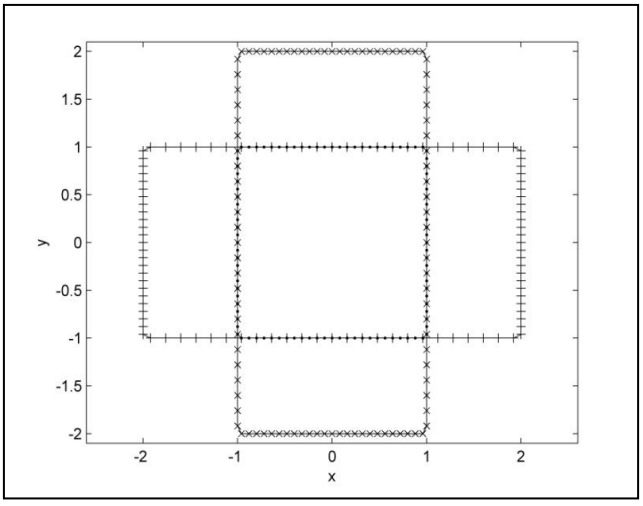

Figure B: Case 4.1.1. The known two reference solutions of the governing equation ($\bullet$: initial layout, $+$: $\bar{u}_x(\mathbf{p}) = p_x$, $\bar{u}_y(\mathbf{p}) = 0\,\text{m}$, $\times$: $\bar{u}_x(\mathbf{p}) = 0\,\text{m}$, $\bar{u}_y(\mathbf{p}) = p_y$.), used in calculation of the desingularized values of fundamental solution in traction boundary condition points, that give erroneous NMFS solution.

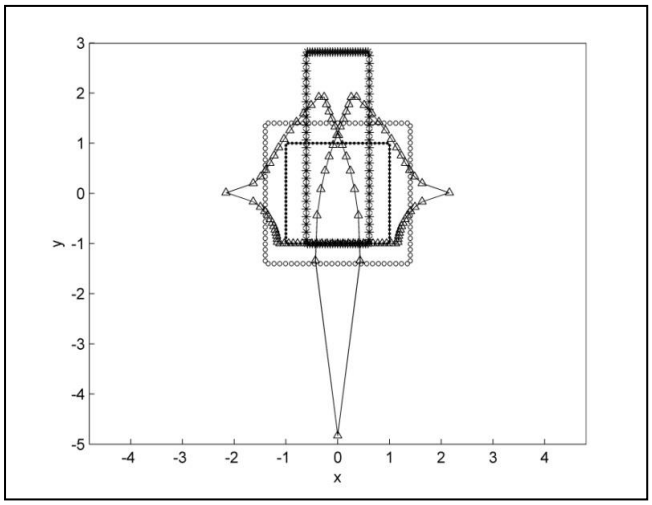

Figure C: Case 4.1.1. The analytical solution, the numerical solution with MFS and the erroneous numerical solution with NMFS with $N^{\Gamma} = 100$ and $c_x = c_y = 0\,\mathrm{m}$. (• : collocation points, ◦ : source points in MFS, + : analytical solution, × : MFS solution, △ : NMFS solution)

References

Aleksidze, M. A. (1991). *Fundamentalnye funktsii v priblizhennykh resheniyakh granichnykh zadach [Fundamental functions in approximate solutions of boundary value problems]*. Spravochnaya Matematicheskaya Biblioteka [Mathematical Reference Library]. “Nauka”, Moscow. (in Russian); (with an English summary).

Aliabadi, M. H. (2002). *The Boundary Element Method, Applications in Solids and Structures*. John Wiley & Sons. Chichester.

Atluri, S .N.; Shen, S. (2002). *The Meshless Method.* Tech Science Press. Encino.

Balakrishnan, K.; Ramachandran, P. A. (2001). Oscilatory interpolation in the method of fundamental solution for nonlinear Poisson problems. *Journal of Computational Physics*. 172: 1–18.

Belytschko, T.; Lu, Y. Y.; Gu, L. (1994). Element-free Galerkin methods. *International Journal for Numerical Methods in Engineering*. 37: 229-256.

Benedetti, I.; Aliabadi M. H. (2013). A three-dimensional grain boundary formulation for microstructural modeling of polycrystalline materials. *Computational Materials Science*. 67: 249-260.

Berger, J. R.; Karageorghis, A. (2001). The method of fundamental solutions for layered elastic materials. *Engineering Analysis with Boundary Elements*. 25: 877-886.

Berger, J. R.; Karageorghis, A.; Martin, P. A. (2005). Stress intensity factor computation using the method of fundamental solutions: mixed-mode problems. *International Journal for Numerical Methods in Engineering*. 69: 469-483.

Beskos, D. E. (1987). *Boundary Element Methods in Mechanics*. Elsevier Science Publishers B. V., Amsterdam.

Bogomolny, A. (1985). Fundamental solutions method for elliptic boundary value problems. *SIAM Journal on Numerical Analysis*. 22: 644–669.

Bower, A. F. (2009). *Applied Mechanics of Solids*. CRC Press. Boca Raton, Florida.

Braccini, M.; Dupeux, M. (2012). *Mechanics of Solid Interfaces*. Wiley. New York.

Burgess, G.; Maharejin, E. (1984). A comparison of the boundary element and superposition methods. *Computers & Structures*. 19: 697-705.

References

Chen, C. S. (1995). Method of fundamental solution for nonlinear thermal explosions. *Communications in Numerical Methods in Engineering*. 11: 675-681.

Chen, K. H.; Kao, J. H.; Chen, J. T.; Young, D. L.; Lu, M. C. (2006). Regularized meshless method for multiply-connected-domain Laplace problems. *Engineering Analysis with Boundary Elements*. 30: 882-896.

Chen, Y. P.; Lee, J.; Eskandarian, A. (2006). *Meshless Methods in Solid Mechanics*, Springer Verlag, Berlin, 2006.

Chen, W.; Lin, J.; Wang, F. (2011). Regularized meshless method for non-homogeneous problems. *Engineering Analysis with Boundary Elements*. 35: 253–257.

Chen, C. S.; Karageorghis, A; Smyrlis, Y. S. (2008). *The Method of Fundamental Solutions - A Meshless Method*. Dynamic Publishers, Atlanta.

Chen, W.; Wang, F. Z. (2010). A method of fundamental solutions without fictitious boundary. *Engineering Analysis with Boundary Elements*. 34: 530-532.

Dong, L.; Atluri, S. N. (2011a). A simple procedure to develop efficient & stable hybrid/mixed elements, and Voronoi cell finite elements for macro - & micromechanics. *CMC: Computers, Materials & Continua*. 24: 61-104.

Dong, L.; Atluri, S. N. (2011b). Development of T-Trefftz four - node quadrilateral and Voronoi cell finite elements for macro- & micromechanical modeling of solids. *CMES: Computers Modeling in Engineering & Sciences*. 81: 69-118.

Dong, L.; Atluri, S. N. (2012). T-Trefftz Voronoi cell finite elements with elastic/rigid inclusions or voids for micromechanical analysis of composite and porous materials. *CMES: Computers Modeling in Engineering & Sciences*. 83: 183-219.

Dong, L.; Atluri, S. N. (2013). SGBEM Voronoi cells (SVCs) with embedded arbitrary shaped inclusions, voids, and/or cracks for micromechanical modeling of heterogenous materials. *CMC: Computers, Materials & Continua*. 26: 1-44.

Fairweather, G.; Karageorghis, A. (1998). The method of fundamental solutions for elliptic boundary value problems. *Advances in Computational Mathematics*. 9: 69-95.

Fan, C. M.; Chen, C. S.; Monroe, J. (2009). The method of fundamental solutions for solving convection-diffusion equations with variable coefficients. *Advances in Applied Mathematics and Mechanics*. 1: 215–230.

Fenner, R. T. (2001). A force field superposition approach to plane elastic stress and strain analysis. *Journal of Strain Analysis for Engineering Design*. 36: 517-529.

Fu, Z.; Chen, W.; Yang, W. (2009). Winkler plate bending problems by a truly boundary-only boundary particle method. *Computational Mechanics*. 44: 757–763.

Gauger, C.; Leinen, P.; Yserentant, H. (2000). The finite mass method. *SIAM Journal Numerical Analysis*. 37: 1768-1799.

Golberg, M. A. (1995). The method of fundamental solutions for Poisson's equation. *Engineering Analysis with Boundary Elements*. 16: 205–213.

Golberg, M. A.; Chen, C. S. (1994). The theory of radial basis functions applied to the BEM for inhomogeneous partial differential equations. *Boundary Elements Communications*. 5: 57–61.

Golberg, M. A.; Chen, C. S. (1997). *Discrete Projection Methods for Integral Equations*. Computational Mechanics Publications. Southampton.

Golberg, M. A.; Chen, C .S. (1998). *The method of fundamental solutions for potential, Helmholtz and diffusion problems: in. Boundary Integral Methods Numerical and Mathematical Aspects, Computational Engineering.* WIT Press/Computational Mechanics Publications. Boston. 103-176.

Golberg, M. A.; Chen, C. S.; Bowman, H.; Power, H. (1998). Some comments on the use of radial basis functions in the Dual Reciprocity Method. *Computational Mechanics*. 21: 141–148.

Gu, Y.; Chen, W.; Zhang, C. Z. (2011). Singular boundary method for solving plane strain elastostatic problems. *International Journal of Solids and Structures*. 48: 2549-2556.

Herrera, I. (1984). *Boundary Methods. An Algebraic Theory*. Pitman Advanced Publishing Program. Boston.

Hon, Y. C.; Wei, T. (2005). The method of fundamental solution for solving multidimensional inverse heat conduction problems. *CMES: Computer Modeling in Engineering & Sciences*. 7: 119–132.

Huang, G.; Cruse, T. A. (1994). On the non-singular traction-BIE in elasticity. *International Journal of Numerical Methods in Engineering*. 37: 2041-2072.

Jiang, X. R.; Chen, W. (2011). Method of fundamental solution and boundary knot method for Helmholtz equations: a comparative study. *Chinese Journal of Computational Mechanics*. 28: 338–344 (in Chinese).

Karageorghis, A. (1987). Method of fundamental solution for the numerical solution of biharmonic equations. *Journal of Computational Physics*. 69: 434-459.

Karageorghis, A.; Fairweather, G. (2000). The method of fundamental solutions for axisymmetric elasticity problems. *Computational Mechanics*. 25: 524-532.

Karageorghis, A.; Lesnic, D. (2011). Application of the MFS to inverse obstacle scattering problems. *Engineering Analysis with Boundary Elements*. 35: 631-638.

References

Karageorghis, A.; Poullikkas, A.; Berger, J. R. (2006). Stress intensity factor computation using the method of fundamental solutions. *Computational Mechanics*. 37: 445-454.

Katsurada, M.; Okamoto, H. (1996). The collocation points of the fundamental solution method for the potential problem. *Computers & Mathematics with Applications*. 31: 123–137.

Kim, S. (2013). An improved boundary distributed source method for two-dimensional Laplace equations. *Engineering Analysis with Boundary Elements*. 37: 997-1003.

Kołodziej, J. A. (1987). Review of applications of boundary collocation methods in mechanics of continuous media. *Solid Mechanics Archives*. 12: 187-231.

Kołodziej, J. A. (2001). *Zastosowanie metody kollokacji brzegowej w zagadnieniach mechaniki [Applications of the Boundary Collocation Method in Applied Mechanics]*. Wydawnictwo Politechniki Poznánskiej. Poznán, (in Polish).

Kołodziej, J. A.; Gorzelanczyk, P. (2012). Application of method of fundamental solutions for elasto-plastic torsion of prismatic rods. *Engineering Analysis with Boundary Elements*. 36: 81–86.

Kołodziej, J. A.; Jankowska, M. A.; Mierzwiczak, M. (2013). Meshless methods for the inverse problem related to the determination of elastoplastic properties from the torsional experiment. *International Journal of Solids and Structures*. 50: 4217-4225.

Kondapalli, P. S.; Shippy, D. J.; Fairweather, G. (1992a). Analysis of acoustic scattering in fluids and solids by the method of fundamental solutions. *Journal of Acoustical Society of America*. 91: 1844–1854.

Kondapalli, P. S.; Shippy, D. J.; Fairweather, G. (1992b). The method of fundamental solutions for transmission and scattering of elastic waves. *Computer Mathods in Applied Mechanics and Engineering*. 96: 255–269.

Kupradze, V. D. (1964). *On a Method of Solving Approximately the Limiting Problems of Mathematical Physics.* Ž. Vyčisl. Mat. i Mat. Fiz. 4: 1118-1121.

Kupradze, V. D.; Aleksidze, M. A. (1964). The method of functional equations for the approximate solution of certain boundary value problems. *USSR Computational Mathematics and Mathematical Physics.* 4: 82–126.

Kupradze, V. D.; Gegelia, T. G.; Basheleshvili, M. O.; Burchuladze, T. V. (1976). *Trekhmernye zadachi matematicheskoi teorii uprugosti i termouprugosti [Three-dimensional problems in the mathematical theory of elasticity and thermoelasticity]*. Izdat. "Nauka", Moscow (in Russian).

Lekhnitskii, S. G. (1981). *Theory of Elasticity of an Anisotropic Plate*. MIR publishers, Moscow.

Liu, G. R. (2009). *Meshfree Methods: Moving Beyond the Finite Element Method, 2nd edition*. CRC Press. Boca Raton, FL.

Liu, Q. G.; Šarler, B. (2013). Non-Singular Method of Fundamental Solutions for Two-Dimensional Isotropic Elasticity Problems. *CEMS. Computers Modeling in Engineering & Sciences*. 91: 235-266.

Liu, Q. G.; Šarler, B. (2014). Non-singular Method of Fundamental Solutions for anisotropic elasticity. *Engineering Analysis with Boundary Elements*. 45: 68-78.

Liu, Y. J. (2010). A new boundary meshfree method with distributed sources. *Engineering Analysis with Boundary Elements*. 34: 914-919.

Maharejin, E. (1985). An extension of the superposition method for plane anisotropic elastic bodies. *Computers & Structures*. 21: 953-958.

Marin, L. (2011). Relaxation procedures for an iterative MFS algorithm for two-dimensional steady-state isotropic heat conduction Cauchy problems. *Engineering Analysis with Boundary Elements*. 35: 415-429.

Marin, L.; Lesnic, D. (2004). The method of fundamental solutions for the Cauchy problem in two-dimensional linear elasticity. *International Journal of Solids and Structures*. 41: 3425-3438.

Mathon, R.; Johnston, R. L. (1977). The approximate solution of elliptic boundary-value problems by fundamental solutions. *SIAM Journal on Numerical Analysis*. 14: 638–650.

Mitchell, A. R.; Griffiths, D. F. (1980). *The Finite Difference Method in Partial Differential Equations*. John Wiley & Sons, Michigan.

Mura, T. (1987). *Micromechanics of Defects in Solids. 2ed*. Martinus Nijhoff Publishers. Leiden.

Nguyen, V. P.; Rabczuk, T.; Bordas, S.; Duflot, M. (2008). Meshless methods: a review and computer implementation aspects. *Mathematics and computers in simulation*. 79: 763-813.

Ooi, E. H.; Popov, V. (2012). An efficient implementation of the radial basis integral equation method. *Engineering Analysis with Boundary Elements*. 36: 716-726.

Panzeca, T.; Fujita Yashima, H.; Salerno, M. (2001). Direct stiffness matrices of BEs in the Galerkin BEM formulation. *European Journal of Mechanics –A/Solids*. 20: 277-298.

Patankar, S. V. (1980). *The Fnite Volume Method*. Hemisphere. New York.

Patterson, C.; Sheikh, M. A. (1982). *On the Use of Fundamental Solutions in Trefftz Method for Potential and Elasticity Problems, In: C.A. Brebbia (Ed.), Boundary*

References

Element Methods in Engineering, Proceedings of the Fourth International Seminar on Boundary Element Methods. Springer. New York. 43-54.

Perne, M.; Šarler, B.; Gabrovšek, F. (2012). Calculating transport of water from a conduit to the porous matrix by boundary distributed source method. *Engineering Analysis with Boundary Elements*. 36: 1649-1659.

Poullikkas, A.; Karageorghis, A.; Georgiou, G. (2002). The method of fundamental solutions for three-dimensional elastostatics problems. *Computers & Structures*. 80: 365-370.

Qu, J.; Cherkaoui, M. (2006). *Fundamentals of Micromechanics of Solids*. John Wiley & Sons, Inc. Hoboken, New Jersey.

Raamachandran, J.; Rajamohan, C. (1996). Analysis of composite plates using charge simulation method. *Engineering Analysis with Boundary Elements*. 18: 131-135.

Redekop, D. (1982). Fundamental solutions for the collocation method in planar elastostatics. *Applied Mathematical Modelling*. 6: 390-393.

Redekop, D.; Cheung, R. S. W. (1987). Fundamental solutions for the collocation method in three-dimensional elastostatics. *Computers & Structures*. 26: 703-707.

Redekop, D.; Thompson, J. C. (1983). Use of fundamental solutions in the collocation method in axisymmetric elastostatics. *Computers & Structures*. 17: 485-490.

Šarler, B. (2009). Solution of potential flow problems by the modified method of fundamental solutions: formulations with the single layer and the double layer fundamental solutions. *Engineering Analysis with Boundary Elements*. 33: 1374-1382.

Šarler, B.; Vertnik, R. (2006). Meshfree explicit local radial basis function collocation method for diffusion problems. *Computers & Mathematics with Applications*. 51: 1269-1282.

Smyrlis, Y.-S. (2009). Applicability and applications of the method of fundamental solutions. *Mathematics of Computation*. 78: 1399-1434.

Stroh, A. S. (1958). Dislocations and cracks in anisotropic elasticity. *Philosophical Magazine* 3:625-646.

Teway, V. K.; Wagoner, R. H.; Hirth, J. P. (1989). Elastic Green's function for a composite solid with a planar interface. *Journal of Materials Research.* 4: 113-123.

Ting, T. C. T. (1996). *Anisotropic Elasticity*. Oxford Science Publications. Oxford.

Tsai, C. C. (2007). The method of fundamental solutions for three-dimensional elastostatic problems of transversely isotropic solids. *Engineering Analysis with Boundary Elements*. 31: 586-594.

Young, D. L.; Chen, K. H.; Chen, J. T.; Kao, J. H. (2007). A modified method of fundamental solutions with source on the boundary for solving Laplace equations with circular and arbitrary domains. *CMES: Computer Modeling in Engineering & Sciences*. 19: 197-222.

Young, D. L.; Chen, K. H.; Lee, C.W. (2005). Novel meshless method for solving the potential problems with arbitrary domain. *Journal of Computational Physics*. 209: 290-321.

Young, D. L.; Tsai, C. C.; Chen, C. W.; Fan, C. M. (2008). The method of fundamental solutions and condition number analysis for inverse problems of Laplace equation. *Computers & Mathematics with Applications.* 55: 1189-1200.

Walker, W. A. (2012). The repeated replacement method: a pure lagrangian meshfree method for comutational fluid dynamics. PLoS ONE 7(7): e39999. doi:10.1371/journal.pone.0039999

Wrobel, L. C. (2002). *The Boundary Element Method, Applications in Thermo-Fluids and Acoustics*. John Wiley & Sons, Chichester.

Zielinski, A. P.; Herrera, I. (1987). Trefftz method. Fitting boundary conditions. *Interntional Journal for Numerical Methods in Engineerin*. 24: 871-891.

Zienkiewicz, O. C.; Taylor R. L. (2000). *The Finite Element Method: the Basis*. Butterworth-Heinemann. Woburn, MA.

References